Nelson Mandela Metropolitan University

for tomorrow

Characterisation of Young's modulus and loss factor of damping materials

by

Markus Nörtemann

BEng Automotive Engineering

A dissertation submitted in fulfilment of the requirements for the degree of Magister in Mechatronic Engineering at the Faculty of Engineering, the Built Environment and Information Technology to be awarded at the Nelson Mandela Metropolitan University

Promoters: Prof. Dr.-Ing U. Becker

Prof. Dr.-Ing T. van Niekerk

June 16, 2014

Markus Nörtemann
Holtenser Weg 13
37186 Moringen
-Germany-

I, Markus Nörtemann, 213508850, hereby declare that the dissertation, *Characterisation of Young's modulus and loss factor of damping materials* for the degree of *Magister in Mechatronic Engineering*, is my own work and that it has not previously been submitted for assessment or completion of any postgraduate qualification to another University or for another qualification.

Port Elizabeth June 16, 2014

Markus Nörtemann

Copyright Statement

Acknowledgments

During the work on my dissertation, several people and institutions contributed towards this study. I would like to thank in particular the following:

- My supervisors, Prof. Dr.-Ing U. Becker and Prof. Dr.-Ing T. van Niekerk, for giving me the opportunity to study at the NMMU and for their guidance as well as constructive suggestions during this work.

- Glynne Erasmus, for taking the SEM pictures in this study.

- Martin Stahlberg from the Ostfalia University, who sent important books from Germany.

- The library team at the NMMU, who helped me obtaining numerous articles and books.

- My parents for their love, support and encouragement. I owe you both everything.

- Last but not least, a special thank you goes to Bomikazi Zeka, who edited the language in this dissertation and moreover filled my life with love and joy.

Abstract

Given the importance of simulation techniques in automotive engineering, there is a lack of implementation regarding these techniques in the acoustics of damping materials for air-borne sound. Biot's calculations have proven its abilities to simulate the acoustic characteristics of these damping materials. However, the characterisation of essential structural parameters, such as Young's modulus and loss factor, in order to conduct Biot's calculations have been inconclusive. Thus, the primary research objective of this study is to propose a new measurement system for the structural Biot parameters.

After a comprehensive literature review has been undertaken on damping materials, as well as measurement apparatuses for Young's modulus and loss factor of damping materials, two causes of measurement errors have been identified. Unknown stresses in measurement apparatuses and inhomogeneous, polytrophic and viscoelastic behaviour of specimens.

A new measurement system that does not affect the specimens with unknown stresses and accounts for their complex behaviour required investigation. Non-contact ultrasound had been selected as a solution to determine the aforementioned parameters, since these methods do not necessarily touch or compress the specimen, which led to unknown stresses and neglection of the complex specimen behaviour with the aforementioned techniques.

Although ultrasound had been used to determine structural parameters on various types of materials, it has never been used to measure soft porous damping materials. In order to find possible solutions, various sources using ultrasonics to investigate struc-

tural parameters had been reviewed. In order to calculate structural parameters, the longitudinal and transversal wave velocity inside the specimen had to be determined.

The main findings showed that non-contact ultrasound will be able to evaluate the Young's modulus, loss factor as well as Poisson's ratio. Consequently, it was shown that longitudinal velocity measurements could be conducted using well known transmission measurements. However, well known approaches would not be sufficient measuring the transversal wave velocity in soft damping materials. This problem was addressed with a special gas to be used, with lower sound speed velocity in the fluid than in the solid. Moreso, a new method determining the transversal wave velocity had been found, as it would enable the use of an even larger range of damping materials, especially ones with heavy frames and lower porosity. It will use refracted waves inside the specimen and the determination of the convertion position of the transversal to the longitudinal wave at the rear specimen surface.

At the end of the study, hardware components were selected and a test rig was constructed, which should be able to prove that a determination of structural Biot parameters with non-contact ultrasound is possible with less errors instead of using mechanical transfer function systems. The development of measurement software as well as the testing of the measurement system and its validation was not under investigation in this dissertation.

This study has expanded on the body of literature knowledge regarding non-contact ultrasound. Furthermore, a significant contribution has been made towards a new measurement system measuring Young's modulus and loss factor which circumvents errors in mechanical transfer function systems. This will contribute to more precise simulations of damping materials and damped enclosures, which may ultimately result in enhanced efficiency of damping materials as well as the acoustic packaging of cars.

Keywords:

Young's modulus, Loss factor, Damping materials, Non-contact ultrasound, Structural Biot parameters

Contents

List of Figures

List of Tables

Nomenclature

Abbreviations

Abbreviation	*Meaning*
TOF	Time of flight
NMMU	Nelson Mandela Metropolitan University
PET	Polyethylene Terephthalate
PU	Polyurethane
SEM	Scanning electron microscope
FEM	Finite element method
KKR	Kramers Kronig relations
DFT	Discrete Fourier transform
PMMA	Polymethyl methacrylate
A/D converter	Analogue to digital converter
ETS	Equivalent-Time sampling

Symbols

Symbol	***Unit***	***Meaning***
a	1	Composite pore shape factor
A	m^2	Surface, perpendicular to applied force
A_p	m^2	Pore surface
b	m	Width of specimen
c	$^m/_s$	Sound velocity
c_{lb}	$^m/_s$	Longitudinal sound velocity in specimen
$c_{lb}(\omega)$	$^m/_s$	Longitudinal phase velocity in specimen
c_{lf}	$^m/_s$	Sound velocity in fluid
c_{tb}	$^m/_s$	Transversal sound velocity in specimen
C_i^ν	1	Curve fit coefficients related to curve ν
c_p	$^J/_{mol} \cdot K$	Heat capacity at constant pressure
c_v	$^J/_{mol} \cdot K$	Heat capacity at constant volume
d	m	Diameter of specimen
D_i^S	1	Curve fit coefficients related to curve S
d_v	$^{N \cdot s}/_{m^2}$	Dynamic viscosity
E	Pa	Young's modulus
e	1	Wave number
E_a	Pa	Apparent Young's modulus

Symbols

Symbol	*Unit*	*Meaning*
E_b	Pa	Young's modulus of specimen
E'	Pa	Dynamic Young's modulus
E''	Pa	Loss Young's modulus
E^*	Pa	Complex Young's modulus
F	N	Force
f_b	Hz	Bandwidth frequency
f_h	Hz	Highest frequency
f_r	Hz	Resonant frequency
f_v	1	Porosity
$F(\omega)$	N	Force measured by force transducer
H_c	1	Correction function
I_a	W/m^2	Acoustic intensity of absorbed sound
I_e	W/m^2	Acoustic intensity of emitted sound
I_r	W/m^2	Acoustic intensity of received sound
k	N/m	Stiffness factor
K	Pa	Bulk modulus
K'	Pa	Dynamic bulk modulus
K_b	Pa	Bulk modulus of specimen
K_f	Pa	Bulk modulus of fluid
$K_m(\omega)$	N/m	Measured compression stiffness
$K_m(0)$	N/m	Static compression stiffness of disc shaped specimen
K_s	Pa	Bulk modulus of solid
$k_s(\omega)$	N/m	Measured compression stiffness of spring
k_0	N/m	Static compression stiffness of spring
$K(0)$	N/m	Static compression stiffness of rod-like specimen
L	Pa	Longitudinal modulus

Symbols

Symbol	***Unit***	***Meaning***
l	m	Thickness of specimen
l_a	$a.u.$	Longitudinal wave amplitude
L_b	Pa	Longitudinal modulus of specimen
l_r	m	Length of array
L'	Pa	Dynamic longitudinal modulus
L''	Pa	Loss longitudinal modulus
m	Kg	Mass of specimen and upper plate with additional mass
M	$^{Kg}/_{mol}$	Molar mass
M'	Pa	Dynamic general modulus
M''	Pa	Loss general modulus
M^*	Pa	Complex general modulus
N	Pa	Shear modulus
n	1	Wave number
N'	Pa	Dynamic shear modulus
N_b	Pa	Shear modulus of specimen
N_s	Pa	Shear modulus of solid
P	Pa	Elastic constant of solid
p	Pa	Pressure
p_e	Pa	Emitted pressure amplitude
p_i	Pa	Incident pressure amplitude
p_r	Pa	Received pressure amplitude
p_{ref}	Pa	Reflected pressure amplitude
$P_\nu(S)$	1	Correction polynom shape factor
$P_S(\nu)$	1	Correction polynom Poisson's ratio
Q	1	Potential coupling
R	Pa	Elastic constant of fluid

Symbols

Symbol	*Unit*	*Meaning*
r	m	Radius of specimen
R	$^{J}/_{mol \cdot K}$	Universal gas constant
R_f	1	Reflection factor
R_l	1	Magnitude of reflected wave amplitude
r_a	m	Distance to microphones
r_{ds}	m	Distance from source to array
r_s	$^{N \cdot s}/_{m^4}$	Length specific flow resistance
$re(f)$	1	Reflection coefficient
r_{ref}	m	Reference distance
r_{fm}	m	Distance from focus to microphone
S	1	Shape factor
s	m	Pore size of specimen
t	s	Time
T	K	Absolute temperature
t_a	m	Transversal wave amplitude
T_e	N	Tension
T_f	1	Transmission factor
T_l	$a.u.$	Magnitude of refracted longitudinal wave amplitude
T_t	$a.u.$	Magnitude of refracted transversal wave amplitude
t_f	s	Emission time
t_{fm}	s	Time from focus to microphone position
t_m	s	Delayed time
$T_m(\omega)$	1	Transfer function general displacements uncorrected
$T_{mc}(\omega)$	1	Transfer function general displacements corrected
t_{rd}	s	Rising time of digitizer
$T_s(\omega)$	1	Transfer function displacements of spring

Symbols

Symbol	*Unit*	*Meaning*
$u(\omega)$	m	Double integrated signal of accelerometer
$\bar{u}_f$	m	Average displacement of fluid
$\bar{u}_s$	m	Average displacement of solid
v	$^m/_s$	Flow velocity of fluid
V_b	m^3	Volume of specimen
V_f	m^3	Volume of fluid in pores
V_p	m^3	Pore volume
w_m	1	Weighting factor
x_p	m	Horizontal position
$x(\omega)$	m	Horizontal displacement
$\tilde{x}_{1,2}$	m	Displacements for accelerometer 1,2
X_1, X_2	m	Complex amplitudes for accelerometer 1,2
x_f	m	Assumed focus position
$X_m(\omega)$	$^N/_m$	Mechanical reactance
y	m	Vertical displacement
y_a	m	Vertical amplitude
y_p	m	Vertical position
z	m	Length of ultrasonic path
Z_{bl}	$^{kg}/_{s \cdot m^2}$	Impedance of specimen for longitudinal wave
Z_{bt}	$^{kg}/_{s \cdot m^2}$	Impedance of specimen for transversal wave
Z_f	$^{kg}/_{s \cdot m^2}$	Impedance of fluid
$Z_m(\omega)$	$^{kg}/_{s \cdot m^2}$	General mechanical impedance uncorrected
$Z_{mc}(\omega)$	$^{kg}/_{s \cdot m^2}$	Mechanical impedance corrected
$\underline{Z_2}$	$^{kg}/_{s \cdot m^2}$	Complex wall impedance
$\mathbf{I}$	$a.u.$	Vector of incident wave
$\mathbf{K_1}$	1	Unit vector in direction of propagation

Symbols

Symbol	*Unit*	*Meaning*
$\mathbf{K_2}$	1	Unit vector orthogonal to direction of propagation
$\mathbf{R}$	$a.u.$	Vector of reflected wave
$\mathbf{r}$	m	Location vector
$\mathbf{T_l}$	$a.u.$	Vector of refracted longitudinal wave
$\mathbf{T_t}$	$a.u.$	Vector of refracted transversal wave
$\mathbf{U}$	$^m/_s$	Displacement velocity vector

Greek symbols

Symbol	***Unit***	***Meaning***
α	1	Sound absorption coefficient
α	$^1/_m$	Attenuation coefficient
β	$degree$	Angle of refracted longitudinal wave
χ	1	Tortuosity
δ	rad	Phase shift
Δd	m	Change in diameter
Δf	Hz	Half power bandwidth
Δl	m	Change in specimen thickness
Δp	Pa	Pressure difference before and after specimen
Δt	s	Time difference TOF measurement in fluid with specimen
ΔV_b	m^3	Change in volume of specimen
Δx	m	Distance from microphones to each other
ϵ_0	$^N/_{m^2}$	Initial strain
ϵ^*	$^N/_{m^2}$	Complex strain
η	1	Loss factor
γ	$degree$	Angle of refracted transversal wave
γ_s	$^N/_{m^2}$	Shear strain
κ	1	Adiabatic index
Λ	m	Viscous characteristic length
Λ'	m	Thermal characteristic length
λ	m	Wavelength of ultrasonic wave
ν	1	Poisson's ratio
ω	$^{rad}/_s$	Angular frequency
ω_{r1}	$^{rad}/_s$	First resonance of system
Ω_b	Ω	Electric resistance with specimen inserted
Ω_f	Ω	Electric resistance with only fluid

Greek symbols

Symbol	***Unit***	***Meaning***
ω_m	1	Weighting factor
Φ	$degree$	Angle of reflected wave
$\phi_{ub}(\omega)$	$^{rad}/_{s}$	Unwrapped phase velocity with specimen
$\phi_{uf}(\omega)$	$^{rad}/_{s}$	Unwrapped phase velocity with fluid
ρ	$^{kg}/_{m^3}$	Linear density
ρ_{12}	$^{kg}/_{m^3}$	Describes mass coupling between fluid and solid
ρ_{ij}	$^{kg}/_{m^3}$	Density terms of solid and fluid
ρ_b	$^{kg}/_{m^3}$	Density of specimen
ρ_f	$^{kg}/_{m^3}$	Density of fluid
ρ_s	$^{kg}/_{m^3}$	Density of solid
σ	$^{N}/_{m^2}$	Stress
σ_0	$^{N}/_{m^2}$	Initial stress
σ^*	$^{N}/_{m^2}$	Complex stress
θ	$degree$	Angle of incidence
τ	$^{N}/_{m^2}$	Shear strain
Ξ	$^{Pa \cdot s}/_{m^2}$	Complex wall impedance

1 Introduction to the Study

1.1. Introduction and Background

The quality standards of cars demanded by customers has risen over the past years. Besides optical and surface characteristics, the acoustic behaviour of automotives is equally important.

The acoustics inside the passenger compartment is influenced by acoustic sources, which produce sound, taken from [33] and described in Figure 1.1.

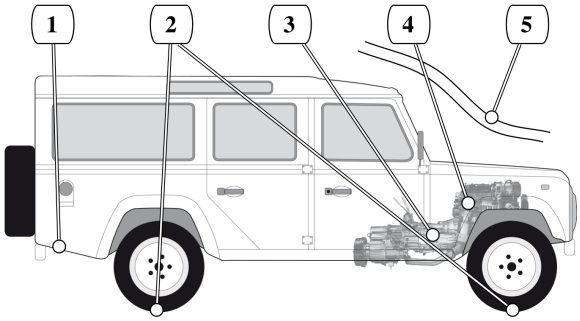

1 : *Exhaust noise*
2 : *Rolling noise*
3 : *Gearbox noise*
4 : *Engine noise*
5 : *Aerodynamic noise*

Figure 1.1.: Acoustic sources of a driving vehicle

In order to minimize noise exposure, there are different types of damping materials available. The term is limited in this dissertation to materials that absorb air-borne sound energy. However, other materials absorbing structural vibrations also exist. To be able to solve the paradox of a car, which has to be light and also have increasing acoustic performance, new damping materials are demanded which have less volume

and are also lighter. In order to investigate new materials and also to make the engineering process of acoustic packages for cars more efficient, companies try to use simulation models. Precise simulation models are based on *inter alia* Biot's theory. [46, 65]

To create realistic results out of Biot's simulations, a number of parameters of the damping materials are required. [15, 16, 65] This dissertation focuses on the structural Biot parameters, Young's modulus[1] and loss factor[2]. The determination of these parameters presents certain challenges as the structure of the materials is inhomogeneous[3] and polytrophic[4]. In addition, the parameters of these viscoelastic[5] materials are easily influenced by testing procedures leading to unknown stresses.

Contrary to the complexity of the materials, today's measurement systems compress the specimens, which leads to unknown stresses. Their correctional attempts only account for a homogeneous isotropic specimen behaviour. [82, 61, 53] It is for this reason that the characterisation of structural Biot parameters of damping materials, to date, is only possible with errors.

False determination of these parameters has lead to insufficient simulation of the acoustic behaviour of damping materials resulting in insufficient simulation inside the car cabin. Therefore, increasing the use of material and engineering effort to achieve a desired acoustic performance in the passenger compartment. Furthermore, suppliers can only inaccurately link material composition and production methods to the parameters, which leads to limitations of material improvements. Quality control of damping materials through suppliers and car manufacturers can only be done imprecisely.

To measure the structural Biot parameters more precisely, a new measurement system has to be proposed which is also able to measure polytrophic and inhomogeneous materials.

[1] Describes the connection between stress and strain of a solid

[2] Describes the part of oscillation energy which is lost due to friction

[3] The matrix consisting of solid and pore structures, where there allocation can change

[4] Independence of a property from its examined direction

[5] In this case: Frequency dependence of elasticity

1.2. Overall Aim, Objectives and Demarcation of the Study

Aim of the Study

The aim of the study is to determine a new measurement system to investigate the structural Biot parameters, Young's modulus and loss factor, of damping materials used to absorb air-borne sound energy in automotive applications. It should be able to measure these parameters more precisely than the commonly used mechanical transfer function systems.

Contrary to today's measurement approaches, the investigation of Young's modulus and loss factor with the new measurement system should be applied directly without the need of correcting measurement results afterwards.

Objectives

Primary Research Objective

The primary research objective is to propose a new measurement system for structural Biot parameters of damping materials used to absorb air-borne sound energy i.e. foams and nonwoven materials.

Secondary Research Objective

In order to address the primary objective of this study, the following secondary objectives have been prepared:

1. To undertake studies of the structure and general behaviour of damping materials for air-borne sound i.e. foams and nonwoven materials.
2. To study commonly used apparatuses to measure structural Biot parameters of these damping materials.
3. To conduct research about measurement issues of commonly used measurement systems.

4. To propose a new measurement concept and formulas, which circumvents the measurement errors.

5. To set up the first steps in order to test and validate the new measurement principle in the future. I.e. to design and select hardware components and to construct a test rig for the measurement system.

Demarcation of the Study

The focus of this study is it to set up the first steps in developing a measurement system of structural Biot parameters, which is circumventing errors in existing methods. Therefore, the new measurement system will not be tested and validated in this dissertation. Furthermore, the software programming will not be covered in this dissertation.

1.3. Brief Literature Review

In the section that follows, a brief literature overview of air-borne sound damping materials as well as the determination of structural Biot parameters of damping materials is provided. The ultrasound measurements of these parameters in general will also be under discussion.

1.3.1. Damping Materials

According to Garibaldi [33], damping is described as the dissipation of vibratory energy by transformation into heat. At the same time the vibration amplitude gets reduced. Restricting the description to air-borne sound, the contemplated vibration is the vibration of air molecules. Consequently, damping materials are used to control noise, which may simply be referred to as unwanted sound.

Damping materials for air-borne sound are mostly porous viscoelastic[1] materials. They may be constructed out of mineral or vegetable fibre, by foamy materials or combina-

[1] A porous medium where the matrix is viscoelastic and the fluid within is viscous.

tions of both of them. [33, 14] Analysis by the Fraunhofer institute [31, 46] showed that a damping material used in automotive applications may be multi-layered and pressed into shape which changes its structure dramatically. It may thus be more complicated than a simple specimen made out of a single material without further treatments.

Damping materials, which can also be characterised as polytrophic and inhomogeneous, depending on the actual specimen, have been reported sensitive in measurement apparatuses leading to disregarded stresses in general. [56, 5, 88, 78]

1.3.2. Apparatuses to Determine Structural Biot Parameters of Damping Materials

In order to simulate damping material's behaviour according to Biot's theory, Biot's acoustic and structural parameters have to be determined. Biot's structural parameters are: [15, 16, 65]

- Young's modulus E,
- loss factor η, and
- Poisson's ratio ν.

Common apparatuses to determine these parameters are based on a simple mechanical transfer function system according to the old DIN 53426 [14, 40] which was cancelled or according to Garibaldi *et. al.* [33]. It may also be described as a mass spring resonance system. [33]

The assumption that the specimen behaves like a spring leads to measurement errors. [53] However, systems using the aforementioned assumptions have been used until now. Even corrected apparatuses following Sim and Kim [82], Mariez *et. al.* [61] and Langlois [53] only account for an isotropic homogeneous specimen. This assumption may be with little errors, valid for only solid materials or foams, but not for a nonwoven material which is rather inhomogeneous and polytrophic.

1.3.3. Ultrasound and its Relation to Structural Parameters

A general description without further explanation about ultrasonics to determine structural Biot parameters can be given in the book by Garibaldi *et. al.* [33]. The equations used by him however do not apply for the measurement system proposed here.

A derivation of equations on how to determine Young's modulus and loss factor out of ultrasonic measurements for elastic or viscoelastic materials in general can be given by Kuttruff *et. al.* [52], Hugh [42], Mc Skimin [64] and Achenbach. [2] However, the equations for Young's modulus do not apply for porous viscoelastic materials. These types of materials have been investigated mostly in the field of medical techniques where research investigated the Young's modulus of bones in order to get better insight into the disease, osteoporosis. In this field, the above mentioned equations have been corrected in terms of their porosity, which was investigated by Bourbie [17] and also described by Pakula *et. al.* [76], Fellah *et. al.* [29] and Lauriks. [57]

A compilation about commonly used apparatuses in medical techniques can be found in the book by Laugier *et. al.* [55]. The researchers in this field had a material to investigate, which is in a much higher Young's modulus range than the damping materials in this dissertation. Therefore, several adaptions have to be made.

1.4. Methods and Materials

As mentioned, the aim of the study is to propose a new measurement system to investigate the structural Biot parameters of air-borne sound damping materials. To achieve the research objectives of this study, a secondary and a primary study will be undertaken.

1.4.1. Secondary Study

To achieve the research objectives set out in this study, information from car manufacturers and suppliers will be gathered in respect of the apparatuses they use to determine structural Biot parameters as well as their experiences. In addition, a comprehensive literature review will be carried out identifying commonly used apparatuses as well as reported measurement issues.

Furthermore, commonly used damping materials will be gathered from suppliers in order to investigate their structure using the SEM microscope at the NMMU. This is supposed to reveal more information about the material's characteristics considering inhomogenities and polytrophic behaviour.

1.4.2. Primary Study

The primary study will focus on circumventing measurement errors reported with commonly used measurement systems. Research has been conducted for years correcting errors with commonly used mechanical transfer function systems without investigating an accurate measurement system for all types of damping materials, including inhomogeneous polytrophic materials. Hence, the new measurement approach proposed in this dissertation will be based on other principles. An overview of various approaches to investigate structural Biot parameters in general can be given by Garibaldi *et. al.* [33]. This leads to a non-contact ultrasonic approach as the most promising solution without

necessarily compressing or affecting specimens with unknown stresses during testing. As a result, the new measurement system will be based on ultrasonics.

More literature of ultrasonics relating to structural parameters will have to be reviewed. In the following fields, ultrasonics have been used to reveal structural parameters of viscoelastic materials:

- Ultrasonics replacing dynamic material analysers (DMA's) for viscoelastic materials. [42]
- Ultrasonics in medical techniques leading to structural parameters of bones, a porous viscoelastic material. [17, 76, 29, 57]

Ultrasonic measurement systems differ from used coupling techniques. Since damping materials are sensitive due to compressing a non-contact approach can only lead to sufficient measurement results. Moreso, water as a coupling fluid will not be used since it would soak the porous specimens, which would make the measurements less practical.

After measurement principles and formulas including adaptions on existing systems have been investigated, hardware will be selected to build a modulable frontend to be able to extend the measurement system if needed, should the project continue in further studies. Furthermore, it should allow programmable software to be used for measurements which will simplify future studies.

The test rig will be constructed using the software CATIA. It will restrict reflected waves inside as well as transmitted ultrasonic waves out of the test rig. Therefore, the danger of measuring reflected waves can be avoided, moreover transmitted waves of high acoustic energy might lead to the damage of ears. The aforementioned properties will require additional solutions about the material's behaviour used for the test rig, considering ultrasonic frequency range. Research articles will be acquired through the library facilities of the Nelson Mandela Metropolitan University (NMMU) and from previously gathered literature in Germany through the Ostfalia University in Wolfsburg. General unpublished information will be gathered using the internet.

1.5. Scope and Significance of the Study

Biot's theory has sufficiently been used for years simulating the acoustic behaviour of porous viscoelastic materials. [46, 65] However, it is known in the automotive industry that simulations do not have to match measured acoustic behaviour. A reason may be because of large errors reported when measuring required Biot's structural parameters of damping materials with mechanical transfer function systems. The errors arise from compressing the specimen and affecting it with unknown stresses. [82, 61, 53] Moreso, the sensitivity of simulated acoustic parameters is described, when slight variations of structural parameters are applied. [53] Correctional attempts compensating the errors and the unknown stresses in mechanical transfer function systems do not account for polytrophic, inhomogeneous and viscoelastic specimen behaviour.

The study will therefore investigate why an isotropic, homogeneous damping material characterisation can lead to measurement errors.

In addition, ultrasound in general has widely been used for non-destructive determination of structural parameters, also for viscoelastic [42] and porous viscoelastic materials. [17, 76, 29, 57] If used as non-contact ultrasound, specimens will not be compressed or affected by unknown stresses, which can be a solution for the aforementioned measurement errors. Following this, non-contact ultrasound will be investigated as a possible solution to determine the Young's modulus and loss factor of damping materials. Therefore, the study will attempt to make a valuable contribution towards the knowledge of ultrasonic determination of structural parameters of porous viscoelastic materials. This can set the start of a new measurement system investigating structural Biot parameters of damping materials. Ultimately, this may result in more efficient damping materials, which have less volume and are lighter. Moreover, engineering time may be reduced in future using simulation techniques.

As previously mentioned, the measurement system will not be tested or validated in this dissertation, which is left for future research.

1.6. Structure of the Research

The structure of the research will be as follows:

Chapter one: Introduction to the Study will introduce the research by describing a background of the subject. This introduction will include a problem statement. Thereafter, the aim of the study as well as the primary and secondary research objectives will be described. A brief literature review comprising of the methods and materials that will be used are highlighted. In addition, the scope and significance of the study will be presented. The chapter will be concluded with an overview of the structure of the study that will follow.

Chapter two: Fundamentals of the Study will summarize Biot's theory as well the acoustic Biot parameters. Thereafter, the structural Biot parameters will be described in more detail as well as their relations to each other. The functionality, along with the complexity of damping materials and final damping products in automotive applications will be discussed. Furthermore, their structure will be investigated using an SEM microscope in respect of inhomogenity and polytrophic behaviour.

Chapter three: Current Measurement Techniques to Characterise Young's Modulus and Loss factor will focus on currently used measurement techniques to characterise Young's modulus and loss factor. The well documented errors, that are made by assuming the specimens behaviour to be spring like, will be documented as well as the correctional attempts trying to compensate these issues. The chapter will end with a conclusion highlighting the limitations of these correctional attempts and also point out the sensitivity of simulated acoustic parameters when structural parameters are slightly varied.

Chapter four: Theory of a New Measurement System to Evaluate Structural Biot Parameters will build on chapter three, where mechanical transfer function systems have been described as insufficient to determine structural parameters of damping materials. It describes the reasons why ultrasonics may lead to a better parameter es-

timation. Furthermore, the theory linking ultrasonic wave propagation and structural material parameters is described.

Chapter five: Evaluation of Parameters to Investigate Structural Parameters will describe well known approaches to determine ultrasonic parameters leading to Young's modulus and loss factor. Limitations of these approaches will be highlighted. This will lead to necessary adaptions and proposed new solutions in determining ultrasonic parameters.

Chapter six: Investigations of the Test Rig will deal with the necessary calculations in order to transfer the theoretical background described in chapter five into a test rig. The test rig will be able to test the described approaches in chapter five. The chapter will include predictions about inner sound speed velocity inside the specimens and investigations about the most suitable coupling fluids. Materials of the test rig will be selected in order to convert the use of known free field measurement techniques in acoustics into the ultrasonic frequency range.

Chapter seven: Measurement Hardware will present the functionality of ultrasonic hardware and a selection of sufficient components. The functionality and implementation of acoustic antennas will be presented, as it is required for a measurement approach proposed in chapter five.

Chapter eight: Construction of the Test Rig will provide the construction of the test rig. It will cover how the idea of free field measurement techniques is combined with the measurement approaches described in chapter five. All measurement approaches will be able to be tested with the measurement chamber shown in this chapter.

Chapter nine: Summary will be the final chapter of the study and will summarize the contents of the preceding eight chapters. The main findings will be highlighted and the contributions and limitations of the study will be presented. In conclusion recommendations and suggestions for future research will be discussed.

2 Fundamentals of the Study

2.1. Introduction

The following chapter describes the fundamentals of the study. The Biot model is presented, as it is widely used to simulate the acoustic behaviour of porous materials. The acoustic Biot parameters are briefly presented and in more detail, the structural Biot parameters i.e. Young's modulus, loss factor and their relation to each other. In addition to that, the term and the functionality of damping materials as well as damping products in general are presented. Their structure and complexity will be further investigated using an SEM microscope.

2.2. Biot's Theory for Porous Absorbing Materials

The following section summarizes Biot's theory for porous absorbing materials based mainly on the book by F.P. Mechel. [65] Maurice Biot introduced his theory in 1956 [15, 16] while he was working as an independent consultant for an oil company. There, he researched the properties of porous rocks and water filled porous cloyey soils. [22] His theory describes in general the wave propagation of fluid[1] filled porous materials. Since then, his study has had several applications including the description of sound propagation in porous media. The application of his theory in acoustics can lead to

[1] Which can be a liquid or a gas. Contrary to a solid it can be described as a substance without a fixed shape. It deforms itself when a shear force is applied.

a better understanding in designing porous damping materials as sound absorbers. Furthermore, it can be part of simulation models of sound damped chambers as they occur inside of cars. Calculations taken out by the Fraunhofer institute showed that a prediction of the sound absorption coefficient of a multi layered damping material using a Biot model are close to measured values. The Fraunhofer institute's study revealed that the Biot model is more exact in the lower frequency range than other models used to predict sound absorption coefficients by Delany-Bazley or Allard-Johnson as can be seen in Figure 2.1. [46]

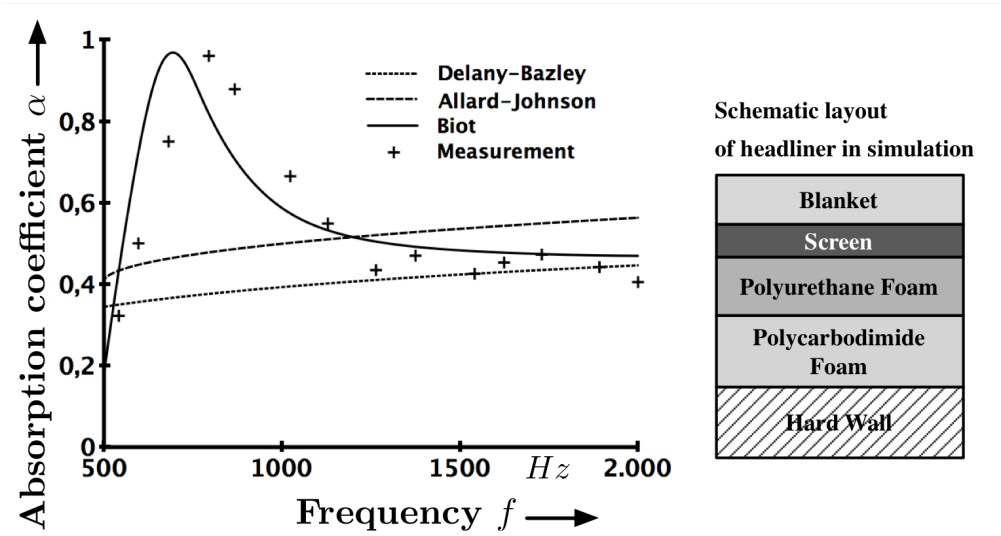

Figure 2.1.: Measured absorption coefficient of a headliner in comparison with different simulation models [46]

An important result of Biot's theory is the statement that two longitudinal waves can travel in a porous fluid filled medium at different velocities when the material is excited with a sound wave. In addition to that, a shear wave occurs. The fast longitudinal wave is influenced by the movement when the fluid and the solid is moving in phase. Conversely, the slow wave describes the relative motion between the fluid and the matrix. Ultimately the slow longitudinal wave has a larger decrease in amplitude when travelling through the material. The shear wave propagates mostly through the matrix through shear stress.

The following assumptions are made for the material as described by Biot's theory:

- The matrix is homogeneous and isotropic and there is a continuous connection between pores and the fluid phase. (Closed pored materials reveal an almost nonporous solid behaviour).
- The pore size is small in relation to the volume of the material and also small in relation to the wavelength.

For the motion equations $\bar{u}_s$ ($s = solid$) is the displacement of a single finite volume element dV. $\bar{u}_f$ is the displacement of the fluid ($f = fluid$). Biot postulates two motion equations. The left part of the equations describes accelerating forces for the fluid and solid phase. This part of the equation is expanded by the inertia forces which overcouple. [49] The motion equation for the solid is defined to be:

$$\overbrace{\rho_{11}\frac{\partial^2 \bar{u}_s}{\partial t^2} + \rho_{12}\frac{\partial^2 \bar{u}_f}{\partial t^2}}^{\text{Accelerating and inertia force}} = \underbrace{P \cdot grad\, div\, \bar{u}_s}_{\text{Compression force}} + \underbrace{Q \cdot grad\, div\, \bar{u}_f}_{\text{Coupling force}} - \underbrace{N_s \cdot rot\ rot\, \bar{u}_s}_{\text{Shear force}} + \underbrace{bF(\omega) \cdot \left(\frac{\partial \bar{u}_f}{\partial t} - \frac{\partial \bar{u}_s}{\partial t}\right)}_{\text{Viscous forces}} \tag{2.1}$$

On the right side of the equation, is the compression force of the solid and the next term is the coupling force between the solid and the fluid. The following subtrahend represents the shear force in the solid. The last term of the equation stands for the description of the frequency dependent viscous forces between fluid and solid. The equation for the fluid is described as:

$$\overbrace{\rho_{22}\frac{\partial^2 \bar{u}_f}{\partial t^2} + \rho_{12}\frac{\partial^2 \bar{u}_s}{\partial t^2}}^{\text{Accelerating and inertia force}} = \underbrace{R \cdot grad\, div\, \bar{u}_f}_{\text{Compression force}} + \underbrace{Q \cdot grad\, div\, \bar{u}_s}_{\text{Coupling force}} - \underbrace{bF(\omega) \cdot \left(\frac{\partial \bar{u}_f}{\partial t} - \frac{\partial \bar{u}_s}{\partial t}\right)}_{\text{Viscous forces}} \tag{2.2}$$

The density terms are defined to be:

$$\rho_{11} = (1 - f_v)\rho_s\rho_{12} \tag{2.3}$$

$$\rho_{22} = f_v\rho_f - \rho_{12} \tag{2.4}$$

$$\rho_{12} = -(\chi - 1)f_v\rho_f \tag{2.5}$$

The term $bF(\omega)$ in equations (2.1) and (2.2) is a viscous coupling factor which can be determined through the flow resistivity Ξ. A simplified equation was developed by Johnson *et. al.* [50] which differs only in small percentages from other equations developed by Biot:

$$bF(\omega) = f_v^2\Xi\sqrt{1 + \frac{4j\chi^2 d_v\rho_f\omega}{\Xi^2\Lambda^2 f_v^2}} \tag{2.6}$$

and:

$$\Lambda = a\sqrt{\frac{8d_v\chi}{\Xi f_v}} \tag{2.7}$$

The parameter a is an adjustment factor accounting for the cross sectional shape of the pores which cannot be analytically determined for real porous materials. It is nearly 1 and can be approximated by precalculated values depending on the shape of the pores which can be found in. [23] Biot introduced elastic constants in his equations (2.1), (2.2), namely P, Q and R. Thought experiments revealed equations which can be solved to determine P, Q, R through the measurable terms N, K_b, K_s and K_f. The bulk modulus of the material, where the absorber is made out of is denoted as K_s. In most sound absorbing materials, it is much higher than the bulk modulus of the actual specimen K_b and also higher than the bulk modulus of the fluid K_f, therefore:

$$K_s \gg K_b \qquad \text{and} \qquad K_s \gg K_f \tag{2.8}$$

With that assumption, the equations solving P, Q and R can be simplified to:

$$P = K_b + \frac{4}{3}N + \frac{(1 - f_v)^2}{f_v}K_f \tag{2.9}$$

$$Q = (1 - f_v)K_f \tag{2.10}$$

$$R = f_v \cdot K_f \tag{2.11}$$

With:

a	=	Composite pore shape factor	1
$bF(\omega)$	=	Viscous coupling factor	1
d_v	=	Dynamic viscosity	$^{N\cdot s}/_{m^2}$
f_v	=	Porosity	1
K_b	=	Bulk modulus of specimen	Pa
K_f	=	Bulk modulus of fluid	Pa
K_s	=	Bulk modulus of solid	Pa
N	=	Shear modulus	Pa
N_s	=	Shear modulus of solid	Pa
P	=	Elastic constant of solid	Pa
Q	=	Potential coupling	1
R	=	Elastic constant of fluid	Pa
t	=	Time	s
$\bar{u}_s$	=	Average displacement of solid	m
$\bar{u}_f$	=	Average displacement of fluid	m
χ	=	Tortuosity	1
Λ	=	Viscous characteristic length	m
ω	=	Angular frequency	$^{rad}/_{s}$
ρ_{ij}	=	Density terms of solid and fluid	$^{kg}/_{m^3}$
ρ_{12}	=	Describes mass coupling between fluid and solid	$^{kg}/_{m^3}$
ρ_s	=	Density of solid	$^{kg}/_{m^3}$
ρ_f	=	Density of fluid	$^{kg}/_{m^3}$
Ξ	=	Flow resistivity	$^{Pa\cdot s}/_{m^2}$

2.2.1. Acoustic Biot Parameters

This subsection describes the acoustic parameters that are required to conduct calculations using the Biot model. For detailed description of the measurements, further literature is referenced. The acoustic Biot parameters which have to be determined in order to conduct Biot's calculations are:

f_v	=	Porosity	1
χ	=	Tortuosity	1
Λ, Λ'	=	Viscous or Thermal characteristic length	m
Ξ	=	Flow resistivity	$Pa{\cdot}s/m^2$

The **Porosity** f_v includes information about the volumetric ratio of solid and pores in the absorbing material. It is defined to be the density ratio of the specimen to the density of the elastic solid (the raw material the absorber is made out of):

$$f_v = 1 - \frac{\rho_b}{\rho_s} \tag{2.12}$$

For porous absorbers, the porosity is usually in the range of $0,9 - 0,99$. When the density of the elastic solid is known, its calculation is straightforward. It can also be determined by the apparatus described by Champoux *et. al.* [20]. However, this method requires the absorber itself not to be compressed in a chamber where the pressure gets increased, which is the main limitation for porous absorbing materials.

The **Tortuosity** χ is an expression of the complexity of the labyrinthine construct of the porous material. The connection of pores and the influences of pores sizes on barrier effects are described by this parameter. [32]

Following Allard *et. al.* [3] the tortuosity can be calculated measuring the radii and length of porous structures. However, this approach is too time consuming for acoustic materials. Another method investigated by Brown [18] measures the tortuosity with an alternating voltage field and the ratio of the resistances of the specimen and an electric

liquid.

$$\chi = f_v \frac{\Omega_b}{\Omega_f} \tag{2.13}$$

Another possibility of measuring the tortuosity of a porous material after Allard *et. al.* [4] and Leclaire *et. al.* [58] is the use of ultrasonics and the ratio of phase velocity in a fluid to the phase velocity inside the specimen:

$$\chi = \left(\frac{c_{lf}}{c_{lb}(\omega)} \right)^2 \tag{2.14}$$

Viscous friction occurs in lower frequencies and leads to a strong decrease in pressure amplitude. In the high frequency range it can be neglected. To estimate the border between the high and low frequency model, the **Characteristic length** Λ Λ' is calculated.

Following Johnson *et. al.* [50], the **Viscous characteristic length** Λ can be calculated with:

$$\Lambda = 2 \frac{\int_{V_p} v^2 \, dV_p}{\int_{A_p} v^2 \, dA_p} \tag{2.15}$$

The viscous characteristic length gets significantly influenced through narrows between pores or smallest pore sizes because it leads to the highest friction of the fluid when it flows through the solid.

With the **Thermal characteristic length** Λ', the interaction between the solid and fluid through thermal energy exchange in the pores is considered. Following Champoux and Allard [19], it is defined as:

$$\Lambda' = 2 \frac{\int_{V_p} dV_p}{\int_{A_p} dA_p} \tag{2.16}$$

The **Flow resistivity** Ξ can be measured with a tube where the specimen is inserted. On one side of the tube, an airflow through the specimen is applied. Using the pressure decrease from one side of the specimen to the another and the measurement of the air flow velocity, the flow resistivity can be measured with: [14]

$$\Xi = \frac{\Delta p}{v \cdot l} \tag{2.17}$$

With:

A_p	=	Pore surface	m^2
$c_{lb}(\omega)$	=	Longitudinal phase velocity in specimen	$^m/_s$
c_{lf}	=	Sound velocity in fluid	$^m/_s$
f_v	=	Porosity	1
l	=	Thickness of specimen	m
v	=	Flow velocity of fluid	$^m/_s$
V_p	=	Pore volume	m^3
χ	=	Tortuosity	1
Δp	=	Pressure difference before and after specimen	Pa
Λ, Λ'	=	Viscous or thermal characteristic length	m
Ω_b	=	Electric resistance with specimen inserted	Ω
Ω_f	=	Electric resistance of only fluid	Ω
ρ_b	=	Density of the specimen	$^{kg}/_{m^3}$
ρ_s	=	Density of the elastic solid	$^{kg}/_{m^3}$
Ξ	=	Flow resistivity	$^{Pa \cdot s}/_{m^2}$

2.2.2. Structural Parameters

The chapter describes structural Biot parameters, which are:

E	=	Young's modulus	Pa
η	=	Loss factor	1
ν	=	Poisson's ratio	1

as well as their relation to each other including other moduli. Current measurement apparatuses to measure Young's modulus E and loss factor η can be found in chapter 3. Measurement systems in Section 3.4 also account for the Poisson's ratio ν. The principles of a new measurement apparatus which circumvents problems with existing systems is carried out in Chapters 4-8.

Elasticity and Elastic Moduli

Every solid material counteracts a deformation with resistance. The force which has to be applied from outside to cause deformation is proportional to it. This coherence is called the elastic displacement. A material is referred to as elastic when the energy, which is applied from the force outside gets saved reversibly as displacement energy. In an ideal case, this behaviour is linear. Hooke's law describes the behaviour between the outside force F and the displacement x with a stiffness factor k as:

$$F = k \cdot x \qquad \text{(Hooke's law)} \tag{2.18}$$

E is the **Young's modulus** and describes the resistance of a material against an elastic displacement. Using Hooke's law to describe the behaviour of stress σ and strain ϵ gives:

$$\sigma = \epsilon \cdot E \tag{2.19}$$

Where:

$$\epsilon = \frac{\Delta l}{l} \qquad \text{(Change in length as a fraction of total length)} \tag{2.20}$$

And:

$$\sigma = \frac{F}{A} \qquad \text{(Outside force applied on the front face of a specimen)} \tag{2.21}$$

If a cylindrical solid gets deformed by stress through an outside force, it will not only undergo an axial displacement. Moreso, the specimen diameter will change, as can be seen in Figure 2.2. The ratio between elastic longitudinal to elastic transversal strain is denoted as the **Poisson's ratio** ν as:

$$\nu = -\frac{\frac{\Delta d}{d}}{\frac{\Delta l}{l}} \tag{2.22}$$

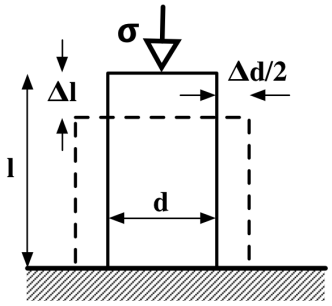

Figure 2.2.: Geometric visualization of displacement of a cylindrical solid under principal stress

If a specimen is surrounded by rigid walls so that only longitudinal displacement Δl is possible, which causes longitudinal strain but no shear strain ϵ, the following relations hold for the longitudinal modulus L. For visualization see Figure 2.3:

$$\sigma = \epsilon \cdot L \tag{2.23}$$

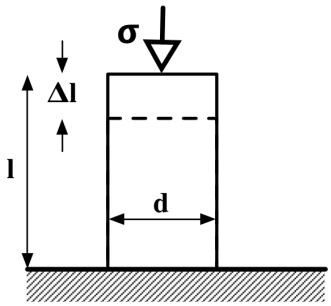

Figure 2.3.: Geometric visualization of displacement of a cylindrical solid under principal stress without shear strain

The shear modulus N is defined as the ratio of shear stress τ and shear strain γ, refer to Figure 2.4, as:

$$\tau = \gamma \cdot N \tag{2.24}$$

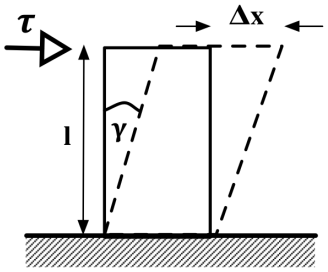

Figure 2.4.: Geometric visualization of displacement of a cylindrical solid under shear stress

The bulk modulus K measures its resistance to uniform compression through a pressure p with:

$$K = -p \cdot \frac{V_b}{\Delta V_b} \tag{2.25}$$

Figure 2.5 shows this behaviour.

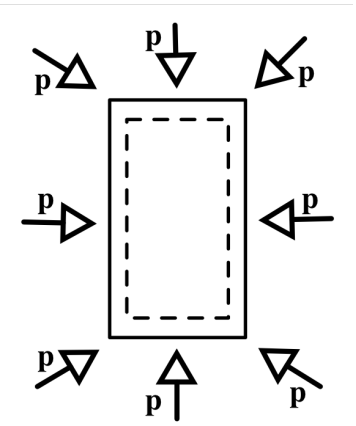

Figure 2.5.: Geometric visualization of displacement of a cylindrical solid under all-round pressure

The moduli are interdependent and can be converted into each other using the following equations [55, 51, 79]:

$$K = E\frac{1}{3(1-2\nu)} \tag{2.26}$$

$$L = E\frac{1-\nu}{(1+\nu)(1-2\nu)} = K + \frac{4}{3}N \tag{2.27}$$

$$N = E\frac{1}{2(1+\nu)} \tag{2.28}$$

Viscoelasticity and Loss Factor

A viscoelastic material is the intermediate between a pure elastic material and a viscous one. The deformation of viscoelastic materials occurs with a time lag. The deformation does not disappear directly after the removal of the load. [30] This can also be observed with porous viscoelastic materials.

Viscoelasticity in materials leads to energy dissipation, as opposed to elasticity where all the input energy gets released. Energy dissipation occurs where the stress-strain curve is different from loading to unloading. This phenomenon is described in Figure 2.6. Here, three regions can be identified according to Gibson [34]:

- Region 1: The linear bending region, in which foam cells bend and stretch. It is limited to small strains. (The elastic parameters can be measured in this region.)
- Region 2: The buckling region, where stress increases slowly with strain due to buckling of foam cells.
- Region 3: The densification region. The cells collapse completely and the foam behaves like a solid.

The area between the curve for loading and unloading is the energy that gets dissipated.

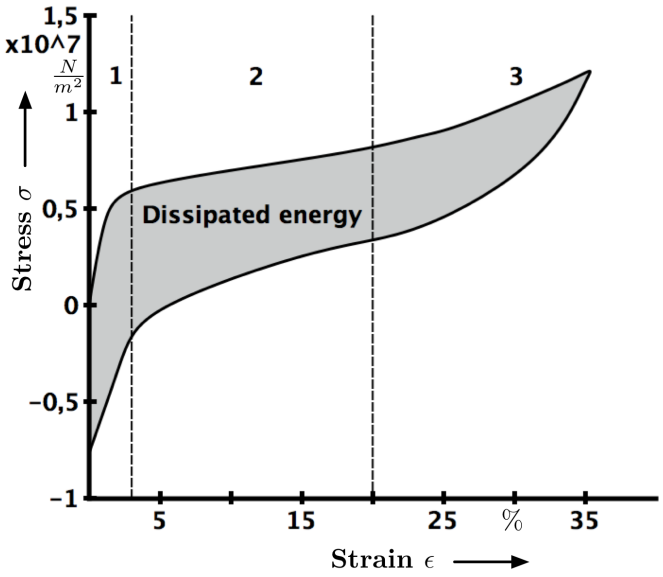

Figure 2.6.: Loading-unloading cycle (hysteresis) of stress-strain curve of melamine foam [34]

Normally, viscoelastic materials are represented as a combination of a spring (elastic) with a dashpot (viscous) model. For these materials, the Young's modulus is complex E^* and can be split up into the real (elastic) E' and imaginary parts (viscous) iE'' of the complex modulus. Taking into account periodic loadings as they are applied in measurement techniques in chapter 4, these moduli are frequency dependent.

$$E^* = E'(\omega) + jE''(\omega) \tag{2.29}$$

$E'(\omega)$ is the storage or dynamic modulus which describes the part of energy which can be converted without losses. $jE''(\omega)$ is the loss module. It describes the part of mechanical energy which gets converted into heat. Figure 2.7 shows the Argand diagram of the Young's modulus for viscoelastic behaviour.

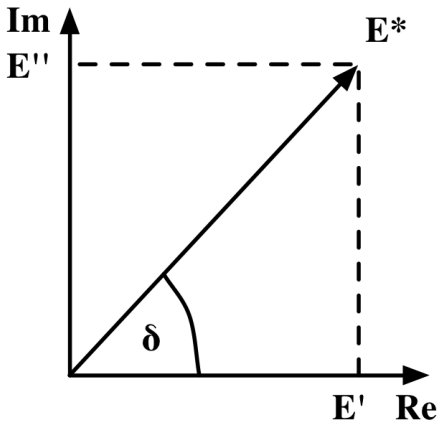

Figure 2.7.: Argand diagram of Young's modulus for viscoelastic behaviour

The tangent of angle δ is the **loss factor** η which is defined to be the ratio of the energy dissipated per cycle to the maximum potential energy stored in a cycle.

$$\tan\delta(\omega) = \eta(\omega) = \frac{E''(\omega)}{E'(\omega)} \tag{2.30}$$

With:

A	=	Surface, perpendicular to applied force	m^2
E	=	Young's modulus	Pa
E'	=	Dynamic Young's modulus	Pa
E''	=	Loss Young's modulus	Pa
E^*	=	Complex Young's modulus	Pa
F	=	Force	N
k	=	Stiffness factor	N/m
K	=	Bulk modulus	Pa
L	=	Longitudinal modulus	Pa
N	=	Shear modulus	Pa
p	=	Pressure	Pa
x	=	General displacement	m
δ	=	Phase shift	rad
$\Delta d, d$	=	Change in diameter, diameter of specimen	m
$\Delta l, l$	=	Change in length, length of specimen	m
$\Delta V_b, V_b$	=	Change in Volume of specimen, Volume of specimen	m^3
ϵ	=	Strain	1
η	=	Loss factor	1
γ	=	Shear strain	N/m^2
ν	=	Poisson's ratio	1
σ	=	Stress	N/m^2
τ	=	Shear stress	N/m^2

2.3. Damping Materials

In the case of automotive applications, several acoustic sources produce noise, which is classified as unwanted sound. These sound sources reach a receiver which, in this dissertation can be persons inside the car cabin, through a transfer path, as described in Figure 2.8.

Figure 2.8.: Noise travelling through a path and reaches a receiver

The system consists of multiple paths and sources. The paths can consist of solid and fluid phases. When noise has to be controlled through the transfer path, several damping materials exist for each path type. Following Garibaldi *et. al.* [33] damping can be described as the dissipation of vibratory energy when it gets transformed into heat. This reduces the vibrational amplitude. In this dissertation, the description is limited to damping materials influencing the fluid path and therefore reducing the vibrational amplitude of air atoms leading to a dissipation of acoustic energy. This origin of sound is also called air-borne sound.

When a sound wave crosses a damping material, the conversion into heat energy is done due to friction because of the relative motion of air molecules and the surfaces of the damping material. This friction counteracts the air flow and therefore dissipates a high portion of sound energy. [33]

The highly porous structure of nonwoven materials consists of fibres which can be made out of cotton or for example, polyethylene terephthalate (PET). Moreover, different bounding techniques or hybrid, multi layer materials combining foams and nonwoven materials exists. Foams such as polyurethane (PU) or melamine foams have a cell structure. An example of damping materials is given in Figure 2.9.

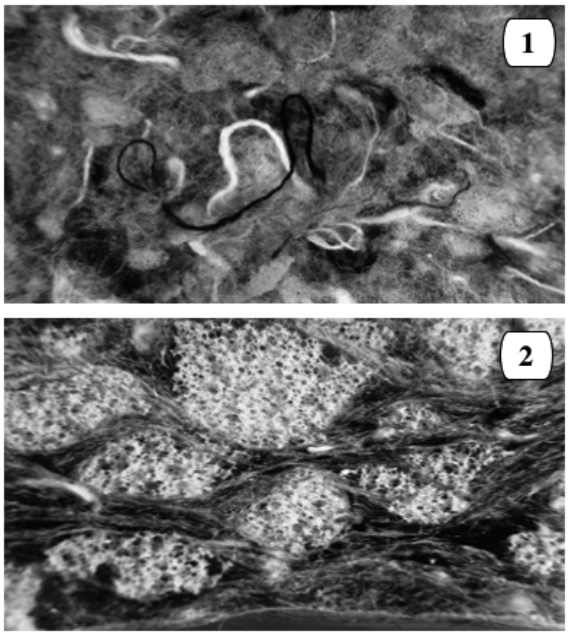

1 : *Thermoplastic bounded nonwoven fabric*
2 : *Thermoplastic bounded cotton nonwoven fabric with PU foam flakes*

Figure 2.9.: Example, damping materials used in automotive applications [14]

Foams can have open or closed pores, which have different advantages. Open porous materials have better absorbing properties, however when the transmission of sound waves have to be restricted, closed pored materials are more advantageous. [69] It has to be noted that Biot's theory cannot be applied to closed pored materials since a requirement is the interconnection of pores. [65] It has also been reported that closed pored materials tend to behave like a solid.

Foams and nonwovens can be divided into two phases:

- solid phase or matrix, and
- fluid phase.

The Figure 2.10 shows the scanning electron microscope (SEM) picture of the melamine foam (BASF Basotect®V with the two phases. The foams matrix appears in white.

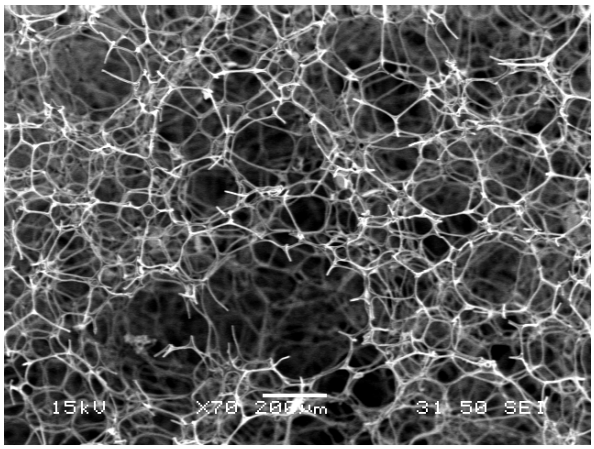

Figure 2.10.: Scanning microscope picture: BASF Basotect®V Melamine foam

2.3.1. Complexity of Damping Materials

Damping materials are highly complex, thus the characterization of their parameters can be difficult because these materials are:

- porous-viscoelastic,
- polytrophic, and
- inhomogeneous.

Several specimens, PU- and melamine foams as well as PET nonwoven materials, have been investigated using the SEM at the NMMU (JEOL JSM-6380) which is displayed in Figure 2.11.

Figure 2.11.: JEOL SEM Microscope JSM-6380

In order to test the nonconductive samples with this technique, specimens were gold coated after they have been attached to specimen holders using double-sided and conductive adhesive tapes. Additional tapes have been placed at the sample sides to increase conductivity, as shown in Figure 2.12.

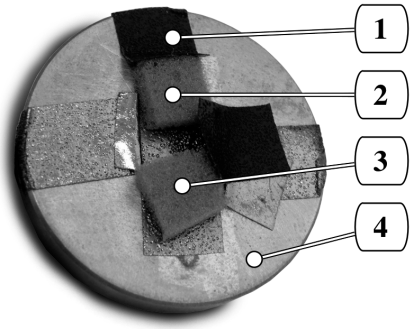

1 : *Conductive adhesive tape*
2 : *Specimen front facing side*
3 : *Specimen side facing side*
4 : *Specimen holder*

Figure 2.12.: Specimen holder with specimen (BASF Basotect®V Melamine foam) gold coated for SEM investigation

Large differences in the general structure, depending on the material, have been investigated and can be seen in Figure 2.13. It can be observed, that foams i.e. Melamine and PU foams may be characterised as almost homogeneous and isotropic contrary

to nonwoven materials. These have to be polytrophic since their structure depends dramatically on the side which is front facing. They are also much more inconsistent in their general structure when considering the front facing side. Other side views from PU and Melamine foams are not presented in Figure 2.13 since they are equal. Other sample comparisons are not presented here, since these observations could be noticed with every sample combination.

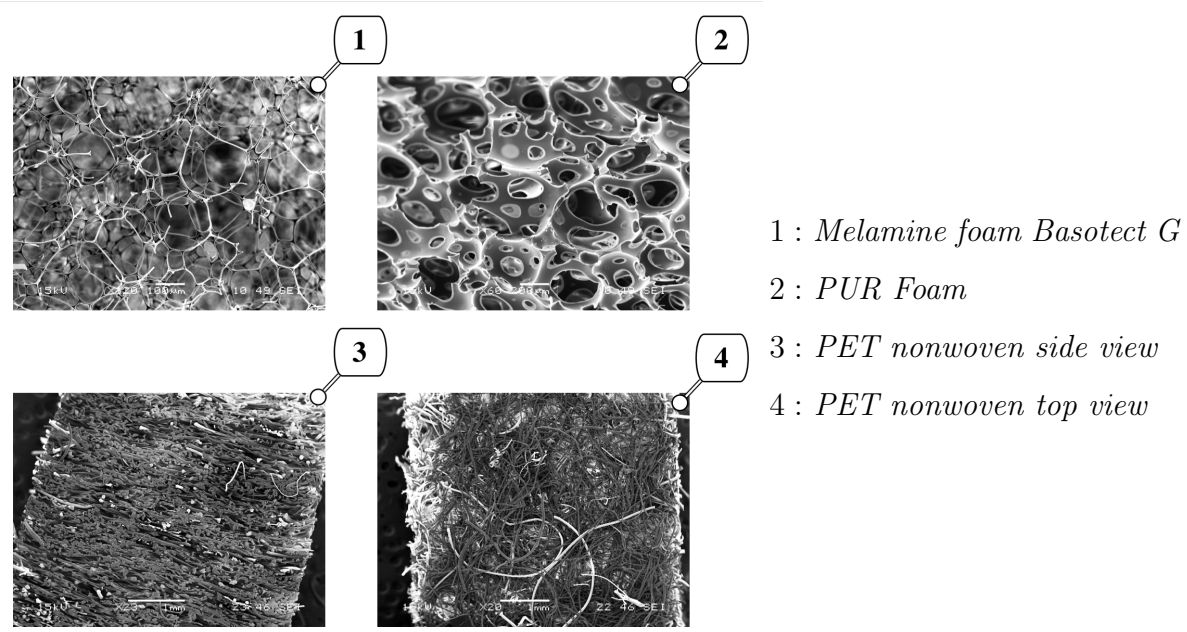

Figure 2.13.: SEM Pictures of different foam and nonwoven materials

Adding to the complexity of damping materials, they are low cost products. That implies that their behaviour measured on one end of a large manufactured product does not need to have the same specifications than on the other end. This differs with different production techniques.

When these materials are bent or pressed into the shape which they are supposed to have for automotive applications, their structure can change dramatically. The Figure 2.14, taken by the Fraunhofer institute [31] shows a nonwoven material which forms the headliner of a car. On several characteristic spots, specimens have been taken out and investigated with a computer tomograph as it can be seen in Figure 2.15.

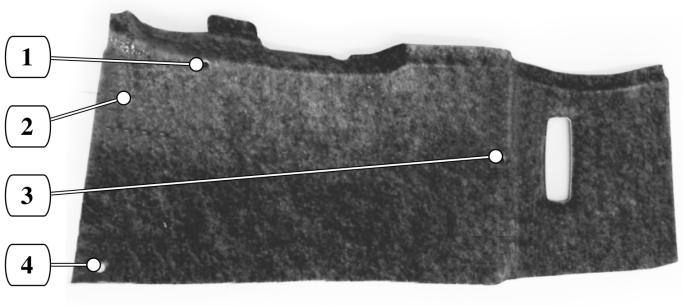

Figure 2.14.: Nonwoven material used as a car headliner [31]

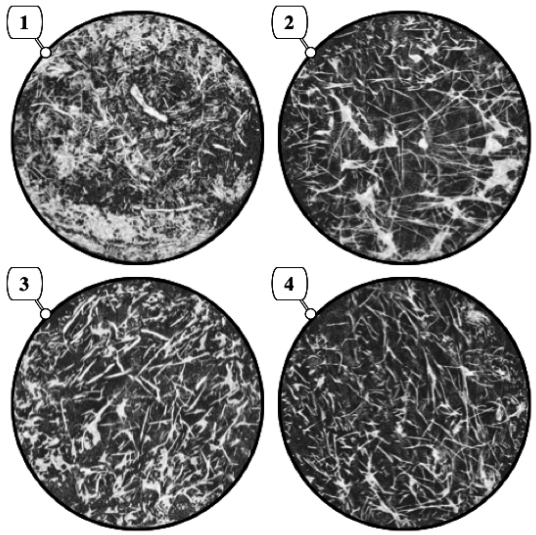

1 : *Edge 1 (highly pressed)*

2 : *Bended zone*

3 : *Edge 2 (moderately pressed)*

4 : *Plain zone*

Figure 2.15.: Computer tomographic pictures: Headliner specimens [31]

It can clearly be seen that the matrix of the nonwoven material changes due to compressing or bending and therefore, the value of the parameters of the material have to change.

The sensitivity of foams and nonwoven materials also affects the Kundt tube measurement which is commonly used to investigate the sound absorption coefficient and other parameters[1] of these materials. Articles exist about the accuracy measuring the acoustic impedance of porous viscoelastic materials with this technique. [56, 5, 88]

[1]Such as: the reflection coefficient, acoustic impedance and admittance, transmission loss

Comparisons of the acoustic impedance between free field measurements have been made and shown that only free field measurements give valid results. The authors claim, the reason for this is because the specimens get compressed and lie directly at the tube walls, which causes friction. [78] In Figure 2.16, it is shown how the specimen is inserted into the Kundt tube and that it gets compressed between the tube walls.

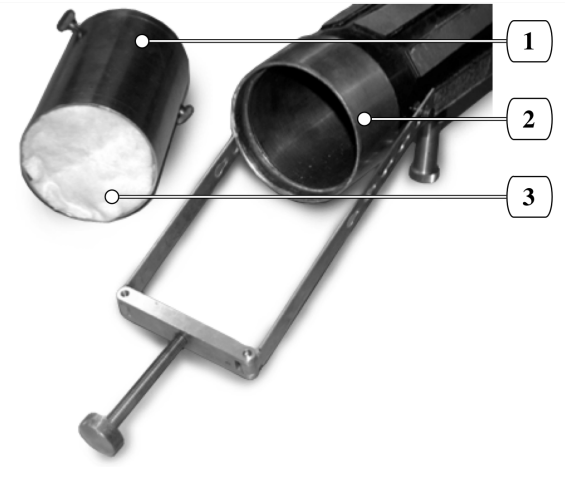

1 : *Kundt tube*

2 : *Specimen holder*

3 : *Specimen*

Figure 2.16.: Specimen compressed in specimen holder of Kundt tube which causes friction between the specimen and the tube walls [67]

From above observations, it is therefore understandable that a correct measurement system to investigate the Young's modulus and loss factor of foams and nonwoven materials should not compress the material's structure and also should not neglect boundary conditions. Furthermore, it should not consider the specimen as isotropic and homogeneous when nonwoven materials are measured.

It has to be noted that parts used for damping purposes in automotive applications may consist of different layers of materials. In order to achieve exact results using Biot's theory, the Fraunhofer institute investigated every layer separately. [46]

2.4. Summary

The aim of this chapter was to explain the Biot model and this chapter also clarified why it is considered sufficient to deliver exact acoustic simulations of open porous viscoelastic damping materials. In order to conduct Biot's calculations, several Biot parameters have to be investigated. The acoustic, as well as the structural parameters have been presented here.

Furthermore, damping materials were explained since they are used to absorb acoustic sound energy. Following microscopic investigations, foams may be characterised as almost homogeneous and isotropic whereas nonwoven materials have larger inhomogenities and are a polytrophic materials. Their structure can change in automotive applications, which must lead to a change in parameters. They have been reported to react sensitively in an other measurement apparatuses, the Kundt tube, in case of compression which changes their structure and therefore their parameters. It was also discussed that friction leading to unknown stresses can cause measurement errors in the Kundt tube.

3 Current Measurement Techniques to Characterise Young's Modulus and Loss Factor

3.1. Introduction

This chapter describes the measurement techniques to determine Young's modulus and loss factor as well as their advantages and disadvantages. A description about measurement issues and attempts to improve them are described in Section 3.4. There are different types of techniques to characterise the Young's modulus and loss factor of damping materials. However, based on research of leading companies in the automotive industry and their suppliers, only the following measurement techniques are considered to be applicable for foams and nonwoven materials:

- Harmonic forced resonance methods, also called dynamic stiffness resonance methods.
- Harmonic forced nonresonance methods also called dynamic stiffness nonresonance methods. [33]

3.2. Harmonic Forced Resonance Methods

This section describes the harmonic forced resonance methods used to evaluate the Young's modulus and loss factor.

The harmonic forced resonance method was also known under the German standard DIN 53426. [14, 40] This standard has been cancelled. All other methods are based on this mechanical transfer function system. It is also known as the mass-spring resonance technique. [33] A description can be seen in Figure 3.1.:

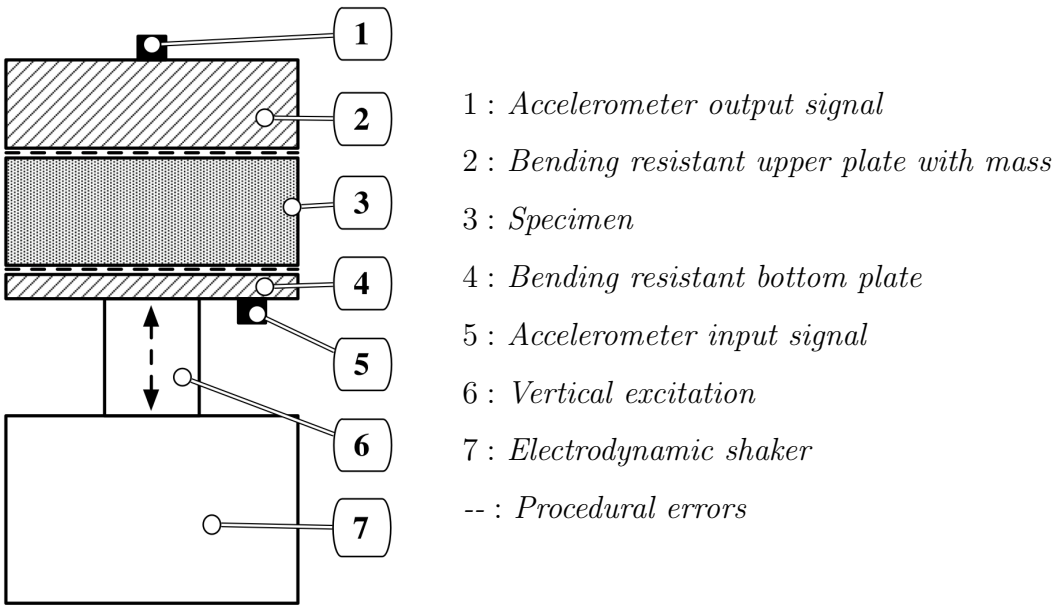

Figure 3.1.: Vibration-test standard: DIN 53426 [14]

The functionality is as follows:

- The specimen is excited by an electromagnetic shaker, which is powered by a continuous sine-sweep oscillator.
- The accelerometer at the bottom plate measures the response of the shaker head.
- The accelerometer at the upper plate measures the response of the specimen.

By shifting the mass of the upper plate, this system can measure the parameters at

different frequencies. The limit frequency is approximately below 1000 Hz [11], however other aspects such as the preload through the upper mass also have to be considered.

The equation to calculate the loss factor can be derived from a single degree of freedom model. The equation of motion for the apparatus in Figure 3.1 is then [82]:

$$m\ddot{\tilde{x}}_2 + (A_b/l)E'(1+j\eta)(\tilde{x}_2 - \tilde{x}_1) = 0 \tag{3.1}$$

With:

$$\tilde{x}_1 = X_1 e^{j\omega t} \qquad \tilde{x}_2 = X_2 e^{j\omega t} \tag{3.2}$$

Here A is the cross sectional area of the specimen and l is the specimen thickness. The complex amplitudes for $\tilde{x}_1$ and $\tilde{x}_2$ are X_1 and X_2. Building the transfer function from equation (3.1) gives:

$$\frac{X_2}{X_1} = \frac{E' + jE'\eta}{(E' - \omega^2 ml/A) + jE'\eta} \tag{3.3}$$

This formula can be written as a combination of its real part Re and imaginary part Im:

$$Re = E'\frac{E'(1+\eta^2) - \omega^2 ml/A_b}{D} \qquad Im = \frac{-\omega m(l/A)E'\eta}{D} \tag{3.4}$$

Where D is defined to be:

$$D = (E' - \omega^2 ml/A)^2 + (E'\eta)^2 \tag{3.5}$$

The ratio B of Im to Re is:

$$B \equiv \frac{Im}{Re} = -\frac{\omega^2 m(l/A)E'\eta}{E'(1+\eta^2) - \omega^2 ml/A} \tag{3.6}$$

Writing E as terms of η and B gives:

$$E' = \frac{\omega^2 m(l/A)(B-\eta)}{B(1-\eta^2)} \tag{3.7}$$

For the ideal resonance without damping where $B = 1$ and $\tan(\delta) = \eta = 0$ equation (3.7) can be simplified to the equation used by major car manufacturers and suppliers:

$$E' = \frac{f_r^2 \cdot 4 \cdot \pi \cdot m \cdot l}{b^2} \tag{3.8}$$

The loss factor is derived by the proportional bandwidth Δf which takes into account the broadening of the resonance peak. This broadening is usually normalized in terms of the resonance frequency f_r. Δf is the span between two half power point frequencies ($-3\,dB$) one above and one below the resonance frequency f_r. [33] As shown in Figure 3.2.

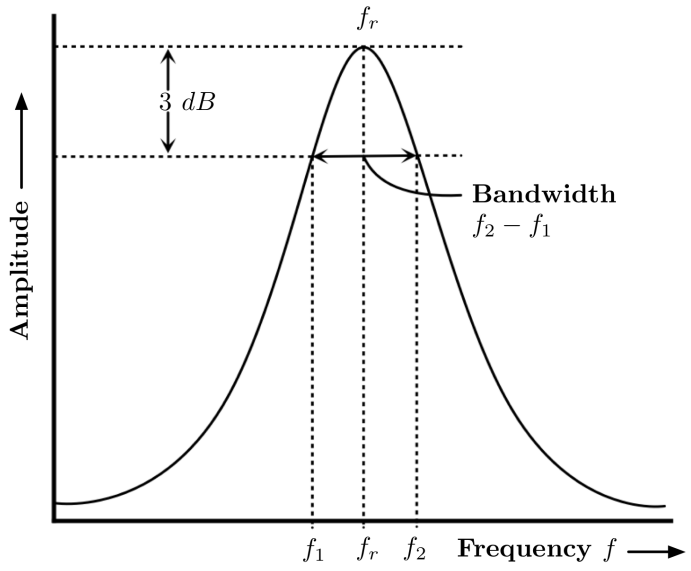

Figure 3.2.: Determination of loss factor by half power bandwidth

The equation for determining loss factor by half power bandwidth is:

$$\eta = \frac{\Delta f}{f_r} \tag{3.9}$$

Or with the following equation using the accelerations on the specimen $\ddot{\tilde{x}}_2$ and the acceleration of the exciter $\ddot{\tilde{x}}_1$ [33]:

$$\eta = \frac{1}{\sqrt{(\ddot{\tilde{x}}_2/\ddot{\tilde{x}}_1)^2 - 1}} \tag{3.10}$$

With:

A	=	Surface perpendicular of applied force	m^2
B	=	Ratio of imaginary to real part	1
b	=	Width of specimen	m
E'	=	Dynamic modulus	Pa
f_r	=	Resonant frequency	Hz
l	=	Thickness of specimen	m
m	=	Mass of specimen and upper plate with additional mass	kg
$\tilde{x}_{1,2}$	=	Displacements for accelerometer 1,2	m
X_1, X_2	=	Complex amplitudes for accelerometer	m
Δf	=	Half power bandwidth	Hz
η	=	Loss factor	1
ω	=	Angular frequency	rad

Advantages [33]:

- The method does not require a lot of equipment.
- It has simple equations, is fast and easy to use.

Disadvantages:

- The mass has to be changed to shift the frequency. [33]
- Neglected boundary conditions and unknown stresses occurring at the bottom and at the upper plate. (Further explanation in Section 3.4)

3.3. Harmonic Forced Nonresonance Methods

This chapter describes nonresonance techniques to evaluate the Young's modulus and loss factor. These techniques can also be summarised under dynamic stiffness methods. [33]

The main change in the measurement setup is that the upper plate is mounted on a force transducer which is rigid. A description can be seen in Figure 3.3.

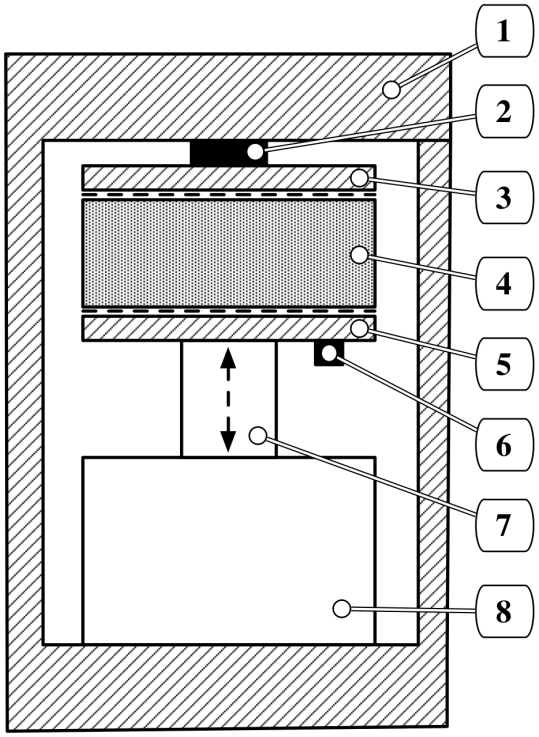

1 : *Fix support*
2 : *Force output transducer*
3 : *Bending resistant upper plate*
4 : *Specimen*
5 : *Bending resistant bottom plate*
6 : *Accelerometer input signal*
7 : *Vertical excitation*
8 : *Electrodynamic shaker*
-- : *Procedural errors*

Figure 3.3.: Nonresonance method [33]

The calculation of the Young's modulus and loss factor is as follows: A sinusoidal tensile strain at the bottom of the specimen occurs due to the shaker. This generates a sinusoidal stress at the other end with a phase shift between these two signals δ. The equations are then:

$$E^* = E' + jE'' = \frac{\sigma^*}{\epsilon^*} = \frac{\epsilon_0}{\sigma_0} \cdot \ e^{j\delta} \tag{3.11}$$

$$\eta = \frac{E''}{E'} = \tan\delta \tag{3.12}$$

With:

E'	=	Dynamic modulus	Pa
E''	=	Loss modulus	Hz
E^*	=	Complex Young's modulus	Pa
δ	=	Phase shift	rad
ϵ^*	=	Complex strain	mm
ϵ_0	=	Initial strain	mm
σ_0	=	Initial stress	N/mm^2
σ^*	=	Complex stress	N/mm^2

Advantages [33]:

- The system can measure at different frequencies.
- Measurement is better defined than the harmonic forced resonance method considering static pre-strains and dynamic strains.

Disadvantages:

- Neglected boundary conditions and unknown stresses at the bottom and at the upper plate (further explanation in Section 3.4).

3.4. Procedural Errors and Correction Attempts

The following subsection describes procedural errors and several derivatives which have been investigated to correct measurement issues with the setups described in Section 3.2 and 3.3.

A foam or a nonwoven material that is considered to behave like a spring will cause several measurement mistakes.

If a long rod-like specimen is tested in a vibration test similar to Figure 3.3, it would hardly bulk sideways when it is compressed comparing to its length. Implying the assumption that the specimen cannot move in the horizontal direction at the upper and the bottom plate. Another behaviour takes place when the specimen is disc shaped. It would bulk sideways[1] heavily which is visualized in Figure 3.4. From this observation, it seems to be clear that a complicated behaviour like this cannot be assumed to be spring-like. Unfortunately, cutting out a sample from a damping material will be, in almost every automotive application, disc shaped. Therefore, methods investigated by Sim and Kim [82], Mariez *et.al.* [61] and Langlois [53] can be considered. These methods correct measurement issues arrising from the assumption of the specimen behaving like a spring. The method proposed by Langlois seems to be the best developed so far, hence it is presented in detail. More information on the other methods can be found in the respective publications.

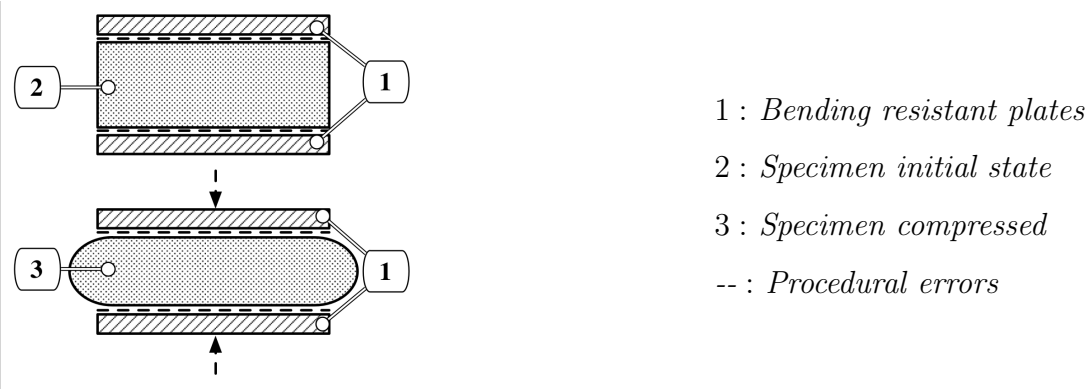

Figure 3.4.: Deformation of homogeneous isotropic foams due to compression and horizontal movement inhibition at the plates

[1]The effect of a horizontal displacement caused by compressing a material is described by the Poisson's ratio.

3.4.1. The Sim and Kim Method

The method by Sim and Kim [82] corrects the harmonic forced resonance method by using two disc-shaped samples with different shape factors. The shape factor is defined to be:

$$S = \frac{r}{2l} \tag{3.13}$$

Where r is the radius of the specimen and l the thickness. The measurement setup is the same as in Figure 3.1. They first measured the specimen with the small shape factor to determine the apparent Young's modulus since the effects of Poisson's ratio are lower.

A static finite element method (FEM) model is built to simulate the mechanical impedance of the second specimen with the larger shape factor.

In the FEM model, the Poisson's ratio is then adjusted until it equals the measurement results of the second sample. The Poisson's ratio, which is found, leads to a better estimation of the Young's modulus from the first sample. The iteration carries on until small changes are found for Young's modulus and Poisson's ratio.

The advantage of this measurement is that no laser vibrometer is used; however this type of measurement is time consuming. It has to be noted that the authors used this method on PU Blocks, not foams or nonwoven materials. No validation is described in their article. [82]

3.4.2. The Mariez, Sahraoui and Allard Method

The main change in the setup of the basic nonresonance method is that not only an accelerometer signal is used to measure the vertical displacement, a laser vibrometer is also used to measure the horizontal displacement, as it can be seen in Figure 3.5. In order to be able to use a laser vibrometer, moving targets have to be glued on the specimen at its centre. Mariez *et al.* [61] uses cubic samples to be able to measure in three orthogonal directions.

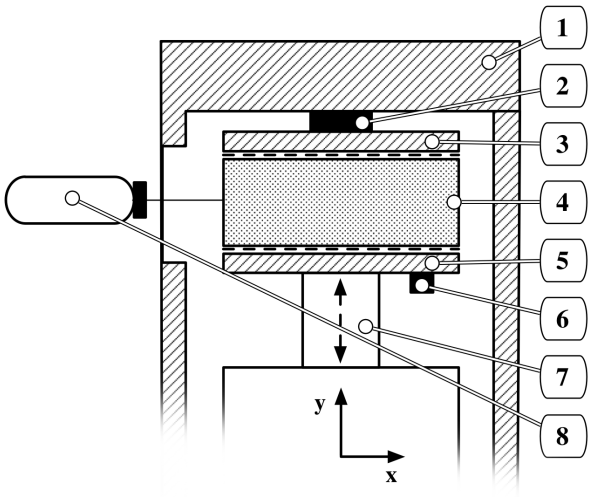

1 : *Fix support*

2 : *Force output transducer*

3 : *Bending resistant upper plate*

4 : *Bending resistant bottom plate*

5 : *Accelerometer input signal*

6 : *Vertical excitation*

7 : *Laser vibrometer*

-- : *Procedural errors*

Figure 3.5.: Nonresonance method with laser vibrometer [61]

Due to the laser vibrometer, both the mechanical impedance $Z_m(\omega)$ and the transfer function of the displacements $T_m(\omega)$ can be measured.

$$Z_m(\omega) = \frac{F(\omega)}{y(\omega)} \tag{3.14}$$

$$T_m(\omega) = \frac{x(\omega)}{y(\omega)} \tag{3.15}$$

Mariez *et. al.* furthermore suggested a calibration technique to reduce undesired effects of the overall measurement system. They used a spring with a frequency resonance much higher than the measurement frequency of the system, so its value k_0 measured on a tensile machine should be equal to its dynamic value on the measurement system $k_s(\omega)$. According to Mariez *et al.* since a spring is used, its transfer function of the displacements for the spring $T_s(\omega)$ should be one as an idealised value. This gives the corrected mechanical impedance and displacement transfer functions:

$$Z_{mc}(\omega) = \frac{F(\omega)}{y(\omega)} \cdot \frac{k_0}{k_s(\omega)} \tag{3.16}$$

$$T_{mc}(\omega) = \frac{x(\omega)}{y(\omega)} \cdot \frac{1}{T_s(\omega)} \tag{3.17}$$

The first measurement step is to determine the Poisson's ratio of the sample using equation (3.17). Secondly, a measurement of the mechanical impedance is done using equation (3.16).

Thereafter, the Young's modulus can be determined inversely using static approximations of $Z_{mc}(0)$ and $T_{mc}(0)$ out of FEM simulations with:

$$Z_{mc}(0) = \frac{F(0)}{y(0)} = \frac{E \cdot b(1-\nu)}{h(\nu)} \tag{3.18}$$

$$T_{mc}(0) = \frac{x(0)}{y(0)} = g(\nu) \tag{3.19}$$

The parameters h and g are functions fitted on FEM results, b is the width of the sample. Assuming quasistatic strain, the functions can be rewritten with their dynamic parameters for Young's modulus and Poisson's ratio:

$$Z_{mc}(\omega) = \frac{E^*(\omega)b(1-\nu^*(\omega))}{h(\nu^*(\omega))} \tag{3.20}$$

$$T_{mc}(\omega) = g(\nu^*(\omega)) \tag{3.21}$$

If the measured Poisson's ratio $\nu^*(\omega)$ is known as well as the measured mechanical impedance $Z_{mc}(\omega)$, then the determination of Young's modulus is straightforward. The angular frequency of this measurement system has to be low to become a good approximation with the static FEM model. In their article, the authors did not describe a validation process. This measurement attempt was used on PU foams. [61]

With:

b	=	Width of specimen	m
E	=	Young's modulus	Pa
E^*	=	Complex Young's modulus	Pa
F	=	Force	N
h, g	=	Functions fitted on FEM results	1
k_0	=	Static compression stiffness for a spring	$^N/_m$
$k_s(\omega)$	=	Measured compression stiffness for a spring	$^N/_m$
$K_m(\omega)$	=	Measured compression stiffness	$^N/_m$
l	=	Thickness of specimen	m
r	=	Radius of specimen	m
S	=	Shape factor	1
$T_m(\omega)$	=	Transfer function general displacements	1
$T_{mc}(\omega)$	=	Transfer function general displacements corrected	1
$T_s(\omega)$	=	Transfer function displacements of spring	1
$x(\omega)$	=	Horizontal displacement	m
$y(\omega)$	=	Vertical displacement	m
$Z_m(\omega)$	=	General mechanical impedance uncorrected	$^{kg}/_{s \cdot m^2}$
$Z_{mc}(\omega)$	=	Mechanical impedance corrected	$^{kg}/_{s \cdot m^2}$
ν	=	Poisson's ratio	1
ω	=	Angular frequency	$^{rad}/_s$

3.4.3. The Method by Christian Langlois *et. al.*

The setup of this method is according to Subsection 3.4.2. Langlois *et. al.* [53] also suggest the method of Mariez *et. al.* [61] to calibrate the measurement system in case of its mechanical impedance. The mechanical impedance is as before:

$$Z_m(w) = \frac{F(w)}{y(w)} \tag{3.22}$$

Then, the corrected function for the mechanical impedance is named as $Z_{mc}(\omega)$, which is complex valued and can be written as a function of its real and imaginary parts:

$$Z_{mc}(w) = K_m(\omega) + jX_m(\omega) \tag{3.23}$$

There, $K_m(\omega)$ is the compression stiffness and $X_m(\omega)$ is the mechanical reactance at the frequency ω. When inertial effects are assumed to be insignificant, equation (3.23) can be written as:

$$Z_{mc}(w) \cong K_m(w) \cdot (1 + j\eta(w)) \tag{3.24}$$

The compression stiffness and the loss factor at the quasistatic range of interest are given by:

$$K_m(w) = Re(Z_{mc}(w)) \tag{3.25}$$

$$\eta(w) \cong \frac{Im(Z_{mc}(w))}{Re(Z_{mc}(w))} \tag{3.26}$$

Langlois *et. al.* used FEM methods to achieve precalculated polynomial factors to correct his mechanical impedance measurement. In the following part, the calculation of these factors is described.

As previously stated, the effect from errors of bulk deformation and unknown stresses become insignificant for long slender columns. Consequently for a long rod-like specimen, the static compression stiffness is not much affected by the Poisson's ratio or boundary conditions. Its characteristic one-dimensional static compression stiffness is

given by:

$$K_0 = \frac{E \cdot A}{l} \tag{3.27}$$

The equation (3.27) refers to a spring-like specimen behaviour. When the column is short, Poisson's ratio and boundary conditions effect the compression stiffness. Solving the equation (3.27) for the Young's modulus can only lead to an apparent Young's modulus given by:

$$E_a = \frac{l}{A} * K_m(0) \tag{3.28}$$

Dividing equation (3.28) by the true value of the Young's modulus, gives the normalised static compression stiffness:

$$\frac{E_a}{E} = \frac{K_m(0)}{K_0} \tag{3.29}$$

The Figure 3.6 shows variations of the normalised static compression stiffness as a function of shape factors and Poisson's ratios. The dots result from an axisymmetrical FEM model.

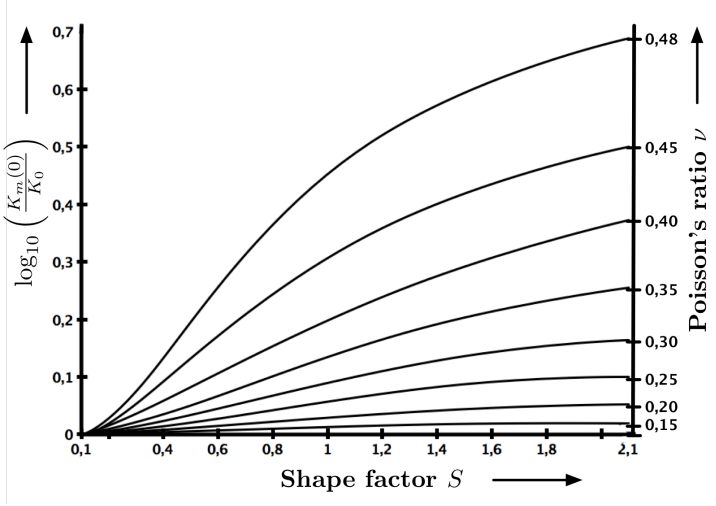

Figure 3.6.: Normalised compression stiffness, shape factor, Poisson's ratio [53]

With:

A	=	Surface, perpendicular to applied force	m^2
E	=	Young's modulus	Pa
E_a	=	Apparent Young's modulus	Pa
F	=	Force	N
K_0	=	Static compression stiffness for a rod-like column	N/m
$K_m(0)$	=	Static compression stiffness for a disc shaped specimen	N/m
$K_m(\omega)$	=	Measured compression stiffness	N/m
l	=	Thickness of specimen	m
$X_m(\omega)$	=	Mechanical reactance	N/m
$y(\omega)$	=	Vertical displacement	m
$Z_m(\omega)$	=	General mechanical impedance uncorrected	$kg/s \cdot m^2$
$Z_{mc}(\omega)$	=	Mechanical impedance corrected	$kg/s \cdot m^2$
η	=	Loss factor	1
ω	=	Angular frequency	rad/s

Keeping Figure 3.6 in mind, each curve related to a specific Poisson's ratio can be written in a polynominal s of order M:

$$P_\nu(S) = \frac{K_m(0)}{K_0} = 1 + \sum_{i=1}^{N} C_i^\nu S^i \tag{3.30}$$

For a given shape factor, a polynominal in v can be built:

$$P_S(\nu) = \frac{K_m(0)}{K_0} = 1 + \sum_{i=1}^{N} D_i^S \nu^i \tag{3.31}$$

It can be noted that the static polynominal relations in equation (3.30) and (3.31) hold because the frequency range of the measurement will be taken out below any resonances, therefore the following substitution can be done with (3.30) and (3.31):

$$K_m(w) \to K_m(0) \quad \text{for } \omega \ll \omega_{r1} \tag{3.32}$$

The following example describes how this method is used.

Two disc shape samples with different shape factors have to be cut out of the acoustic product. Their thickness is the same, but their diameter differs.

To build the polynominals, first the equation (3.30) is used to evaluate the polynominals for the two samples with shape factors S_1 and S_2 for the different Poisson's ratios in Figure 3.6. With equation (3.31) the computed dots in Figure 3.7 are used to form the polynominals in terms of the Poisson's ratios, which leads to Figure 3.7b.

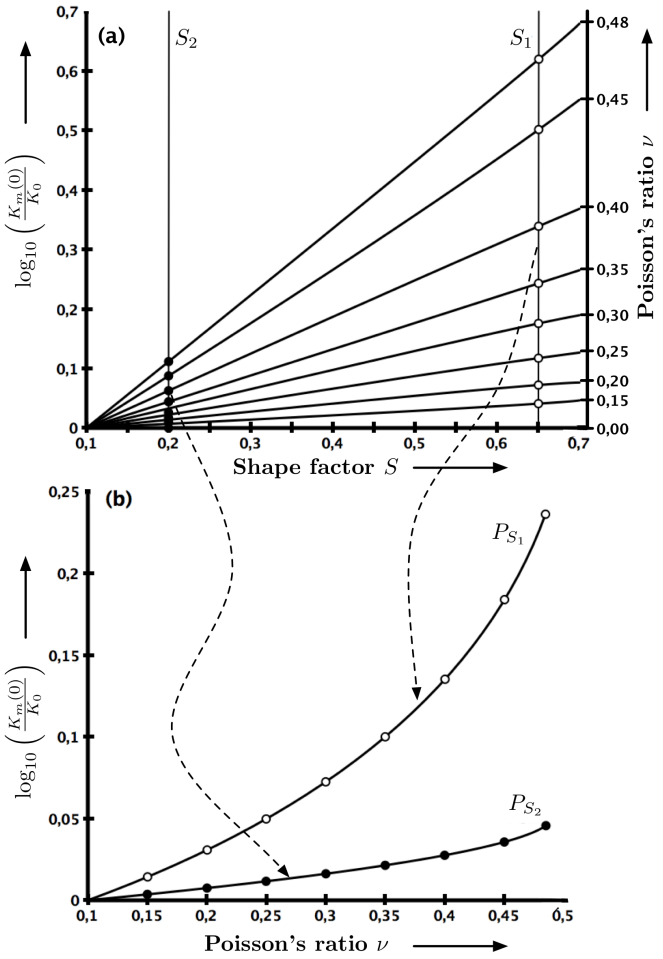

Figure 3.7.: Forming the correction polynoms [53]

To evaluate the parameters, a normal mechanical impedance measurement using the apparatus in Figure 3.1 is taken out with the two specimens. Thereafter, the Poisson's

ratio can be determined. The two specimens share the same Young's modulus, Poisson's ratio and damping loss factor. Therefore, using equation (3.32) and combining equations (3.27),(3.28),(3.30) and (3.31), leads to:

$$E(\omega) = \frac{K_{m,S_1}(\omega) l_{S_1}}{P_{S_1}(\nu) A_{S_1}} = \frac{E_{aS_1}(\omega)}{P_{S_1}(\nu)} \tag{3.33}$$

and

$$E(\omega) = \frac{K_{m,S_2}(\omega) l_{S_2}}{P_{S_2}(\nu) A_{S_2}} = \frac{E_{aS_2}(\omega)}{P_{S_2}(\nu)} \tag{3.34}$$

Combining equations (3.33) and (3.34) leads to:

$$\frac{E_{aS_1}(\omega)}{P_{S_1}(\nu)} - \frac{E_{aS_2}(\omega)}{P_{S_2}(\nu)} = 0 \tag{3.35}$$

With:

C_i^v	=	Curve fit coefficients related to curve ν	1
D_i^s	=	Curve fit coefficients related to curve S	1
$P_\nu(S)$	=	Correction polynom shape factor	1
$P_S(\nu)$	=	Correction polynom Poisson's ratio	1
ω_{r1}	=	First resonance of system	Hz
ω	=	Angular frequency	Hz

Since the apparent Young's moduli are determined from the mechanical impedance measurement and the geometry of the samples, the equation (3.35) has the Poisson's ratio as the only unknown parameter.

As soon as the Poisson's ratio is determined, the Young's modulus can be calculated using equations (3.33) or (3.34). These equations make use of the correction polynoms given in (3.30) and (3.31).

The damping loss factor can be directly computed by dividing the imaginary from the real parts of the mechanical impedance in equation (3.26).

Validation of the method:

This method was validated by use of the Biot model described in Section 2.2. In addition to the above evaluated parameters, being Young's modulus E', Poisson's ratio ν and damping loss factor η; the acoustic Biot parameters such as:

- Porosity [45, 39],
- Static airflow resistance [45, 39],
- Tortuosity [39],
- Viscous characteristic length [9], and
- Thermal characteristic length [9]

have to be determined. Characterisation methods are described in Subsection 2.2.1. However, Langlois referred in his paper to other articles in order to determine the acoustic Biot parameters which are referenced behind the respective parameter.

Using the Biot model, the sound absorption coefficient for normal incidence of the two samples can be computed. This is then compared to a standing wave tube measurement following the standard ASTM E 1050-86. The Figure 3.8 shows how the sample is inserted into the tube.

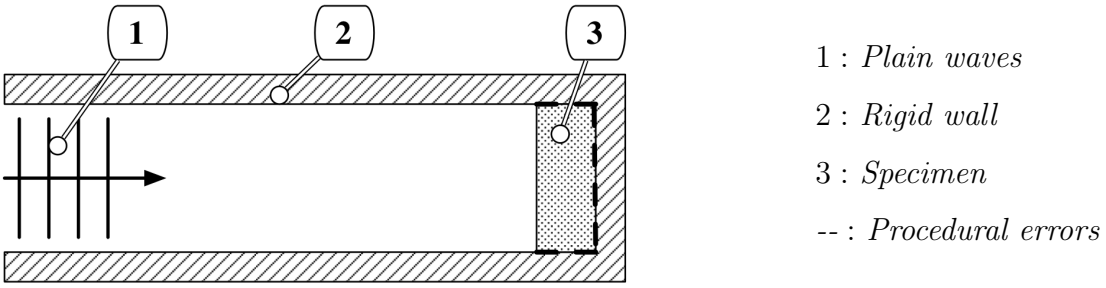

Figure 3.8.: Validation measurement setup in standing wave tube [53]

In this case, it is bonded all around its contour and the rear face with an adhesive. As previously described in Subsection 2.3.1, foams and nonwoven materials are sensitive due to friction between the specimen and the tube walls and in general to boundary

conditions. As a result of that, the outcome of the Biot model has to be corrected using FEM methods in order to compare them with the standing wave tube measurements. The results are presented in Figure 3.9.

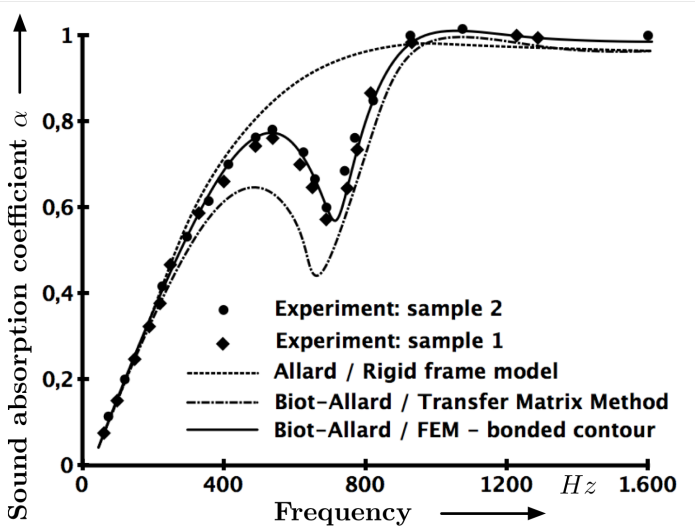

Figure 3.9.: Validation comparison with Biot Model [53]

3.5. Summary

As described in Section 3.4, procedural errors occur for current resonance as well as nonresonance methods. The correctional attempts applied to these methods by Sim and Kim [82], Mariez *et. al.* [61] and Langlois *et. al.* [53] do not seem to be well-conceived.

All the researchers made an assumption that they use a homogeneous and isotropic material. With Sim and Kim, it was a PU block. Mariez *et. al.* and Langlois *et. al.* used a PU foam. However, most likely their correction based on FEM calculations will be with large errors when applied to an inhomogeneous polytrophic material such as a nonwoven material. An isotropic homogeneous foam might bulk sideways and have the normalised static compression stiffness as it is predicted in Figure 3.6. A nonwoven material with randomly directed fibres, also depending on the respective layer of the material, will not show this exact behaviour, see also Subsection 2.3.1. Furthermore,

the FEM calculations of all researchers where static ones, which means that there is another error created, since damping materials are viscoelastic and therefore Young's modulus and loss factor change over the frequency range.

The most developed correctional attempt and also the only one with a validation described, has been proposed by Langlois. This method also makes use of static FEM calculations for correction. However, a validation is described but it is not clear that the measurement system works correctly even on homogeneous and isotropic materials. This is be because he had to correct his validation using FEM methods until the simulated sound absorption coefficient fitted the measured one, see Figure 3.9. Furthermore, the sound absorption coefficient of porous material reacts sensitively on a change of Young's modulus and Poisson's ratio, as it can be seen in Figure 3.10 and Figure 3.11.

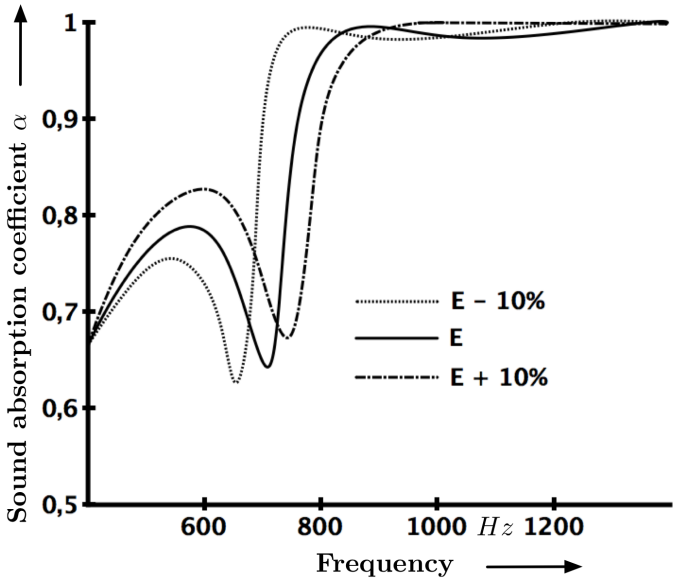

Figure 3.10.: Effects of 10 percent variation of Young's modulus at normal incidence [53]

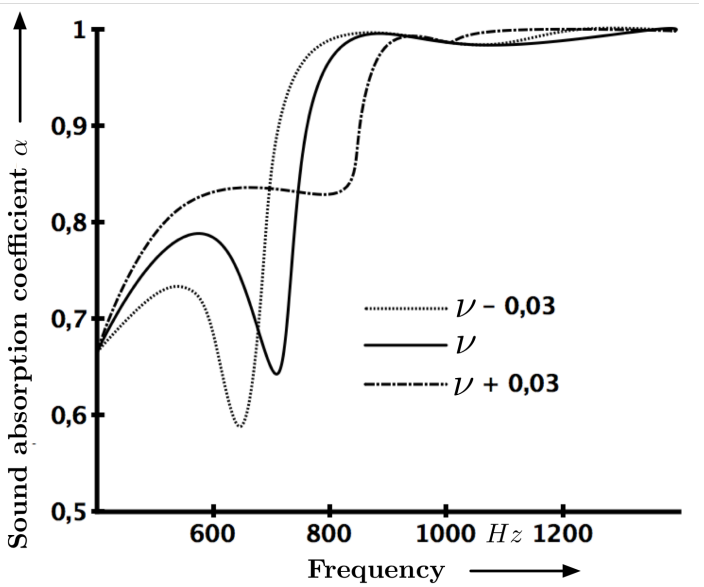

Figure 3.11.: Effects of 7 percent variation of Poisson's ratio at normal incidence [53]

Hence, it is not clear if it is possible to correct the dynamic behaviour of an isotropic and homogeneous foam with quasistatic FEM methods. Furthermore, the parameters of the specimen will change slightly after every measurement due to compression, which creates errors especially for the methods proposed by Mariez *et. al.* and Sim and Kim. No correctional attempt accounts for polytrophic inhomogeneous behaviour of nonwoven materials.

Due to difficulties in characterisation, especially for the Young's modulus and loss factor of nonwoven materials, these techniques still need further development. This problem will be addressed in the following chapters.

4 Theory of a New Measurement System to Evaluate Structural Biot Parameters

4.1. Introduction

As described in Chapter 3, there have been problems reported measuring a foam or a nonwoven material with mechanical impedance methods due to neglected boundary conditions and unknown stresses. Their correctional attempts do not account for inhomogeneous and polytrophic specimens. Furthermore, the only validation reported for homogeneous and isotropic specimens, by Langlois [53], had to be corrected. Therefore, a measurement system has to be found which avoids the aforementioned problems, by not effecting the materials with unknown stresses in the measurement apparatus.

A measurement which comes close to that idea is to use ultrasonics to determine Young's modulus as well as loss factor. Although not being fully understood, ultrasonics have been used for years in nondestructive testing measuring engineering constants.

For ultrasonic measurements, acoustic energy may be transmitted from transducers to a specimen using a coupling fluid such as water. Here, the transmitter, the receiver and the sample are immersed in a water tank. It is also called the ultrasonic immersion method. A description can be seen in Figure 4.1.

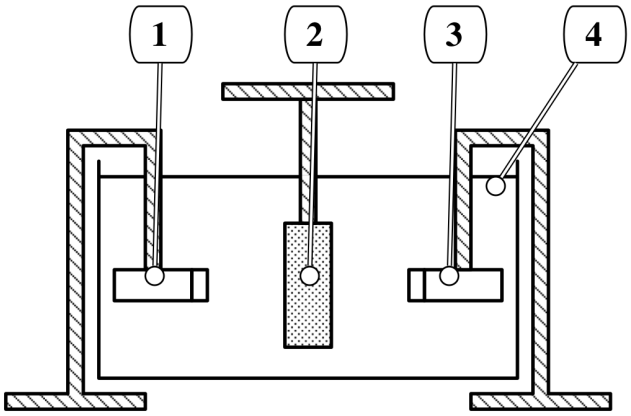

1 : *Emitter*

2 : *Specimen*

3 : *Receiver*

4 : *Water bath*

Figure 4.1.: Ultrasonic immersion method [33]

This measurement system does not affect the material by compressing it, which led to unknown stresses in mechanical transfer function systems. Therefore, an ultrasonic measurement system may be able to evaluate the Young's modulus and loss factor more precisely than the mechanical transfer function systems. Hence, a link between structural Biot parameters and ultrasonic measurements has to be provided.

4.2. Wave Propagation and Relation to Structural Parameters

Ultrasonic testing is based on sound waves forcing atoms inside materials into an oscillatory movement. This movement propagates as a wave through the specimen. When these atoms are displaced, binding forces apply which can be visualised to be like small springs following Hooke's law. The input energy gets saved in this mass spring system, which forces the atoms back to their original position. Their inertia creates an oscillatory movement.

Waves can be divided into longitudinal (pressure) and transversal (shear) waves. An oscillatory movement of atoms in the direction of propagation creates a longitudinal or pressure wave. An oscillatory movement of atoms perpendicular to the direction

of propagation is called a transversal or shear wave. Transversal waves only occur in a solid, since shear strain can only be absorbed in solids. Therefore, a fluid can only contain longitudinal waves, whereas a solid contains both wave types. The basic wave equation describes the motion of waves as:

$$c = \lambda \cdot f \tag{4.1}$$

Where c is the speed of sound, λ the wavelength and f the frequency.

Figure 4.2 shows the longitudinal wave propagation and Figure 4.3 shows the transversal wave propagation.

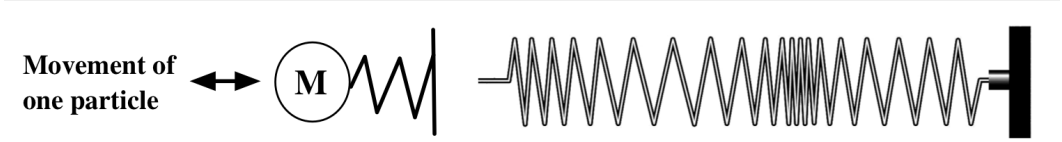

Figure 4.2.: Longitudinal wave propagation

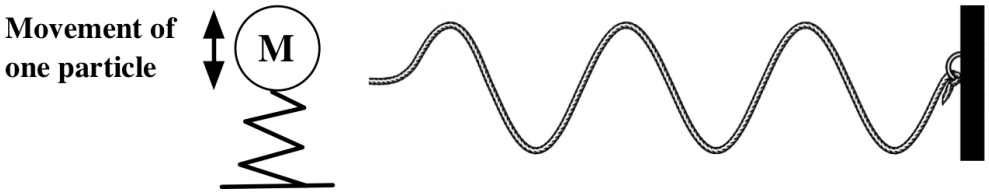

Figure 4.3.: Transversal wave propagation

Mechanical waves can only propagate in a medium, a fluid or a solid. The wave motions are described by laws for harmonic oscillations such as Hooke's law which would be an idealistic elastic motion of a mass on a spring as previously described. Their equations can be derived imagining a transversal wave with simple harmonic oscillations with a displacement y which is changing as the wave passes through the medium. It is the displacement of one element in the direction of propagation of the sound wave x_p at a time t. Therefore, y is a function of (x_p, t). The wave equation described by *inter*

alia [52, 42] is then:

$$\frac{\partial^2 y}{\partial x_p^2} = \frac{1}{c^2}\frac{\partial^2 y}{\partial t^2} \tag{4.2}$$

Writing $c^2 = T_e/\rho$, where T_e is the required restoring force or tension and ρ is linear density ($^{mass}/_{length}$), which gives:

$$T_e\frac{\partial^2 y}{\partial x_p^2} = \rho\frac{\partial^2 y}{\partial t^2} \tag{4.3}$$

The solution of equation (4.2) has the form:

$$y(x_p, t) = G(x_p - ct) + H(x_p + ct) \tag{4.4}$$

Where G and H are arbitrary functions with existing second derivatives. Describing a plain progressive wave, G is specified as a sine or cosine function and $H = 0$. The equation of a harmonic oscillator is [42, 52]:

$$y = y_a \sin(\omega t - \delta) \tag{4.5}$$

Here, y_a is the amplitude, ω is the angular frequency and δ is the phase which determines the starting point of the sine wave at x_0. Inserting the following expressions for angular frequency ω and phase lag δ in respect of the wave number n and speed of sound c:

$$\delta = \frac{2\pi x_p}{\lambda} \qquad \text{and} \qquad \omega = n \cdot c = \frac{2\pi c}{\lambda} = 2\pi f \qquad \text{and} \qquad n = \frac{2\pi}{\lambda} \tag{4.6}$$

gives

$$y(x_p, t) = y_a \sin(\omega t - \delta) = y_a \sin n(ct - x_p) = y_a \sin\frac{2\pi}{\lambda}(ct - x_p) \tag{4.7}$$

Where $(ct - x_p)$ is expressed in radians. When equation (4.7) has to expressed by the wave number n, it leads to:

$$y(x_p, t) = y_a \sin(\omega t - nx_p) \tag{4.8}$$

This is a solution sufficient for equation (4.2), describing an elastic material. Another solution is the expression with both sine and cosine functions with [42, 52]:

$$y = y_a(\sin(\omega t - nx_p) + i\cos(\omega t - nx_p)) = y_a e^{i(\omega t - nx_p)} \tag{4.9}$$

As described in Subsection 2.2.2, viscoelastic materials can be described by a combination of an elastic with a viscous model through the complex modulus, which is genrerally described as:

$$M^* = M' + iM'' \tag{4.10}$$

Integrating this into equation (4.2) gives:

$$\rho\frac{\partial^2 y}{\partial t^2} = M^*\frac{\partial^2 y}{\partial x_p^2} = M'\frac{\partial^2 y}{\partial x_p^2} + iM''\frac{\partial^2 y}{\partial x_p^2} \tag{4.11}$$

The decrease in amplitude because of viscoelasticity or damping, is usually expressed through the factor $(e^{-\alpha x_p})$. The larger the attenuation coefficient α, the more rapid is the reduction of amplitude. Integrating this factor into equation (4.11) gives:

$$y = y_a(\sin(\omega t - nx_p) + i\cos(\omega t - nx_p))e^{-\alpha x_p} = e^{-\alpha x_p}y_a e^{i(\omega t - nx_p)} \tag{4.12}$$

The following solution to find relations between the real and imaginary part of the complex modulus M^* in respect of sound velocity c, angular frequency ω and density ρ was described in short by Hugh [42], taken from McSkimin [64]. After the differential components and the real M' and imaginary terms iM'' in equation (4.11) have been evaluated, two equations can be formed:

$$M' = \rho \cdot c^2 \left(\frac{1 - \left(\frac{\alpha c}{\omega}\right)^2}{\left(1 + \left(\frac{\alpha c}{\omega}\right)\right)^2} \right) \tag{4.13}$$

$$M' = \rho \cdot c^2 \qquad \text{when} \qquad \frac{\alpha c}{\omega} \ll 1 \tag{4.14}$$

$$M'' = \rho \cdot c^2 \left(\frac{\frac{\alpha c}{\omega}}{\left(1 + \left(\frac{\alpha c}{\omega}\right)\right)^2} \right) \tag{4.15}$$

$$M'' = \frac{\rho c^3 \alpha}{\omega} \qquad \text{when} \qquad \frac{\alpha c}{\omega} \ll 1 \tag{4.16}$$

As it can be seen, the equations (4.13) and (4.15) can be simplified when:

$$r = \frac{\alpha c}{\omega} = \frac{\alpha \lambda}{2\pi} \ll 1 \tag{4.17}$$

Values of r can be found in literature for polymers where it is assumed to be $r = 0,1$. However, for special high attenuating stadiums, it can reach up to $r = 0,8$. [42] No information can be found for porous viscoelastic materials. The simplified equations may lead to errors although they have been used not only for polymers, but also been described by numerous authors investigating porous viscoelastic materials. [52, 2, 55]

Using the equation (2.30) and (4.13)-(4.16), gives the parameter $\tan\delta$ or the loss factor η with:

$$\tan(\delta) = \eta = \frac{M''}{M'} = 2c \cdot \alpha \frac{\omega}{\omega^2 - c^2\alpha} \tag{4.18}$$

$$\tan(\delta) = \eta = \frac{M''}{M'} = 2\frac{c \cdot \alpha}{\omega} = \frac{\alpha \cdot \lambda}{\pi} \qquad \text{when} \qquad \frac{\alpha \cdot c}{\omega} \ll 1 \tag{4.19}$$

Until now, the description was limited to a modulus in general not taking into account which modulus is evaluated. Since the wave equations above apply for longitudinal as well as shear waves, the above equations are valid for the longitudinal modulus L, as well as the shear modulus N. Here, c_{lb} has to be inserted as longitudinal wave velocity and c_{tb} for transversal wave velocity respectively.

Combining (4.14) with the equations (2.26), (2.27) and (2.28) relating the moduli to each other, gives the equation to determine the bulk modulus out of ultrasonic measurements. This equation is also described by [2, 52, 55]:

$$K' = L' - \frac{4}{3}N' = \rho \cdot (c_{lb}^2 - \frac{4}{3}c_{tb}^2) \tag{4.20}$$

Not stated by any of these authors, are the equations for greater values for r than 0,1. However, using (4.13) and (2.26) (2.27) (2.28) gives:

$$K' = -\frac{1}{3}\rho \frac{(3\alpha^2 c_{lb}^2 c_{tb} - 4\alpha^2 c_{lb} c_{tb}^2 - 3\alpha\omega c_{lb}^2 - \alpha\omega c_{lb} c_{tb} + 4\alpha\omega c_{tb}^2 - 3\omega^2 c_{lb} + 4\omega^2 c_{tb})}{(\alpha c_{tb} - \omega)(\alpha c_{lb} - \omega)} \tag{4.21}$$

The Young's modulus is as described in Subsection 2.2.2:

$$E' = K' \cdot 3(1 - 2\nu) \tag{4.22}$$

With:

c	=	Sound velocity	$^{m}/_{s}$
c_{lb}	=	Longitudinal sound velocity in specimen	$^{m}/_{s}$
c_{tb}	=	Transversal sound velocity in specimen	$^{m}/_{s}$
E'	=	Dynamic Young's modulus	Pa
f	=	Frequency	Hz
G, H	=	Arbitrary functions	1
K'	=	Dynamic bulk modulus	Pa
L'	=	Dynamic longitudinal modulus	Pa
M'	=	Dynamic general modulus	Pa
M''	=	Loss general modulus	Pa
M^*	=	Complex general modulus	Pa
n	=	Wave number	1
N'	=	Dynamic shear modulus	Pa
r	=	Relation of attenuation coefficient, sound velocity to angular frequency	$^{dB}/_{rad}$
t	=	Time	s
T_e	=	Tension	N
x_p	=	Horizontal position	m
y	=	Vertical displacement	m
y_a	=	Vertical amplitude	m
α	=	Attenuation coefficient	$^{1}/_{m}$
δ	=	Phase shift	s
η	=	Loss factor	1
λ	=	Wavelength of ultrasonic wave	m
ν	=	Poisson's ratio	1

ω	=	Angular frequency	$^{rad}/_{s}$
ρ	=	Linear density	$^{kg}/_{m^3}$

The above equations only hold for a homogeneous, isotropic and elastic solid in which bulk waves can propagate. The requirement for that is that the wavelength λ is much smaller than the sample dimensions and much larger than inhomogenities.

The Poisson's ratio is expected to vary in the range $0 \leq \nu \geq 0,5$, it follows that $c_{lb} > c_{tb}$. [2]

Equation (4.20) holds for an isotropic elastic solid. A porous medium consists in its natural state not only of a solid material but of a mixture of a solid and a fluid. However, a porous medium can be considered to be a solid due to simplicity when the equation (4.20) is corrected. This is done by the percentage of solid matrix material forming the porous specimen. It is expressed by the term $(1 - f_v)$, where f_v is the porosity of the specimen. The corrected equation was also used in medical techniques by researchers investigating the Young's modulus of bones, a porous viscoelastic material. [76, 29, 57] This was previously investigated by Bourbie [17]. Again, this only holds for an isotropic homogeneous "solid" which requires the wavelength λ to be much smaller than sample dimensions and in case of a porous material, the wavelength should be much larger than pore sizes. [2, 76, 55]

$$K_b = (1 - f_v)\rho_s \cdot (c_{lb}^2 - \frac{4}{3}c_{tb}^2) \tag{4.23}$$

Hereafter, $_s$ stands for the solid material and $_b$ for the porous specimen. The Young's modulus of the specimen, where the moduli are still considered dynamic, can be calculated with:

$$E_b = K_b \cdot 3(1 - 2\nu) \tag{4.24}$$

The shear modulus can be corrected in terms of the porosity in the same way [17, 80]:

$$c_{tb} = \sqrt{\frac{N_b}{(1 - f_v) \cdot \rho_s}} \tag{4.25}$$

With:

E_b	=	Young's modulus of specimen	Pa
f_v	=	Porosity	1
K_b	=	Bulk modulus of specimen	Pa
N_b	=	Shear modulus of specimen	Pa
ν	=	Poisson's ratio	1
ρ_s	=	Density of solid	$^{kg}/_{m^3}$

4.3. Summary

The purpose of this chapter was to describe the theory of the new measurement system based on ultrasonic immersion methods.

It is shown that structural Biot parameters of porous viscoelastic damping materials can be evaluated when several specimen parameters are given including parameters, which have to be evaluated conducting ultrasonic measurements. These are the speed of sound of the longitudinal and transversal wave inside the specimen, as well as the attenuation coefficient of the longitudinal wave. The derivation of these relationships were based on general wave theories.

5 Evaluation of Parameters to Investigate Structural Parameters

5.1. Introduction

The unknown parameters to investigate the moduli E_b, N_b, L_b and loss factor η from equations (4.23)(4.25)(4.19) can be divided into parameters which have to be determined using ultrasound and general parameters. The general parameters are:

ρ_s	=	Density of solid	$^{kg}/_{m^3}$
f_v	=	Porosity	1
ν	=	Poisson's ratio	1

The ultrasonic parameters are:

c_{lb}	=	Longitudinal sound velocity in specimen	$^{m}/_{s}$
c_{tb}	=	Transversal sound velocity in specimen	$^{m}/_{s}$
α	=	Attenuation coefficient	1
ω	=	Angular frequency	$^{rad}/_{s}$

The determination of the general as well as the ultrasonic parameters are described in this chapter.

5.2. Determination of General Parameters

The density of the elastic solid (matrix) ρ_s, porosity f_v, Poisson's ratio ν can easily be evaluated using general approaches.

ρ_s: The density of the solid, is equivalent to the material the specimen is made out of. It can be given by the manufacturers of the foam or the nonwoven material.

f_v: The porosity of the specimen can be determined by the density ratio of the specimen ρ_b and the solid ρ_s using the following equation:

$$f_v = 1 - \frac{\rho_b}{\rho_s} \tag{5.1}$$

ν: The Poisson's ratio can be determined when other moduli are known, using for example equation:

$$L_b = E_b \frac{1-\nu}{(1+\nu)(1-2\nu)} = K_b + \frac{4}{3} N_b \tag{5.2}$$

With:

ν	=	Poisson's ratio	1
f_v	=	Porosity	1
ρ_s	=	Density of solid	kg/m^3
ρ_b	=	Density of specimen	kg/m^3
L_b	=	Longitudinal modulus of specimen	Pa
N_b	=	Shear modulus of specimen	Pa
K_b	=	Bulk modulus of specimen	Pa
E_b	=	Young's modulus of specimen	Pa

5.3. Determination of the Speed of Sound from the Longitudinal Wave in Ultrasonics

To measure the speed of sound of the longitudinal wave velocity inside the specimen c_{lb}, a transmission measurement can be conducted. There, the ultrasonic transducer emits an ultrasonic pulse which propagates through the fluid and the specimen until it gets received. The time the ultrasonic pulse needs to propagate from the emitter to the receiver is measured. The longitudinal velocity in the specimen can thereafter be calculated from propagation time differences with the specimen inserted into the fluid and a measurement only with fluid. The setup is presented in Figure 4.1.

5.3.1. Group and Phase Velocity

There are two types of wave velocities, the group velocity and the phase velocity. A wave consisting of different frequency components can be summarised as a group, where each frequency has different wave shapes. The whole group, also called the wave envelope, conveys energy along the direction of propagation. Ultimately, the group velocity is the speed in which the energy of the wave travels.

The phase velocity, on the other hand, describes the propagation velocity of a phase. This is equivalent to a single frequency component of the whole wave group.

In a perfectly elastic medium, the group velocity is equal to the phase velocity. However, if the medium is viscoelastic, dispersion occurs. In this instance, group velocity differs from phase velocity. [55, 42]

5.3.2. Determination of the Speed of Sound from the Longitudinal Wave Using Group Velocity

The speed of sound of the ultrasonic wave can be determined using group velocity measurements. The procedure is described as follows. At first, the ultrasonic measurement is taken out without the specimen in order to determine the speed of sound in the fluid. It can be measured from the distance between the emitter and the receiver and the time the sound wave needs to travel this distance. This procedure is repeated with the specimen inserted into the tank. In addition, the specimen's thickness is measured.

When conducting group velocity measurements, the equation to determine the longitudinal wave velocity in the specimen is:

$$c_{lb} = \frac{c_{lf}}{1 - c_{lf}\frac{\Delta t(f)}{l}} \tag{5.3}$$

With:

c_{lb}	=	Longitudinal sound velocity in specimen	$^m/_s$
c_{lf}	=	Longitudinal sound velocity in fluid	$^m/_s$
Δt	=	Time difference of the measurement in water and with specimen	s
l	=	Thickness of specimen	m

When researchers used the group velocity to determine the speed of sound inside the specimen, they used a marker such as a zero-crossing in the emitted signal. Different markers are shown in Figure 5.1.

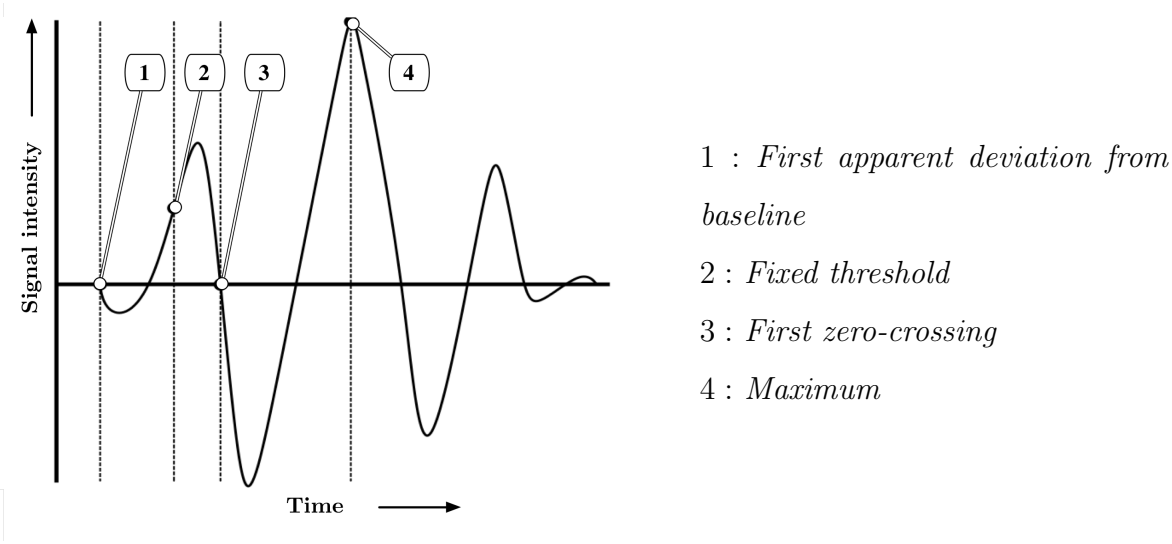

Figure 5.1.: Variation of markers to measure the group velocity [55]

The time this marker needs to travel from the emitter to the receiver gives the measurement time. However, ultrasonic transducers operate in a range of frequencies and are characterised by their middle frequency, where they reach the highest pressure amplitude in the magnitude frequency spectrum. That means the ultrasonic pulse always contains a number of different frequency components. Foams and nonwoven materials have dispersive velocities, which implies that the phase velocity differs from the group velocity. At the same time, frequency dependent attenuation occurs which leads to alternating waveforms where locations of markers might shift. Therefore, the measurement of the speed of sound might be incorrect. Researchers compared group velocity with phase velocity measurements of dispersive media and stated that group velocity measurements might lead to errors in sound speed measurements. [92, 54, 74, 85, 25, 66] The Figure 5.2 shows how different marker positions in the reference pulse leads to different velocity estimations using the group velocity. In this case, the attenuated pulse was displayed assuming linear frequency dependent attenuation. Several works exists to correct these effects [92], or to modulate other waveforms which lead to a better estimation. [85] However, the speed of sound might differ over the measured frequency range and therefore also the Young's modulus. In order to take this into account, the measurement of the phase velocity will lead to a more precise measurement system.

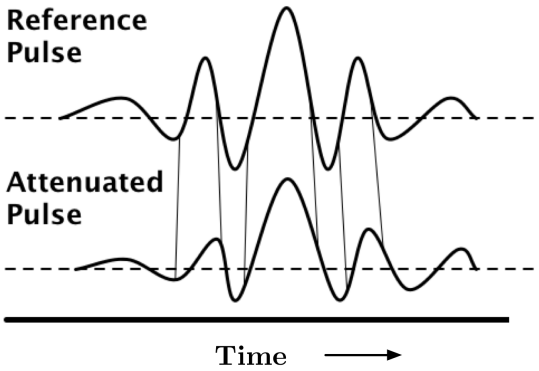

Figure 5.2.: Frequency dependent attenuation leads to errors using group velocity [92]

5.3.3. Determination of the Speed of Sound from the Longitudinal Wave Using Phase Velocity

It has been reported for viscoelastic polymers as well as for porous viscoelastic materials that their attenuation coefficient increases linear with frequency. [42, 37, 55] Kramers Kronig relations (KKR) are connecting the real to imaginary parts of physical response functions. They predict the phase velocity of these materials to increase logarithmically with frequency and therefore to have dispersive properties. [55] The same can ultimately be assumed for foams and nonwoven materials.

To account for that dispersive behaviour, phase velocity measurements can be conducted. Following [85, 55, 74, 25, 93, 94], the phase velocity can be calculated using the time difference or phase difference between measurements with and without the specimen, which is defined to be:

$$\Delta\Phi(\omega) = \phi_{uf}(\omega) - \phi_{ub}(\omega) \tag{5.4}$$

Changing Δt to $\Delta\Phi(\omega)$ in equation (5.25) gives the longituinal phase velocity inside the specimen:

$$c_{lb}(\omega) = \frac{c_{lf}}{1 - c_{lf}\frac{\Delta\Phi(\omega)}{\omega l}} \tag{5.5}$$

Note that c_{lf} remains a group velocity, since water or a gas is not dispersive. For the measurement of the phase velocity, the phase at each frequency can be calculated by using a discrete Fourier transform (DFT). This is done once for a measurement with coupling fluid ($\phi_{uw}(\omega)$) and once for when the specimen is inserted into the fluid ($\phi_{ub}(\omega)$). For a continuous phase spectrum, both signals have to be unwrapped to remove the 2π periodicity. The unwrapped phase is defined to be:

$$\phi_{uf,b}(\omega) = \phi_{f,b} \pm 2i\pi \tag{5.6}$$

Here, i is an integer. [55] In some cases when the signal has a poor signal to noise ratio at low frequencies, multiples of 2π phase errors can occur. This can be solved fitting the different points to a straight line using a least squares method. The correction is done for the range where the resulting intercept is close to multiples of $+-2\pi$. [85, 48]

With:

$c_{lb}(\omega)$	=	Longitudinal phase velocity in specimen	$^{m}/_{s}$
c_{lf}	=	Sound velocity in fluid	$^{m}/_{s}$
l	=	Thickness of specimen	m
ω	=	Angular frequency	$^{rad}/_{s}$
$\phi_{uf}(\omega)$	=	Unwrapped phase velocity in fluid	$^{rad}/_{s}$
$\phi_{ub}(\omega)$	=	Unwrapped phase velocity with specimen	$^{rad}/_{s}$
$\Delta\Phi(\omega)$	=	Phase difference of phase velocity in fluid and with specimen	rad

5.3.4. Interfering Fast and Slow Longitudinal Waves

As described in Section 2.2, the Biot's theory predicts two longitudinal waves in porous materials which can be characterised as a fast and slow longitudinal wave. [15, 16, 65] They also have been spotted in measurements of bones. [41, 36, 43] The fast longitudinal wave occurs when the fluid oscillates in phase with the matrix, the slow longitudinal wave occurs when the fluid oscillates out of phase with the matrix. However, no

information could be found if a fast and slow longitudinal wave will be spotted in foams or nonwoven materials.

In previously described equations, no difference has been made between the fast and slow longitudinal wave. Researchers in the field of medical techniques measuring bones, neglected the slow longitudinal wave in calculations of moduli. Fellah and Sebaa stated that is due to the fact that the fluid particles moving out of phase do not have enough mass to generate a motion in the heavy frame. [28, 80]

The measurement of bones were conducted using water as a coupling fluid, its density is $1000\,{}^{kg}/_{m^3}$. The bone frame has a density of an averaged $1902\,{}^{kg}/_{m^3}$, taken from studies of [76, 41, 29, 92, 81, 59, 43]. This gives a density ratio of $1{,}902\,{}^{kg}/_{m^3}$. Since a noncontact ultrasound approach is investigated in this dissertation, the used coupling gases have the highest density of $12{,}25\,{}^{kg}/_{m^3}$ (see table 6.1). The matrix of the damping materials have the lowest density of $267\,{}^{kg}/_{m^3}$ (see table 6.2). Its density ratio is therefore much higher than the bone measurement with $21{,}36\,{}^{kg}/_{m^3}$. The assumption of neglecting the slow longitudinal velocity in Young's modulus calculations will therefore be valid in this dissertation.

If the two waves can be spotted separately, then no difficulties arise. However, if they are interfering as it is reported in several works existing for measuring bones with ultrasound measurement, results might be false. In that case, negative dispersion i.e. decrease of phase velocity with frequency, has been reported. This is not conclusive according to the KKR. [91] The KKR relate the attenuation coefficient to dispersion. Their relations state that a medium with a linear frequency increase in attenuation coefficient shows an increase of phase velocity with frequency (positive dispersion). Since the attenuation coefficient of bones increases approximately linear with frequency, the negative dispersion cannot be explained. [25, 91] The same relations can be assumed for foams and nonwoven materials.

The Figure 5.3 shows the prediction of phase velocity by the KKR and the measured phase velocity over the frequency of a bone.

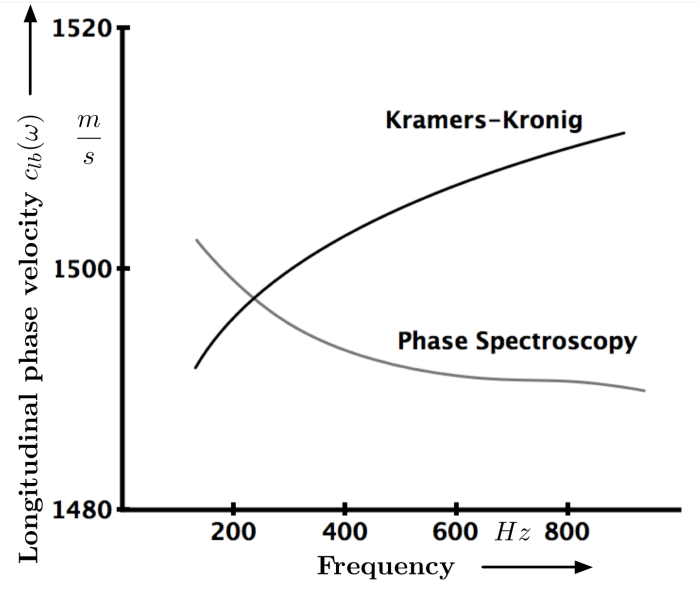

Figure 5.3.: Negative dispersion is not conclusive with KKR [62]

Researchers have proposed a hypothesis in which the negative dispersion arises from interfering fast and slow waves. If the two waves do not interfere, they would show positive dispersion as predicted by the KKR. [63]

Hence, if a fast and a slow wave interfere, it would lead to false results measuring foams and nonwoven materials. Therefore if interfering waves are measured, they will have to be split up into the slow and the fast longitudinal wave. Figure 5.4 shows a fast and a slow simulated longitudinal wave, which split up, showing a positive dispersion. A different behaviour can be observed when they are overlapping. In this case, they show negative dispersion.

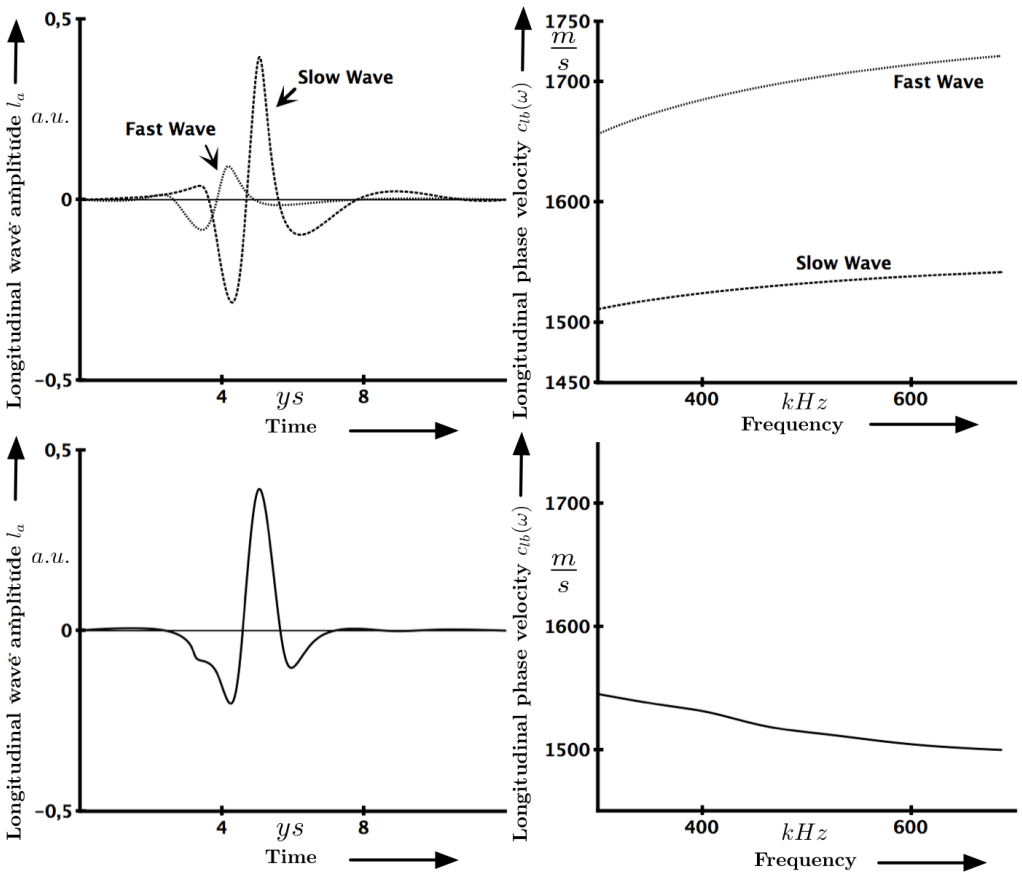

Figure 5.4.: Split up and overlapping fast and slow longitudinal waves [55]

To recover the original fast and slow waves, the Bayesian probability theory can be applied. In this approach, a model is constructed for the received signal by specifying velocity and attenuation parameters for the fast and the slow wave. The dispersions of these waves should be dependent on the frequency dependence of their attenuation coefficients, as it is predicted by the KKR. Therefore, the attenuation coefficient and the phase velocity of the fast and slow waves can be estimated, even if the waves are overlapping and interfering.

The Figure 5.5 shows in the upper diagram, a signal which is acquired from a bone. Moreso, it shows the signal of the constructed model using Bayesian probability theory. The probability theory can determine the individual fast and slow waves which can be seen in the lower diagram.

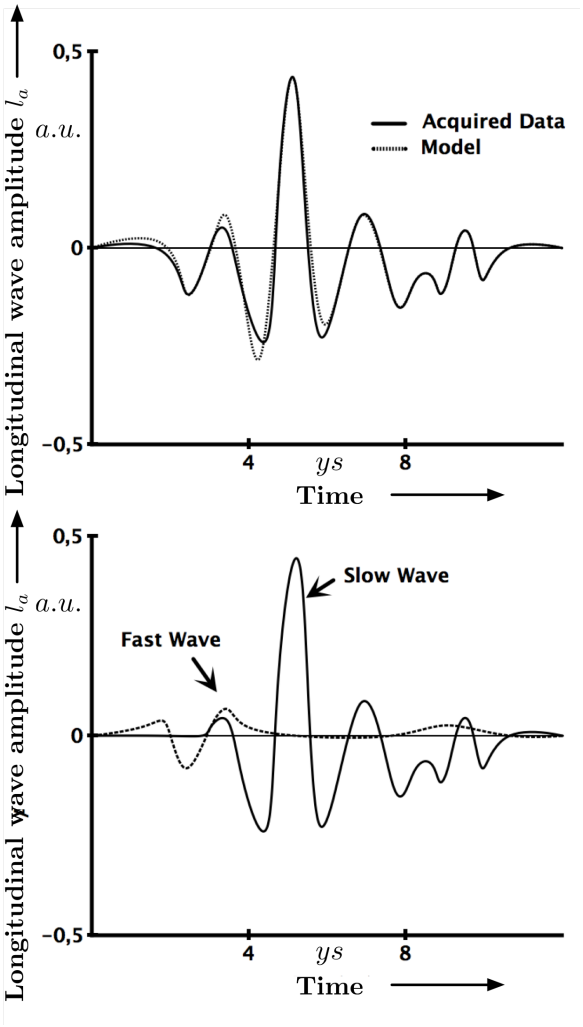

Figure 5.5.: Bayesian theory applied to interfering fast and slow waves [55]

The overlap of the fast and slow compressional wave is dependent on a number of factors including porosity, structural anisotropy, ultrasonic path length and angle of insonification relative to the pore orientation. [73] Therefore, it is not clear that an overlap occurs measuring the foams and nonwoven materials. Hence, the first step in the measurement system proposed here is to estimate whether two waves can be spotted separately over the bandwidth. If not, the diffraction characteristics of the ultrasonic wave has to be measured and compared if it is not conclusive to the KKR. Examples for Bayesian calculations can be found in the literature. [62, 6]

5.4. Determination of the Speed of Sound from the Transversal Wave in Ultrasonics

To determine the Young's modulus with equation (4.23), the transversal wave velocity also has to be measured. A method used for polymers [42] and for bones is to directly bond the ultrasonic transducer to the specimen.

However, directly bonding a shear wave transducer to the foam or the nonwoven material would affect its boundaries. Specimens are reported sensitive for compression and neglected boundary conditions as described in Subsection 2.3.1 and Section 3.4. Therefore, this approach will not be applied. Three other possibilities to measure the transversal wave velocity are carried out in this section.

The first approach measures the velocity of the shear wave by using reflected waves. The second approach uses refracted waves and shifting wave patterns. The third approach uses refracted waves and the position, where a wave convertion between the longitudinal and transversal wave occurs.

5.4.1. Refraction and Reflection of the Ultrasonic Waves

If an ultrasonic wave hits a surface of a solid material, a part of it is reflected and a part propagates into the medium as a longitudinal and a transversal wave. The waves propagate at different angles depending on the waves velocities, when the angle of incidence differs from the normal of the specimens surface. Additionally, reflection occurs. Figure 5.6 shows this behaviour.

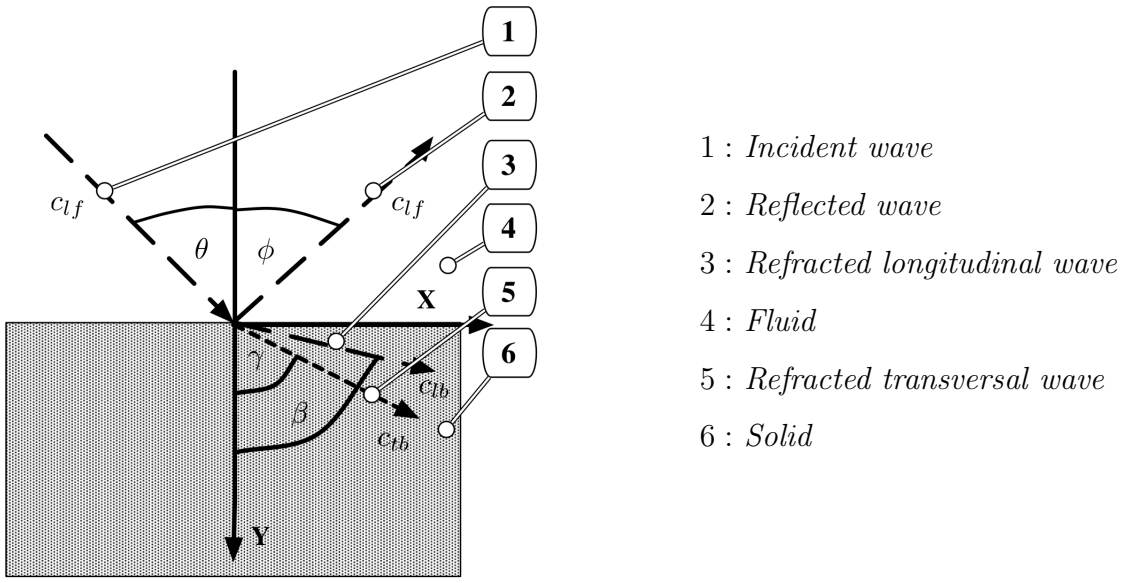

Figure 5.6.: Reflection and refraction of ultrasonic waves [7]

In this figure, there were no differences made between the fast and the slow longitudinal wave.

The following relations describe the behaviour of the longitudinal, the transversal and the reflected wave. They have been summarised from knowledge gained out of [7, 55, 52].

A plain wave in an isotropic medium can be described as:

$$\mathbf{U} = \mathbf{k_1} l_a(\mathbf{r} \cdot \mathbf{k_1} - c_{lb}t) + \mathbf{k_2} t_a(\mathbf{r} \cdot \mathbf{k_1} - c_{tb}t) \tag{5.7}$$

Vector quantities are expressed in bold type, all following equations based on Figure 5.6. Here, $\mathbf{k_1}$ is a unit vector parallel to the direction of propagation and $\mathbf{k_2}$ is a unit vector perpendicular to $\mathbf{k_1}$. $\mathbf{U}$ is the displacement velocity vector. The location vector is $\mathbf{r}$, which represents the position of a point in a space. The longitudinal and transversal wave amplitudes are l_a and t_a. The velocity of the longitudinal wave in the specimen is expressed as c_{lb} and that of the shear wave as c_{tb}.

If a coordinate system similar to Figure 5.6 is given, a wave vector, for the incident

wave $\mathbf{I}$ can be written as:

$$\mathbf{I} = \mathbf{y} \cdot \cos\theta + \mathbf{x} \cdot \sin\theta \tag{5.8}$$

With $\theta < 90°$. The incident wave $\mathbf{I}$, Reflected wave $\mathbf{R}$, Refracted longitudinal wave $\mathbf{T_l}$, Refracted transversal wave $\mathbf{T_t}$ can be written as:

$$\mathbf{I} = (\mathbf{x} \cdot \sin\theta + \mathbf{y} \cdot \cos\theta) \cdot e^{\frac{-i\omega(x_p \sin\theta + y_p \cos\theta - c_{lf}t)}{c_{lf}}} \tag{5.9}$$

$$\mathbf{R} = R(\mathbf{x} \cdot \sin\phi - \mathbf{y} \cdot \cos\phi) \cdot e^{\frac{-i\omega(x_p \sin\phi - y_p \cos\phi - c_{lf}t)}{c_{lf}}} \tag{5.10}$$

$$\mathbf{T_l} = T_p(\mathbf{x} \cdot \sin\beta + \mathbf{y} \cdot \cos\beta) \cdot e^{\frac{-i\omega(x_p \sin\beta + y_p \cos\beta - c_{lb}t)}{c_{lb}}} \tag{5.11}$$

$$\mathbf{T_t} = T_s(\mathbf{x} \cdot \cos\gamma - \mathbf{y} \cdot \cos\gamma) \cdot e^{\frac{-i\omega(x_p \sin\gamma + y_p \cos\gamma - c_{tb}t)}{c_{tb}}} \tag{5.12}$$

Where R_l, T_l and T_t are the magnitudes of the wave amplitudes.

Solving the equations derived from conservation laws gives the following equations for an analytic expression of the wave amplitudes:

The generalised Snells law is:

$$\frac{\sin\theta}{c_{lf}} = \frac{\sin\phi}{c_{lf}} = \frac{\sin\beta}{c_{lb}} = \frac{sin\gamma}{c_{tb}} \tag{5.13}$$

Equations which relating the amplitudes to each other are:

$$(1 - R_a)cos\theta = T_l \cos\beta - T_t \sin\gamma \tag{5.14}$$

$$\rho_f c_{lf}(1 + R_a) = \rho_b c_{lb} T_l \cos 2\gamma - \rho_b c_{tb} T_t \sin 2\gamma \tag{5.15}$$

$$\rho_b c_{tb}(T_l \cos\beta \sin\gamma + T_t \cos 2\gamma/2) = 0 \tag{5.16}$$

The impedances for the different waves can be described as:

$$Z_{lf} = \frac{\rho_f c_{lf}}{\cos\theta} \tag{5.17}$$

$$Z_{lb} = \frac{\rho_b c_{lb}}{\cos\beta} \tag{5.18}$$

$$Z_{tb} = \frac{\rho_b c_{tb}}{\cos\gamma} \tag{5.19}$$

This gives the general reflection factor as:

$$R_f = \frac{Z_{lb}\cos^2 2\gamma + Z_{tb}\sin^2 2\gamma - Z_{lf}}{Z_{lb}\cos^2 2\gamma + Z_{tb}\sin^2 2\gamma + Z_{lf}} \tag{5.20}$$

The reflection factor can be simplified for normal incidence to:

$$R_f = \frac{Z_{lb} + Z_{tb} - Z_{lf}}{Z_{lb} + Z_{tb} + Z_{lf}} \tag{5.21}$$

The transmission factor can be determined when the amplitude of the refracted wave is divided by the one of the incident wave. It is described as:

$$T_f = \frac{2 \cdot (Z_{lb}\cos^2 2\gamma + Z_{tb}t\sin^2 2\gamma)}{Z_{lb}\cos^2 2\gamma + Z_{tb}\sin^2 2\gamma + Z_{lf}} \tag{5.22}$$

It can also be simplified for normal incidence to:

$$T_f = \frac{2 \cdot (Z_{lb}l + Z_{tb})}{Z_{lb} + Z_{tb} + Z_{lf}} \tag{5.23}$$

If the velocities in the solid are greater than the ones in the fluid, there are incident angles θ_1 and θ_2 for which the longitudinal and transversal wave gets completely reflected. This angle for the longitudinal wave is called the first critical angle θ_1. Consequently, the transversal wave gets completely reflected at the second critical angle θ_2. The equations above only hold when $\theta < \theta_1$. Relations in other regions can be found in. [7] The critical angles are [52, 8, 55]:

$$\arcsin\frac{c_{lf}}{c_{lb}} = \theta_1 \tag{5.24}$$

and:

$$\arcsin\frac{c_{lf}}{c_{tb}} = \theta_2 \tag{5.25}$$

With:

c_{lb}	=	Longitudinal sound velocity in specimen	$^m/_s$
c_{lf}	=	Sound velocity in fluid	$^m/_s$
c_{tb}	=	Transversal sound velocity in specimen	$^m/_s$
l	=	Thickness of specimen	m
l_a	=	Longitudinal wave amplitude	$a.u.$

R_f	=	Reflection factor	1
R_l	=	Magnitude of reflected wave amplitude	1
t_a	=	Transversal wave amplitude	$a.u.$
T_f	=	Transmission factor	1
T_l	=	Magnitude of refracted longitudinal wave amplitude	1
T_t	=	Magnitude of refracted transversal wave amplitude	1
x_p	=	Horizontal position	m
y_p	=	Vertical position	m
Z_{lf}	=	Impedance of fluid	$^{kg}/_{s \cdot m^2}$
Z_{lb}	=	Impedance of longitudinal wave in specimen	$^{kg}/_{s \cdot m^2}$
Z_{tb}	=	Impedance of transversal wave in specimen	$^{kg}/_{s \cdot m^2}$
$\mathbf{I}$	=	Vector of incident wave	$a.u.$
$\mathbf{k_1}$	=	Unit vector in direction of propagation	1
$\mathbf{k_2}$	=	Unit vector orthogonal to direction of propagation	1
$\mathbf{R}$	=	Vector of reflected wave	$a.u.$
$\mathbf{r}$	=	Location vector	m
$\mathbf{T_l}$	=	Vector of refracted longitudinal wave	$a.u.$
$\mathbf{T_t}$	=	Vector of refracted transversal wave	$a.u.$
$\mathbf{U}$	=	Displacement velocity vector	$^{m}/_{s}$
β	=	Angle of refracted longitudinal wave	$degree$
γ	=	Angle of refracted transversal wave	$degree$
ϕ	=	Angle of reflected transversal wave	$degree$
θ	=	Angle of incidence	$degree$

5.4.2. Determination of the Transversal Wave Velocity using Reflected Waves

A solution which is called the ultrasound critical-angle reflectometry has been investigated by Antich. [7, 8] It measures the critical angles of bones and derives the velocity of the longitudinal as well as the velocity of the shear wave by using equation (5.24) and equation (5.25). This solution requires the ultrasonic transducer to be placed in the path, where the reflected waves should propagate. Ultimately, the angle of incidence is the same as the angle of reflection. During the measurement, the angle has to be shifted for each measurement step in order to determine the critical angles.

Measuring the phase and the amplitude over the incident angle gives the critical angles, as it can be seen in Figure 5.7 and 5.8. In these figures, equations taken from Antich [7] have been used to create a numerical simulation in which the values c_{lb}, c_{tb} and c_{lf} have been chosen to match the data in the experiment.

Figure 5.7 shows the real part of the reflected amplitude as it is measured in the experiment (full curve) and calculated in the simulation (broken curve). Here, the first critical angle θ_1 can be spotted at the first peak of the wave amplitude which is followed by an abrupt drop. It has to be noted that Antich only spotted one longitudinal wave, contrary to Biot's theory.

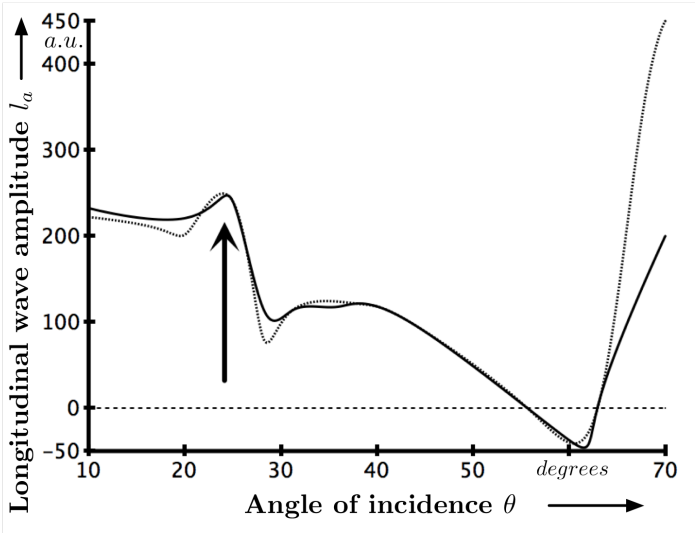

Figure 5.7.: Reflected wave amplitude over incident angle [7]

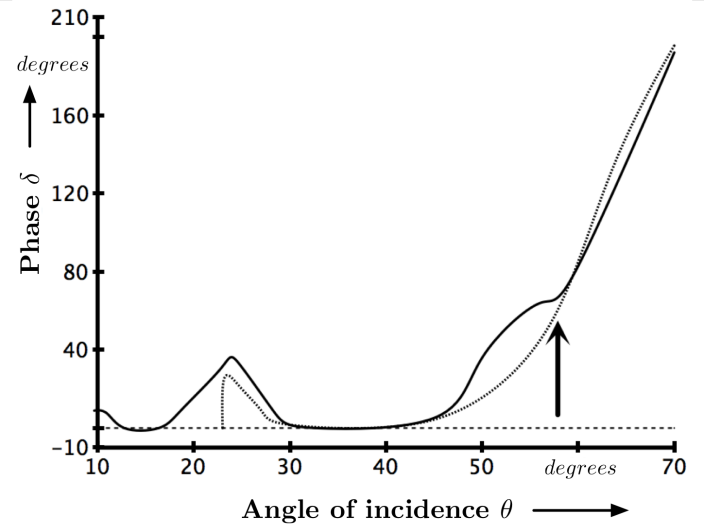

Figure 5.8.: Reflected wave phase over incident angle [7]

Figure 5.8 shows the phase spectrum of the reflected wave as it is measured in the experiment (full curve) and calculated in the simulation (broken curve). Here, the second critical angle θ_2 can be spotted where its phase rises rapidly after it passes through a 90° phase shift. This corresponds to the minimum in the amplitude spectrum as it can be seen in Figure 5.7.

The velocities of the longitudinal and the shear wave can be obtained through the equations (5.24) (5.25).

Antich used $0,7$ degrees as an angle resolution. Therefore, this process requires a lot of time. Figure 5.9 shows the measurement setup.

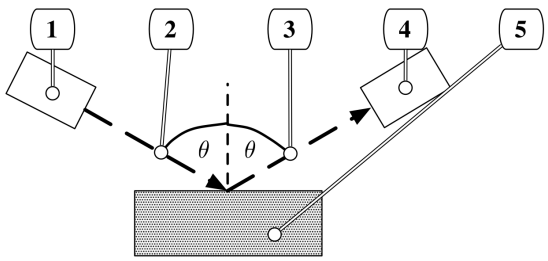

1 : *Emitter*
2 : *Longitudinal incident wave*
3 : *Longitudinal reflected wave*
4 : *Receiver*
5 : *Specimen*

Figure 5.9.: Measurement of critical angles to determine transversal wave velocity

This approach requires the sound speed in the specimen for the longitudinal wave c_{lb} as well as the one for the transversal wave c_{tb} to be greater than in the fluid c_{lf}. More exact, since the incident angle has to be less than $90\,°$, this approach is only valid for $c_{lf} < c_{tb}\sqrt{2}$ This can be critical according to velocity predictions made in Chapter 6.

5.4.3. Determination of the Transversal Wave Velocity using Refracted Waves and Shifting Wave Patterns

The method of shifting wave patterns uses the refracted transversal wave inside the specimen. The method is also applicable to measure the longitudinal velocity and transversal wave attenuation. It has been described by Waterman [89, 90] and uses a rotating plate measurement taken from Maeda [60] , Bär and Walti. [12]

If a specimen is inserted into the beam path, the wave pattern of the received wave shifts. This has been previously visualized in Figure 5.2. By moving the transmitter, the wave pattern can be returned to its original position. The velocities can be determined measuring the distance that the transmitter has to be moved.

If the sample is mounted perpendicular to the beam, the longitudinal velocity in the

specimen c_{lb} can be determined using the equation:

$$c_{lb} = \frac{c_{lf} \cdot l}{l - e} \tag{5.26}$$

If the transversal velocity has to be determined, the specimen is turned at an angle larger than the total reflection of the longitudinal wave. This can be determined using equation (5.24). The wave pattern then shifts and is returned to its original position by distance e. The equation is:

$$c_{tb} = \frac{c_{lf} \cdot l}{l \cos(\theta - \gamma) - e \cos\gamma} \tag{5.27}$$

or:

$$c_{tb} = \frac{c_{lf} \cdot l}{\sqrt{l^2 + e^2 - 2le\cos\theta}} \tag{5.28}$$

As described in Subsection 5.3.1, the waves amplitudes can change due to frequency dependent attenuation. This creates difficulties to set a correct marker for the measurement. However, Waterman stated that adjusting the attenuator to the same pulse height minimizes this effect. Moreover, when the velocities of the sample and the coupling fluid are strongly different and the adjustment of pulse height is not sufficient, an iteration method can be used.

In this process, the sample is turned to an angle larger than the total reflection of the longitudinal wave, until a peak in the waves group faces a given time mark. Afterwards, the specimen is turned to larger angles, until the same peak faces the nearest time mark. Using iteration γ_1, γ_2 and c_{tb} can be found with:

$$\frac{\sin\theta_1}{\sin\gamma_1} = \frac{c_{lf}}{c_{tb}} \tag{5.29}$$

$$\frac{\sin\theta_2}{\sin\gamma_2} = \frac{c_{lf}}{c_{tb}} \tag{5.30}$$

$$c_{tb} = \frac{c_{lf} \cdot l(\cos\gamma_1 - \gamma_2)}{l[\cos\gamma_1 \cos(\theta_2 - \gamma_2) - \cos\theta_2 \cos(\theta_1 - \gamma_1)] - 10^{-6} c_{lf} \cos\gamma_1 \cos\gamma_2} \tag{5.31}$$

The derivations of the equations above can be found in Waterman [89]. Similar to the method in Subsection 5.4.2, this one can only be used for incident angles $\theta \leq 1$ and therefore only for $c_{lf} < c_{tb}\sqrt{2}$. This requirement can be critical according to Chapter 6.

With:

$c_{lb}(\omega)$	=	Longitudinal phase velocity in specimen	$^m/_s$
c_{lf}	=	Sound velocity in fluid	$^m/_s$
$c_{tb}(\omega)$	=	Transversal sound velocity in specimen	$^m/_s$
e	=	Distance to return wave patterns	m
l	=	Thickness of specimen	m
γ	=	Angle of refracted transversal wave	$^\circ$
θ	=	Angle of incidence	$^\circ$

5.4.4. Determination of the Transversal Wave Velocity using Refracted Waves, Convertion Position

Both approaches in Subsection 5.4.2 and 5.4.3 have critical requirements about the velocity in the fluid being less than the longitudinal and transversal velocity in the solid. Chapter 6 will reveal that, whichever fluid is used, these requirements might not be able to be fulfilled. Therefore, another approach has to be found.

To the knowledge of the researcher of this dissertation, this approach has never been used before. It measures the convertion position of the transversal to the longitudinal wave at the rear surface of the specimen. From trigonometrical relations, the transversal wave velocity can be obtained. The process is explained as follows.

If a longitudinal wave with a refraction angle β travels through the sample and hits the rear surface of the specimen (the one from solid to fluid), its refraction angle behaves conversely. This leads to a propagating wave after the specimen, which travels parallel to the incident wave. Figure 5.10 describes that behaviour:

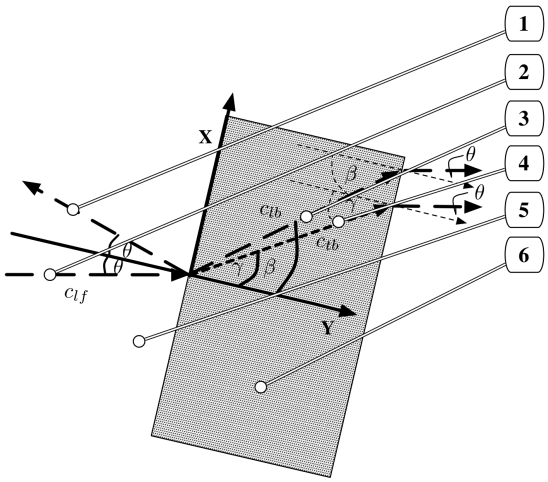

1 : *Reflected wave*

2 : *Incident wave*

3 : *Refracted longitudinal wave*

4 : *Refracted transversal wave*

5 : *Fluid*

6 : *Solid*

Figure 5.10.: Refraction at second surface of specimen in transmission measurements

The same behaviour can be assumed for the transversal wave as shown above. A transversal wave cannot propagate in the fluid, only its longitudinal component creates another longitudinal wave. This behaviour exists only when the angle of incidence is not perpendicular to the rear surface of the specimen. The process of wave convertion is described in Figure 5.11

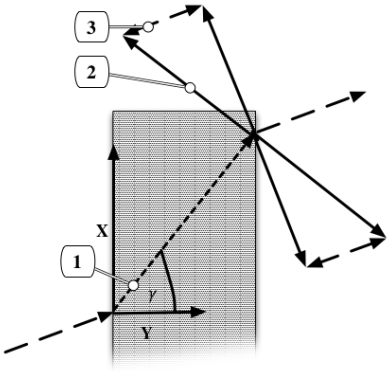

1 : *Transversal wave*

2 : *Transversal oscillating particles*

3 : *Longitudinal oscillating vector*

Figure 5.11.: Creation of a longitudinal wave out of a transversal wave at the rear surface of the specimen

The longitudinal wave will be totally reflected to avoid measuring an interfering wave. Following Achenbach [2], the longitudinal wave in a solid is expected to have higher velocities than the transversal wave. If the angle of incidence θ is higher than θ_1,

total reflection occurs and the longitudinal wave is no longer transmitted into the solid. Turning the specimen to angles larger than θ_1 will lead to a transversal wave measurement, where the longitudinal wave inside the specimen does not have to be considered, similar to Subsection 5.4.3. The idea is therefore, to first evaluate the speed of sound for the two longitudinal waves and thereafter turn the specimen to an angle larger than the first critical angle in equation (5.24). The only longitudinal wave which can still propagate into the fluid after the specimen, will be the one which is created out of the converted transversal wave. It can be seen from Figure 5.11 that the longitudinal wave which gets created, will have larger amplitudes when the angle θ is close to the second critical angle given in (5.25). This will lead to better signal to noise ratios. The setup can be seen in Figure 5.12.

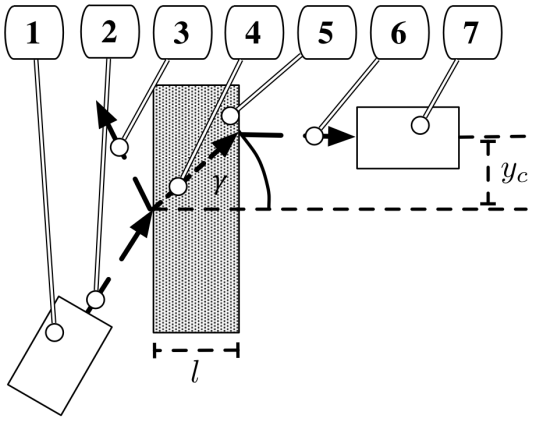

1 : *Emitter*
2 : *Emitted longitudinal wave*
3 : *Reflected longitudinal wave*
4 : *Refracted transversal wave*
5 : *Specimen*
6 : *Second longitudinal wave*
7 : *Receiver*

Figure 5.12.: Measurement of the convertion position y, to determine transversal wave velocity

The determination of the position, where the wave convertion occurs, is derived from acoustic antenna measurements. A description can be found in Section 7.5. After the position of wave convertion y is obtained, the transversal wave velocity can be given using trigonometric relations and Snells law with:

$$c_{tb} = \frac{c_{lf} \cdot \sin\left(\frac{y_c}{l}\right)}{\sin\theta} \tag{5.32}$$

Contrary to other measurement procedures in Subsection 5.4.2 and 5.4.3, this method has the advantage that only the longitudinal waves need to have a higher sound velocity

in the fluid than in the solid. According to sound velocity predictions in Chapter 6, this will be possible for a large range of materials using a special gas as a coupling fluid.

With:

c_{lb}	=	Sound velocity in fluid	$^m/_s$
c_{tb}	=	Transversal wave velocity	$^m/_s$
l	=	Specimen thickness	m
y_c	=	Vertical position of wave convertion	m
θ	=	Incident angle	$degree$

5.5. Determination of the Loss Factor in Ultrasonics

The loss factor is related to the complex modulus E^* with:

$$E^* = E' + E'' \tag{5.33}$$

The loss module E'' is related to the loss factor η with:

$$E'' = E' * \eta \tag{5.34}$$

Following Section 4.2, the loss factor can be determined using equations (4.18) and (4.19). Hugh [42] used the equation (4.18) and replaced the general modulus M with the longitudinal modulus L and therefore c_{lf} with c_{lb}, which gives:

$$\tan(\delta) = \eta = \frac{L''}{L'} = 2c_{lb}\alpha\frac{\omega}{\omega^2 - c_{lb}^2\alpha} \tag{5.35}$$

$$\tan(\delta) = \eta = \frac{L''}{L'} = 2\frac{c_{lb}\alpha}{\omega} = \frac{\alpha\lambda}{\pi} \qquad \text{when} \qquad \frac{\alpha c_{lb}}{\omega} \ll 1 \tag{5.36}$$

This solution is sufficient for the measurement system proposed here and is also described by Garibaldi *et. al.* [33].

The attenuation coefficient can be determined using the difference between the incident and received pressure amplitudes or the intensities respectively [55, 42]:

$$p_r = p_e * e^{-\alpha * z} \tag{5.37}$$

$$I_r = I_e * e^{-2\alpha * z} \tag{5.38}$$

Solving these equations to the attenuation coefficient gives:

$$\alpha = -\frac{ln(\frac{p_r}{p_e})}{z} \tag{5.39}$$

or:

$$\alpha = -\frac{ln(\frac{I_r}{I_e})}{2z} \tag{5.40}$$

The slope of attenuation described by the attenuation coefficient, does not have to remain steady through the frequency range. To take this into account, the equations can also be described in terms of frequency:

$$\alpha(\omega) = \frac{1}{z} * ln\frac{p_r(\omega)}{p_e(\omega)} \tag{5.41}$$

Reflections occurs at the specimen boundaries as well as attenuation when the ultrasonic wave propagates through the fluid. This behaviour is described in Figure 5.13, where the decrease in longitudinal pressure amplitude is shown linear for simplicity:

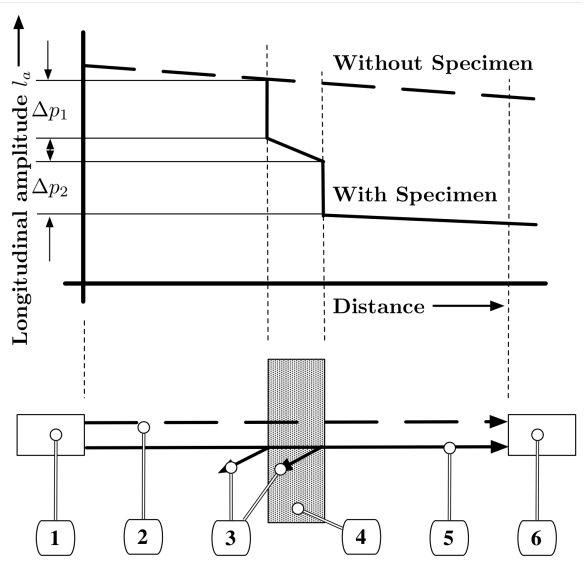

1 : *Emitter*
2 : *Longitudinal wave in fluid*
3 : *Longitudinal reflected wave*
4 : *Specimen*
5 : *Longitudinal wave with specimen*
6 : *Receiver*

Figure 5.13.: Decrease in pressure amplitude due to specimen attenuation, reflection at specimen surface and propagation through a coupling fluid

Therefore, attenuation coefficients of the coupling fluid will have to first be determined. Furthermore, the reflected pressure amplitudes from the first and second specimen borders will have to be evaluated. Since a plain wave cannot be assumed, especially in the near field range of the transducers [52], the pressure amplitudes for the measurement in the fluid will have to be conducted at several distances.

The reflection of the first specimen border can be measured using the ultrasonic emitter as a receiver. The second surface reflection can also be measured. however, it also has to cross the first border. This makes measurements impractical.

It is possible to circumvent the measurement of the second surface reflection by using the ratio of the reflected to the incident acoustic pressure amplitude. This is described by the reflection coefficient R_f, which is defined earlier as [7, 55, 52]:

$$R_f = \frac{Z_{lb} + Z_{tb} - Z_{lf}}{Z_{lb} + Z_{tb} + Z_{lf}} \tag{5.42}$$

Z_{lb}, Z_{lf} and Z_{tb} are the characteristic impedances for the media which are defined as described in Subsection 5.4.1. However, in this case the incident angles do not have to be considered.

$$Z_{lf} = \rho_f c_{lf} \tag{5.43}$$

$$Z_{lb} = \rho_b c_{lb} \tag{5.44}$$

$$Z_{tb} = \rho_b c_{tb} \tag{5.45}$$

The reflection coefficient R_f is the same at the first specimen border $x1$ and at $x2$. Therefore, measuring the received pressure amplitude p_r and using the transmitted pressure amplitude with $T + R = 1$, will lead to Δp_2. Consequently, the reflection at the rear specimen surface will not have to be measured.

With:

c_{lb}	=	Longitudinal wave velocity	$^m/_s$
c_{lf}	=	Sound velocity in fluid	$^m/_s$
c_{tb}	=	Transversal wave velocity	$^m/_s$

E'	=	Dynamic Young's modulus	Pa
E''	=	Loss Young's modulus	Pa
E^*	=	Complex Young's modulus	Pa
I_e	=	Acoustic intensity of emitted sound	W/m^2
I_r	=	Acoustic intensity of received sound	W/m^2
L'	=	Dynamic longitudinal modulus	Pa
L''	=	Loss longitudinal modulus	Pa
p_e	=	Emitted pressure amplitude	Pa
p_r	=	Received pressure amplitude	Pa
R_f	=	Reflection factor	1
z	=	Length of ultrasonic path	m
Z_{lb}	=	Impedance in specimen for longitudinal wave	$kg/s \cdot m^2$
Z_{tb}	=	Impedance in specimen for transversal wave	$kg/s \cdot m^2$
Z_{lf}	=	Impedance in fluid	$kg/s \cdot m^2$
α	=	Attenuation coefficient	$1/m$
η	=	Loss factor	1
λ	=	Wavelength of ultrasonic wave	m
ω	=	Angular frequency	rad/s
ρ_b	=	Density of specimen	kg/m^3
ρ_f	=	Density of fluid	kg/m^3
δ	=	Loss angle	$degree$

Attenuation in porous media occurs due to [55]:

- Viscous friction effects, in this case between the relative motions of the fluid and the matrix,
- Scattering because of inhomogenities, and

- Conversation losses from longitudinal to shear wave modes.

There are limitations in measuring the loss factor with ultrasonics since scattering occurs. It results from the interaction between an ultrasonic wave at boundaries of particles. This occurs when the oscillatory movement of scatterers are different from their surrounding medium. This creates a scattered wave and ultimately leads to more attenuation. It ultimately results in non-specular reflections. Scattering can be visualised as a sound wave passing an edge of a rigid wall. This wall has to be small compared to the wavelength. The process is shown in Figure 5.14. There, the decrease in pressure amplitude does not show an abrupt drop. Instead, there is a "shadow" which leads to a smooth decrease to zero. Furthermore, fluctuations can be seen resulting from scattered waves. [52]

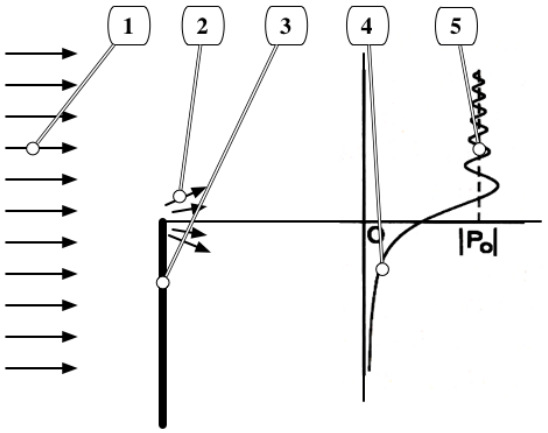

1 : *Transversal wave*

2 : *Transversal oscillating particles*

3 : *Longitudinal oscillating vector*

Figure 5.14.: Scattering of a plain sound wave at the straight edge of a rigid wall [52]

Scattering is dependent on the wavelength compared to heterogenities. If λ is much smaller than the heterogenities, the laws of reflection hold. [55] In order to achieve exact results, the measurement frequency to determine the loss factor should be rather high. The same applies for the measurement of the transversal wave with approaches described in Section 5.4.

5.6. Summary

The description about the evaluation of general parameters is provided in this chapter, as well as the ones for parameters which have to be investigated using ultrasonics.

The general parameters can be investigated using well known approaches. Whereas adaptions have to be made using the ultrasonic techniques to measure the longitudinal and transversal velocity.

Research in the field of medical techniques revealed that a transmission measurement is sufficient in investigating longitudinal velocity. However, it is important to measure the phase velocity, since damping materials are expected to show a dispersive behaviour. Furthermore, two longitudinal waves are expected in a porous material, see Section 5.3. There, the slow longitudinal wave can be neglected because it can be considered not to be able to create a motion in the heavier frame. The two waves can cause measurement errors when they interfere. However, Bayesian calculations have been reported to successfully divide the two waves.

Several transversal wave measurements are possible which do not require the transducers to be bonded directly on the sample. This is the only way to not compress or affect the specimen with unknown stresses. However, all reported approaches so far require the longitudinal wave velocity as well as the transversal velocity to be faster in the solid than in the fluid. This can be critical according to Section 6.2. Therefore, a new approach is presented which only requires the longitudinal velocity inside the specimen to be faster than in the fluid.

The loss factor is determined using a transmission measurement. It can be evaluated by measuring the overall decrease in amplitude. At the same time, the decrease of pressure amplitude through the fluid as well as the reflected pressure amplitudes have to be determined.

6 Investigations of the Test Rig

6.1. Introduction

The purpose of this chapter is to predict the sound speed in a solid in order to account for the transversal measurements presented in Section 5.4. Furthermore, a coupling fluid with the lowest sound speed as possible had to be found. In addition, calculations of the recommended frequency range of the measurement system will be undertaken. Moreover, general measurements on a range of damping materials will be conducted. Finally, materials as well as the structures for the test rig will be investigated.

6.2. Prediction of the Sound Speed in the Specimen

The approaches in Section 5.4 for measuring the transversal wave velocity, emphasize the need of the wave velocity in the fluid to be less than in the solid. Therefore, the sound speed in the specimen has to be predicted.

In order to calculate the sound speed which is expected in the foams and nonwoven materials, data for the Young's modulus has been gathered from manufacturers. Depending on where the parts are used, their Young's modulus E_b is expected to vary between: $50000\,Pa$ and $200000\,Pa$. This is also stated by Ogam. [75] The Poisson's ratio ν has been chosen to vary between $0,40$ and $0,48$. [75] However, a large variety of Poisson's ratios exist depending on materials and their cell structures. [35] The porosity of the materials f_v are expected to be in the range of $0.8 - 0,97$, see [75] and Table

6.2. Depending on the material, the density of the solid skeleton ρ_s is expected to vary between $200 - 1400\,{}^{Kg}/_{m^3}$. This was calculated out of foam densities ρ_b and their porosities f_v, taken from [75] and from Table 6.2.

Combining the equations (2.26),(4.23),(4.25) and converting the result to c_{lb}, gives a rough prediction, without taking into account dispersion, of the sound speed of the longitudinal wave:

$$c_{lb} = \sqrt{\frac{E_b}{(1-f_v)\cdot\rho_s\cdot 3(1-2\cdot\nu)} + \frac{4\cdot N_b}{3\cdot(1-f_v)\cdot\rho_s}} \tag{6.1}$$

Simulations have been made with the software Maple 17, resulting in Figure 6.1. In this program, the porosity f_v, Poisson's ratio ν_b and density of the elastic solid ρ_s can be adjusted in the given range to see the influences of the parameters:

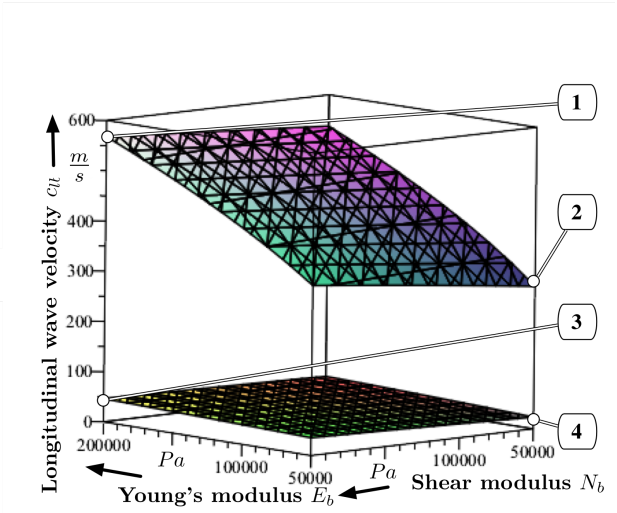

1 : *Highest longitudinal velocity setup A*

2 : *Lowest longitudinal velocity setup A*

3 : *Highest longitudinal velocity setup B*

4 : *Lowest longitudinal velocity setup B*

Figure 6.1.: Prediction of the velocity from the fast longitudinal wave inside the specimen over a range of Young's and shear modulus with settings revealing extreme velocities

The setups A and B are displayed in Figure 6.2:

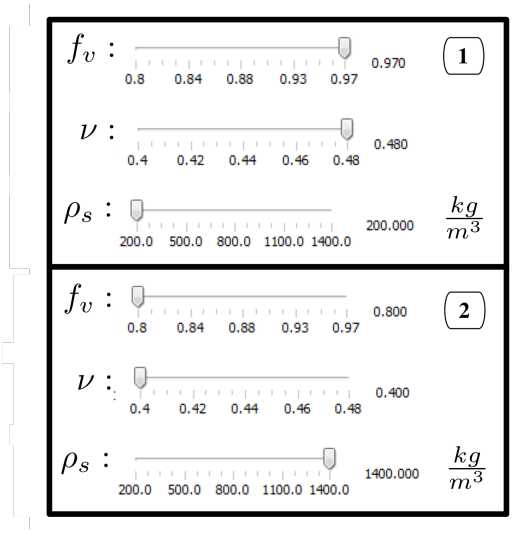

1 : *Setup A for longitudinal velocity*

2 : *Setup B for longitudinal velocity*

Figure 6.2.: Setup A and B for the fast longitudinal velocities

The fast longitudinal velocity reaches up to $570\,{}^{m}/_{s}$ for high porosities and Poisson's ratios with a low density material. On the other hand, for materials with small porosities, low Poisson's ratios and high density materials, the longitudinal wave velocity reaches up to $50\,m/s$.

The transversal wave velocity can be predicted using the equation (4.25) described by Bourbie and Sebaa [17, 80]:

$$c_{tb} = \sqrt{\frac{N_b}{(1 - f_v) * \rho_s}} \tag{6.2}$$

With:

c_{lb}	=	Longitudinal wave velocity	${}^{m}/_{s}$
c_{tb}	=	Transversal wave velocity	${}^{m}/_{s}$
E_b	=	Young's modulus of specimen	Pa
f_v	=	Porosity	1
N_b	=	Shear modulus of specimen	Pa
ν	=	Poisson's ratio	1
ρ_s	=	Density of solid	${}^{kg}/_{m^3}$

The same specimen properties according to setup A and B have been chosen for the simulation of the transversal wave. However, the respective equation does not require information about the Poisson's ratio. Furthermore, the shear modulus would normally be expected to be less than the Young's modulus. In Figure 6.3 however, it is computed in the same range.

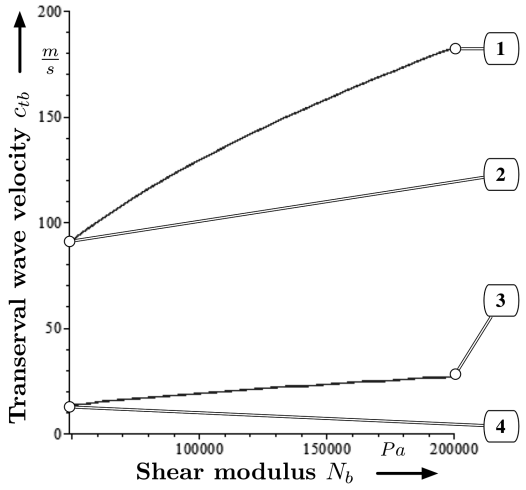

1 : *Highest transversal velocity setup A*

2 : *Lowest transversal velocity setup A*

3 : *Highest transversal velocity setup B*

4 : *Lowest transversal velocity setup B*

Figure 6.3.: Prediction of the velocity from the transversal wave inside the specimen over a range of shear modulus with settings revealing extreme velocities

It can be seen that the transversal velocity is very low, even with the same values for the shear modulus as the Young's modulus. For Setup A, it reaches up to 180 $^{m}/_{s}$, whereas for setup B it would only reach up to 13 $^{m}/_{s}$.

Both waveforms can have a large spread of velocity depending on the respective specimen parameters. Low velocities inside the specimen can be problematic when transversal wave measurements are conducted according to Section 5.4. These approaches require at least the longitudinal wave to have a lower velocity in the specimen than in the surrounding fluid.

6.3. Investigation of the Coupling Fluid

Since the approaches to measure the transversal velocity with refracted or reflected ultrasonic waves require the speed of sound to be less in the fluid than in the solid, a fluid with a low speed of sound has to be found.

Water has a sound speed velocity of 1484 $^{m}/_{s}$ and air of 343,2 $^{m}/_{s}$, both calculated at 20 °C. Therefore, they are not suitable as a coupling fluid. Gases have in general a lower sound speed velocity as liquids. Consequently, a gas has to be found which is safe and easy to use and most importantly fits the requirement of the lowest sound speed as possible.

To investigate a gas which is suitable for the measurement system, its velocity over temperature can be calculated using the equation for ideal gases:

$$c_{lf} = \sqrt{\kappa \frac{R * T}{M}} \tag{6.3}$$

Where:

$$\kappa = \frac{c_p}{c_v} \tag{6.4}$$

With:

c_{lf}	=	Sound velocity in fluid	$^{m}/_{s}$
c_p	=	Heat capactiy at constant pressure	$^{J}/_{mol \cdot K}$
c_v	=	Heat capactiy at constant volume	$^{J}/_{mol \cdot K}$
M	=	Molar mass	$^{kg}/_{mol}$
R	=	Universal gas constant	$^{J}/_{mol \cdot K}$
T	=	Absolute temperature	K
κ	=	Adiabatic index	1

Gases which have been computed in terms of their velocity over a temperature range from $270 - 320\,K$ at an absolute pressure of 101,325 Pa or 1 atm can be found in the

Appendix A. They have been computed using the NIST database. [70] Gases which are suitable as a fluid for applications in this measurement system are presented in Table 6.1.

Gas (CAS number)	Bp in $°C$	c_{lf} in $^{m}/_{s}$	Hazards	ρ_f in $^{kg}/_{m^3}$
Decafluorobutane (355-25-9)	-2	100	Xi	10,4
Dodecafluoropentane (678-26-2)	29	90,5 (32 $°C$)	Xi	12,25 (32 $°C$)
Sulfur hexafluoride (2551-62-4)	-64	134	-	6,15
Chloropentafluoroethane (R115) (76-15-3)	-39	128	Xi	6,5
Octafluorocyclobutane (RC318) (115-25-3)	-6	110	Xi	8,6
1,1,1,3,3,3-Hexafluoro-propane (R236fa) (690-39-1)	0	127	Xi	6,5
1,1,1,2,3,3-Hexafluoro-propane (R236ea) (431-63-0)	6,5	126	Xi	6,6
1,1,1,2,3,3,3-Heptafluoro-propane (R227ea) (431-89-0)	-16,4	120	Xi	7,4
Octafluoropropane (R218) (76-19-7)	-39	114	Xi	8

Table 6.1.: Suitable gases and their properties, [70, 87, 1] temperature dependent values are calculated at 20 $°C$ if not marked differently

The gas which is going to be used on the measurement system firstly, will be Sulfurhexafluorid. It is nontoxic and chemically inactive. Due to its high insulating properties, it is used in high-voltage applications. Moreover, it can be used as contrast agent for ultrasonics. [84] For specimens which require a lower sound speed velocity in the fluid, Decafluorobutane will be used. The gas is colourless and relatively inert. It is

currently used as an extinguishing agent. Toxicologic tests conducted by several researchers showed, that it cannot be classified as genotoxic. [10] If a measurement with the gases mentioned above does not lead to sufficient results, the measurement chamber can be heated. Therefore, Dodecafluoropentane can be used. The investigated specimens and the measurement chamber have to prove that they do not get affected by the irritant gases, which is not part of this dissertation.

Sulfurhexafluorid as well as Decafluorobutane and Dodecafluoropentane have a high global warming potential. [26] An emission of these gases lead to a photochemical degradation in the upper stratosphere. This increases the warming potential of the atmosphere. Consequently, the measurement chamber has to include a cycle in which less gas volatilizes. This concept is carried out in Chapter 8.

Within the parameter range of interest, the effect of the material density range on the inner sound speed of the specimen, taken from Section 6.2, is higher compared to the other parameters. Taking that into account, only the PET nonwoven materials (parameters taken from Table 6.2 have a very low expected sound velocity inside the specimen. Therefore, some PET nonwoven materials might not be able to be measured in the system proposed in this dissertation. This is dependent on the other parameters, Poisson's ratio, porosity, Young's and shear modulus. When the inner sound speed velocity of the transversal wave is low, the safest approach to measure transversal velocity is given in Subsection 5.4.4. With this method, only the longitudinal wave has to be totally reflected and therefore only the longitudinal wave needs to have a higher velocity inside the specimen than in the fluid. This requirement can be fulfilled with Sulfurhexafluid and Decafluorobutane as well as Dodecafluoropentane for a large range of materials partially excluding the PET nonwoven materials.

6.4. Measurement Frequency Range and Additional Measurements for Young's Modulus Determination

Allowed Frequency Range f: The assumptions of equations (4.23) and (4.25) only hold for a homogeneous isotropic and porous medium in which bulk waves propagate. [2, 76, 55] This can be assumed, as long as the wavelength of the ultrasonic wave λ is much smaller than the smallest dimension of the specimen. The smallest dimension of a disc shaped specimen is its thickness. Furthermore, the pore sizes of the specimen, heterogenities, is important. It can be roughly determined by using a microscope. To assume a homogeneous medium, its pore size should be much smaller than its wavelength, see Section 4.2. This gives the measurement frequency range of:

$$l >> \lambda >> s \tag{6.5}$$

To determine the pore sizes of the specimens, the SEM from Section 2.3 is used. Consequently, the same conductivity procedures apply.

Density of Elastic Solid ρ_s and Porosity f_v: In equation (4.23), the density of the elastic solid influences the specimen's bulk and therefore its Young's modulus. It is given by the manufacturers of the foam or the nonwoven material. The porosity of the specimen can be determined with equation (5.1) described in Section 5.2:

$$f_v = 1 - \frac{\rho_b}{\rho_s} \tag{6.6}$$

With:

f_v	=	Porosity	1
l	=	Thickness of specimen	m
s	=	Pore size of specimen	m
λ	=	Wavelength of ultrasonic wave	m
ρ_b	=	Density of specimen	kg/m^3
ρ_s	=	Density of solid	kg/m^3

To determine the density of the specimens, their volume and weight was measured. The precision scale which was used for that purpose is the Swiss Quality Precisa 205A. It is displayed in Figure 6.4.

Figure 6.4.: BASF Basotect®V melamine foam on the precision scale

Specimens from several suppliers have been investigated with equations above to calculate their allowed frequency range, porosity and densities:

- Melamine foams (BASF, Basotect®)
- PET nonwoven materials (Sandler, Sawaform)
- PUR foam carpet (BASF)

The results of the measurements are presented in Table 6.2

Specimen	s in ym	l in mm	f in kHz	ρ_s in kg/m^3	ρ_b in kg/m^3	f_v
S.form 4676-1000-12	450	12	51,667-344,444	1380	83,33	0,940
S.form 4676-1000-15	430	15	41,333-360,465	1380	66,67	0,952
S.form 4676-1000-7	500	7	88,571-310,000	1380	142,86	0,896
S.form 4676-1000-10	400	10	62,000-187,500	1380	100,00	0,928
S.form 4676-2000-8	248	8	77,500-625,000	1380	250,00	0,819
S.form 4676-2000-10	521	10	62,000-297,505	1380	200,00	0,855
S.form 4676-2000-15	390	15	41,333-397,436	1380	133,33	0,903
S.form 3072-2000-11	255	11	56,364-607,843	1380	181,81	0,868
S.form 3072-1000-18	393	18	34,444-394,402	1380	55,55	0,960
S.form ac+ 3077-600	390	10	62,000-397,436	1380	60,00	0,957
S.form ac+ 3077-800	300	12	51,667-516,667	1380	66,67	0,952
S.form ac+ 3077-1000	570	14	44,286-271,930	1380	71,43	0,948
Melamine Basotect V	300	29	21,379-516,667	267	10,27	0,959
Melamine Basotect G	210	12	51,667-738,095	267	9,33	0,965
Melamine Basotect UF	234	14	44,286-662,393	267	9,87	0,963
PUR Foam Carpet	681	8	77,500-227,606	705	28,20	0,960

Table 6.2.: Properties of investigated damping materials

The values for the frequency range were calculated for the Young's modulus measurement by doubling or dividing the allowed wavelength borders by two, depending if the border was influenced by pore size or specimen thickness. Therefore, the much smaller or much larger requirement for the wavelength is fulfilled. The velocity inside the specimen is strongly dependent on its elastic properties. It was chosen to be in the middle range as calculated in Section 6.2, with $310\,^m/_s$.

As it can be seen in Table 6.2, the thickness of common specimens limits the lower

measurement frequency to 88,571 kHz for damping materials of 7 mm thickness. The pore sizes limits the allowed frequency to 227,606 kHz for the PUR foams.

Measuring sound velocities would require the measurement frequency close to the audible frequency range due to viscoelasticity. Furthermore, the damping of ultrasonic waves increases at higher frequencies for many propagating media. [3, 81, 29, 86] This might lead to uninterpretable measurements of the transversal wave velocity described in Subsection 5.4.4, due to poor signal-to-noise ratios. However, the approaches to measure transversal wave velocities using reflection and refraction laws need higher frequencies to account for scattering. Moreover, longer wavelengths leads to less spatial resolution. [55] The measurement of the loss factor also needs higher frequencies to reduce the influence of scattering, see Section 5.5. Therefore, the chosen frequency range might have be shifted upwards close to the upper allowed frequency border.

Consequently, the measurement should be taken out for different frequencies starting at approximately 50 kHz upwards. An idea is to find relations of the frequency dependence of all parameters which have to be investigated using ultrasound. Therefore, a measurement in the higher frequency range can be taken out with less influence of scattering. The values for the high frequency range could thereafter be corrected to reduce the influence of frequency dependent parameters.

6.5. Damping and Insulation of the Measurement Chambers

The measurement chambers in which the ultrasonic measurements will be taken out are damped, in order to avoid standing waves or measurement faults resulting from reflected ultrasonic waves.

In this case, the intensity of the reflected sound has to be as low as possible. The solution is found close to the construction of free field measurement chambers in acoustics using porous viscoelastic materials. These are attached to the wall for damping pur-

poses as can be seen in Figure 6.5. It has to be noted that free field chambers are only used within the audible frequency range of $20\,Hz$-$20\,KHz$. The same guidelines are applied in this dissertation since no information can be given for the ultrasonic range.

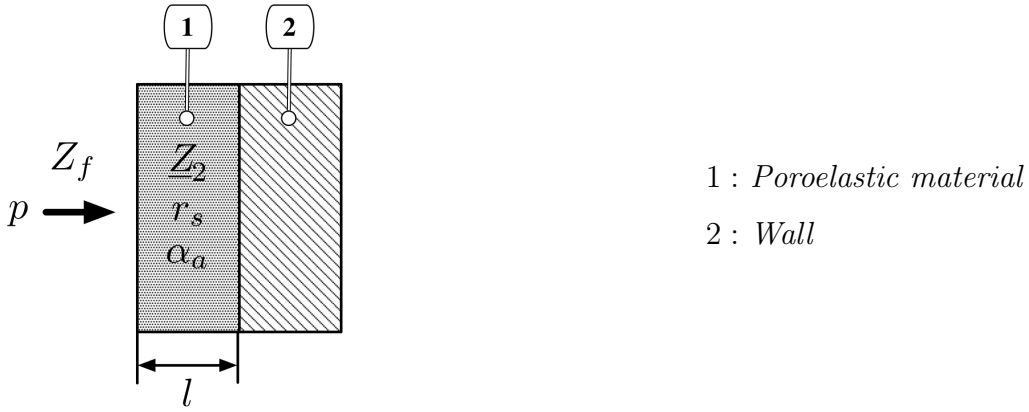

Figure 6.5.: Damped wall with porous viscoelastic material

The dissipation effect of a porous viscoelastic material is dependent on its resistance. This implies that high velocities inside the material are required with small pores. However, this resistance cannot be made as big as possible because the high impedance of the poroelastic material will lead to a higher reflection. Thus, for good absorption an optimal flow resistance is required.

Parameters which have to be set up for the optimal absorber are:

- Complex wall impedance $\underline{Z}_2$,
- Length specific flow resistance r_s,
- Thickness of absorber l, and
- Sound absorption coefficient α_a.

According to Hemm [38], the complex wall impedance $\underline{Z}_2$ should be times 1-2 of the impedance of the fluid which can be calculated with:

$$Z_f = \rho_f * c_{lf} \tag{6.7}$$

The density of the tested BASF Basotect®melamine foam is close to $10\,{}^{kg}/_{m^3}$ and its porosity is 0,96, see Section 6.4. This leads to a longitudinal velocity of about 200-360 ${}^{m}/_{s}$, depending on the Poisson's ratio. The complex wall impedance being 1-2 times larger than in the fluid, should therefore be fulfilled for the most gases in Table 6.1.

The length specific flow resistance r_s should be in the range of [27]:

$$5\,{}^{kNs}/_{m^4} < r_s < 50\,{}^{kNs}/_{m^4} \tag{6.8}$$

The length specific flow resistance of Basotect®melamine foam is between 8-20 ${}^{kNs}/_{m^4}$, according to BASF. [13] This fulfills the aforementioned requirement.

The thickness of the absorbing material l should be adjusted on the highest possible wavelength with:

$$l > \frac{\lambda}{4} \tag{6.9}$$

The lowest frequency is assumed to be at the beginning of the ultrasonic range at 20 kHz. The highest velocity in the fluid can be assumed to be the one in air at 20°C with 343,2 ${}^{m}/_{s}$. This gives the required thickness of the damping material to be larger than 4,3 mm.

The following equation applies for the intensity of the absorbed sound I_a, the intensity of the sound incidence I_i and the absorption coefficient α:

$$\alpha_a = \frac{I_a}{I_i} \tag{6.10}$$

With:

c_{lf}	=	Sound velocity in fluid	${}^{m}/_{s}$
I_a	=	Acoustic intensity of absorbed sound	${}^{W}/_{m^2}$
I_i	=	Acoustic intensity of incidence sound	${}^{W}/_{m^2}$
l	=	Thickness of absorber	m
r_s	=	Length specific flow resistance	${}^{N \cdot s}/_{m^4}$

Z_f	=	Impedance in fluid	$^{kg}/_{s \cdot m^3}$
$\underline{Z}_2$	=	Complex wall impedance	$^{kg}/_{s \cdot m^3}$
α_a	=	Absorption coefficient	$^{dB}/_{mm}$
λ	=	Wavelength of ultrasonic wave	m
ρ_f	=	Density of fluid	$^{kg}/_{m^3}$
ρ_s	=	Density of solid	$^{kg}/_{m^3}$

Therefore, α_a has to be close to 1 in the measurement frequency range. Data of sound absorption coefficients in the ultrasonic range for damping materials cannot be given by manufacturers. However, a measurement of the decrease in sound pressure level can be done using a small reverberation room based on the ISO 354:2003 [47] described by Dobrucki [24]. In an article of Simon *et. al.* [83] several highly absorbing materials at high frequencies have been used as a target for temperature measurements in an ultrasonic standing wave field at $20\,kHz$. They stated that Insulfrax-M-Matte and Basotect®melamin foam showed the highest temperature due to the transformation of sound energy into heat. Thus, Basotect Melamin foam can be considered as a damping material due to its high absorption at ultrasonic frequencies.

Besides the reflected ultrasonic waves, the radiated sound energy out of the measurement chamber has to be considered. Since the ultrasonic pulse needs high intensity, it could damage the ears of users of the measurement system. The Figure 6.6, describes the sound energy balance at a wall.

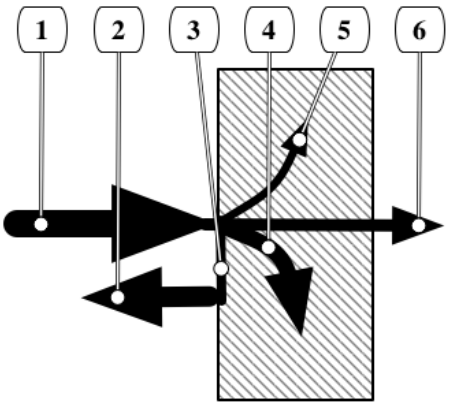

1 : *Incident energy*

2 : *Reflected energy*

3 : *Absorbed energy*

4 : *Virbrational energy*

5 : *Dissipated energy*

6 : *Transmitted (radiated) energy*

Figure 6.6.: Sound energy balance of a wall [38]

To avoid a high amount of transmitted sound energy, the material of the measurement chambers needs high damping properties. Other than its damping properties, the material should have a sufficient strength. Materials contemplated for the measurement system are listed in Table 6.3, including their damping properties in the ultrasonic range.

Material	Frequency in MHz	Damping in $^{dB}/_{cm}$
Iron	2	0,3
Aluminium	2,5	0,02
Polymethyl methacrylate (PMMA)	1,46	2,3

Table 6.3.: Damping properties of materials in ultrasonic range [68]

The table shows that PMMA would be suitable as a wall material. It has also been used by Dorbrucki as a material to insulate enclosures of a welding machine, which radiated ultrasound. [24] The sound reduction of PMMA cannot be calculated. [24] Hence, exact calculations of how the sound reduction index is expected for PMMA is not possible. Nevertheless, since PMMA has high damping properties, offers high strength (Young's modulus 1,8-3,1 GPa) and is resistant against alkalis and acids, the walls of the measurement chambers will be made out of this material.

6.6. Summary

In this chapter, the sound speed of the transversal wave, as well as of the longitudinal wave in the solid was predicted through simulations with the software Maple. This accounts for the critical requirement of the approaches to measure the transversal wave velocity in Section 5.4. The requirement for these approaches are that the sound speed in the fluid has to be less than in the solid. The simulations revealed that this requirement cannot be fullfilled when commonly used coupling fluids, i.e. water or air, are chosen. The problem was addressed with the investigation of several gases, which led to Sulfurhexafluid and Decafluorobutane as suitable coupling fluids. The aforementioned velocity requirement, even with special gases, might not be fulfilled for every damping material used in automotive applications. Therefore, a recommendation for using the transversal velocity measurement in Subsection 5.4.4 is given. This approach only needs the longitudinal wave in the specimen to be faster than the wave velocity in the fluid. Given these solutions, only the heaviest framed material investigated in this chapter, the PET nonwoven material, might not be able to be measured with this measurement system. However, this is also dependent on other material parameters such as Poisson's ratio, porosity, Young's modulus and shear modulus, a measurement can be possible for some PET materials. Calculations of the frequency range of the measurement system have been taken out. The range is influenced by specimens pore sizes and their thickness. In order to determine pore sizes, the SEM from Subsection 2.3.1 was used. Commonly used damping materials restrict the measurement frequency range from roughly50 kHz to 500 kHz.

A test rig, which avoids reflected waves inside the measurement chamber was investigated using guidelines from free field measurement chambers. They usually operate within the audible frequency range. However, no information regarding the restriction of reflected waves could be found in the ultrasonic range. As a damping material for the walls, Basotect®melamine foams from BASF were selected. They have been reported to have high absorption properties, even for the ultrasonic range. The wall material

for the test rig should restrict radiated sound energy. PMMA was selected, because it has high damping properties in the ultrasonic range, as well as suficient strength.

7 Measurement Hardware

7.1. Introduction

This chapter describes the selection of the measurement hardware. Researchers in the field of ultrasonics used a combination of an oscilloscope, occasionally with an additional computer, to acquire signals from the ultrasonic transducers. In this dissertation however, a PXI system will be utilised. Due to the modularity of a PXI system, it can be combined with additional functions, required by a more precise, automatic and faster measurement system. The block diagram of the basic measurement setup is shown in Figure 7.1.

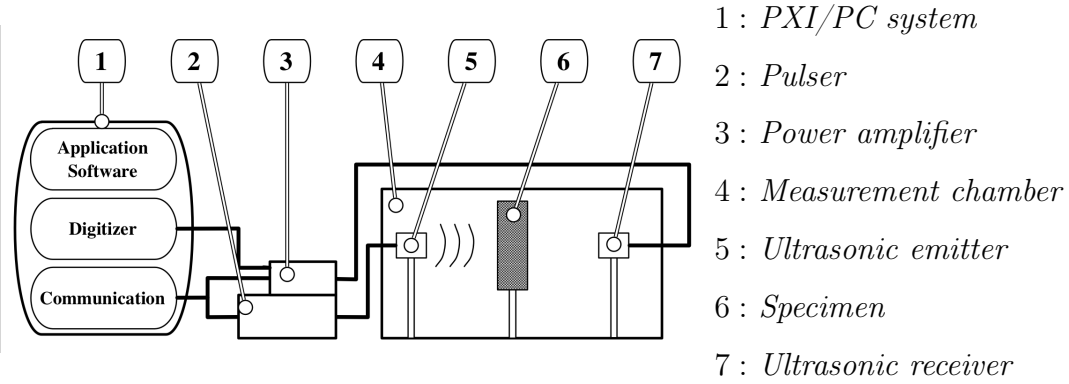

Figure 7.1.: Basic measurement setup

The following hardware modules are required for a basic measurement system:

- Transducers (Transmitter, Receiver) to emit and receive an ultrasonic pulse,
- Pulse generating module to power the emitter,

- Power amplifier to amplify the signal from the receiver, and
- Oscilloscope with integrated filters and calculations for evaluation.

A special solution for the transversal wave measurement proposed in Subsection 5.4.4 is required, which will be addressed using acoustic antenna principles.

7.2. Ultrasonic Transducers

The ultrasonic transducers have been used by researchers to emit an ultrasonic pulse and to receive it. Common ultrasonic transducers create an ultrasonic wave through a piezoelectric disc or a thin film. Through the inverse piezoelectric effect, an alternating pressure is produced on both sides of the piezoelectric crystal depending on the applied alternating voltage.

Other components are the backing material and at times, an impedance matching layer to enhance efficiency, depending on the coupling fluid. The backing material is used to reduce and spread the ultrasonic pulse on that side of the piezoelectric crystal, where an emission of a pressure pulse is not useful. [21]

Figure 7.2 shows the layout of an ultrasonic transducer.

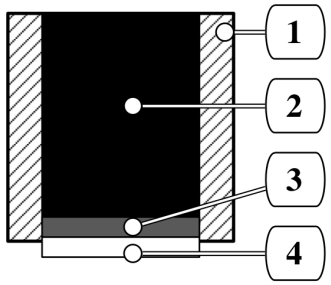

1 : *Housing*
2 : *Backing material*
3 : *Piezoelectric element*
4 : *Impedance matching layer*

Figure 7.2.: Layout of an ultrasonic transducer

Air-coupled transducers that have an impedance which is matched to air, will also be able to be used in the coupling fluids investigated in Section 6.3. These transducers can be delivered from Sonotec. Following the information of the manufacturer, an

ultrasonic measurement with these transducers is possible in air up to $300\,kHz$. The upper frequency is limited due to frequency dependent attenuation and signal to noise ratios. The transducers listed in the table below are selected to enable a measurement from $50\,kHz$ to $300\,kHz$. Data sheets can be found in Appendix B.

Ultrasonic Transducer	Center Frequency in kHz
Sonotec Sonoscale AS 50	50
Sonotec Sonoscale AS 120	120
Sonotec Sonescale AS 300	300

Table 7.1.: Selected ultrasonic transducers

7.3. Power Amplifier and Pulse Generating Module

To create and receive the high voltage pulse demanded by the ultrasonic emitter, an ultrasonic pulser is used. Moreover, to amplify the signal received from the receiving transducer, a power amplifier is required. The pulser/receiver unit which will be used is the OPTEL OPLabBox. The integrated amplifier allows an amplitude gain up to $92\,dB$. However, the output voltage of its pulser with up to $360\,V$, does not come close to the maximum allowable voltage of the transducers. Therefore, an additional pulser, Optel OPGUD HV, will be utilised. It emitts a triangle, high voltage pulse up to $1250\,V$. Data sheets can be found in Appendix C and D.

7.4. Oscilloscope with Integrated Filters and Calculations

The oscilloscope is used to visualise and calculate input and output signals. In this measurement system, since it should be adaptable, a modulable PXI system will be used. This enables the automation of the measurement system in future studies. Moreover,

the programable software, National Instruments, can be used. This has the benefit that the measurement results of Young's modulus and loss factor can be automatically calculated out of ultrasonic parameters.

The PXI platform, including its functions, is visualised in Figure 7.3.

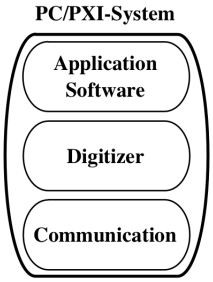

Figure 7.3.: Functions combined in the PXI System

The application software LabVIEW allows the user to interact and program the application in order to set up test parameters and to visualise results. The digitizer converts the voltage signals to bits using analogue to digital converters (A/D converters). The communication allows to set up operational parameters for the pulser/receiver when a programmable pulser/receiver is used. This is not the case in the basic measurement system. The communication will also trigger the pulse generating module. [72]

7.4.1. Digitizer

The digitizer of the frontend returns the voltage information of the receiving transducer into digital information. There are a few characteristics which have to be considered when selecting the correct digitizer for the measurement system in this dissertation, such as: [71]

- Bandwidth,
- Sampling rate,
- Sampling method,

- Resolution and dynamic range,
- Integrated Storage, and
- Channel density.

Bandwidth

The bandwidth describes the frequency range of the input signal which allows the analogue input to be converted into digital information with minimal decrease in amplitude. It is defined as the frequency for which the sinusoidal input signal gets 70,7 % minimized, compared to its original amplitude. This is also described as the -3 dB border. This implies that the measurement system at its specific bandwidth limit will have an amplitude error of 3 dB or 29,3 %.

Besides this error, the minimum bandwidth of a digitizer is recommended to be more than double the signal of the highest frequency. Ideally, a digitizer is selected with a bandwidth to be according to the following equation:

$$f_b \geq 5 * f_h \tag{7.1}$$

The highest allowable rising time of the signal can be calculated, which is defined as the time the signal needs to rise from 10 % to 90 % with:

$$tr_d = \frac{0,35}{f_b} \tag{7.2}$$

With:

f_b	=	Bandwith frequency	Hz
f_h	=	Highest frequency	Hz
tr_d	=	Rising time of digizer	s

The selected digitizer, NI PXI-6250 from National Instruments, delivers a bandwidth of more than the minimum allowed bandwidth with 1,25 MHz. This leads to a rising time of 0,00028 s.

Sampling Rate

The bandwidth was described as a sinusoidal curve which can be digitized with minimal damping. The sampling rate defines, how often the digitizer samples the signal per second. A high sampling rate leads therefore to a better resolution of the signal. The Nyquist theorem states that the sampling rate should be at least more than double the highest frequency. However, that may not be enough to precisely define a signal in the time domain.

Figure 7.4 shows the difference between an adequate and an inadequate sampling rate. The signal which appears after digitization appears as the dashed line.

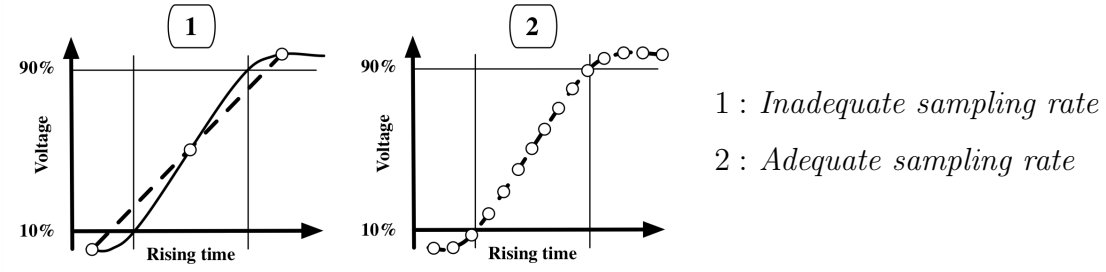

Figure 7.4.: Difference in sampling rate and signal appearance after digitization

As stated above, the required sampling rate is at least double the highest frequency and therefore for this measurement system, it should be at least 600 $^{kS}/_{s}$. The selected digitizer, NI PXI-6250, has a sampling rate of 1,25 $^{Ms}/_{s}$, which is therefore sufficient. [71]

Sampling Method

There are two types of sampling methods, real time sampling and synchronised sampling. The synchronised sampling is also called Equivalent-Time Sampling or ETS. The real time sampling is as described above, based on the clock speed of the A/D converter. If synchronised sampling is used, the signal can be sampled based on a series of triggered signals which recreates the original signal. This leads to a higher sampling rate, however it takes more time and requires the signals to be repeated. In this dissertation, the selected digitizer, NI PXI-6250, has the ETS function, however the sampling rate is sufficient without ETS. [71]

Resolution and Dynamic Range

As stated above, an analogue signal has to be converted into a digital signal using A/D converters. The number of bits at the output of the A/D converter describes the vertical resolution of the digitizer. It influences the minimum voltage step size within a voltage range.

The analog input of the A/D converter gets divided into 2^b steps and the smallest detectable voltage is given by $Input/2^b$. Here, b stands for the bits of the digitizer. Therefore, an 8-bit digitizer would divide an input of 10V into 2^8 steps of $39\,mV$. Whereas, a 24-bit digitizer would divide the same signal it into steps of $596\,nV$.

A digitizer with a higher resolution is used when the measured signals combine very large and very small amplitudes. The signals in this dissertation require a high resolution, since large differences in amplitude can be expected. Figure 7.5 describes that behaviour.

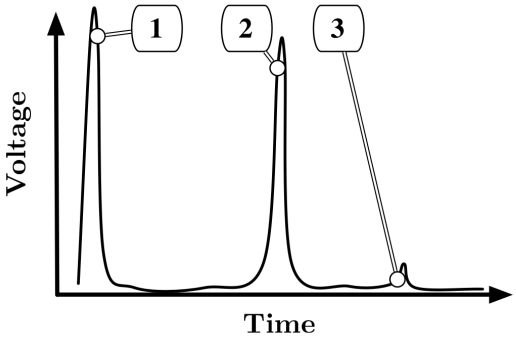

1 : *Initial pulse*

2 : *Reflection of longitudinal wave*

3 : *Longitudinal wave created out of transversal wave*

Figure 7.5.: Differences in expected amplitude signal height during measurements in this dissertation

It cannot be predetermined how high the resolution must be for the measurement system in this dissertation. A 16-bit digitizer however, should be sufficient. Furthermore, the signal from the receiver can be adjusted in the amplifier should the digitizer have insufficient vertical resolution. [71]

Integrated Storage

Measurement systems transfer data for analysing and measurement purposes from the digitizer to the computer. This can be an issue, when the digitizer measures with multiple $^{Gs}/_{s}$ and the data gets transferred through communication buses to the PC, which have less bandwidth. However, using bus systems such as PCI Express and PXI Express, this problem can be solved because they allow a data transfer of multiple $^{GB}/_{s}$. If this is not enough, the data cannot get exchanged simultaneously with the PC. It gets stored in an internal storage. This is not required for the measurement system in this dissertation.

Channel Density

It is important to select a digitizer with enough channels to digitize every sensor. Fortunately, using a PXI system enables a scalable measurement system, where channels can be added as needed.

7.4.2. Selected Oscilloscope, PXI System

The selected PXI system is currently available at the Ostfalia University combining a NI PXI-1033 chassis with a digitizer card NI PXI-6250.

The Card NI PXI-6250 has enough bandwidth and sampling rate for measurements up to $300\,kHz$. Two out of four available channels are going to be used. Calculating their maximum throughput for these two channels will lead to a bus occupancy of:

$$2 \cdot 1250\,^{kS}/_{s} \cdot 16\,bit = 40\,^{Mb}/_{s} \tag{7.3}$$

Since the bus of the MXI-Express controller has a throughput of $110\,^{MB}/_{s}$, this solution is sufficient. The data sheets of the chassis and digitizer is presented in Appendix E and F.

7.5. Acoustic Antennas

The measurement setup to determine transversal velocity as proposed in subsection 5.4.4 needs an acoustic antenna to measure the position, where the longitudinal wave gets converted into the transversal wave at the rear surface of the specimen. Normally, these antennas are used within the audible frequency range and require a microphone array, which measures the received pressure amplitudes for each microphone and analyses these, to find the position of the sound source.

This is possible due to the time differences the signal needs to travel between the sound source and each microphone. [67] Figure 7.6 shows the sound source and an experimentally adopted focus position. They have different time variations for each microphone.

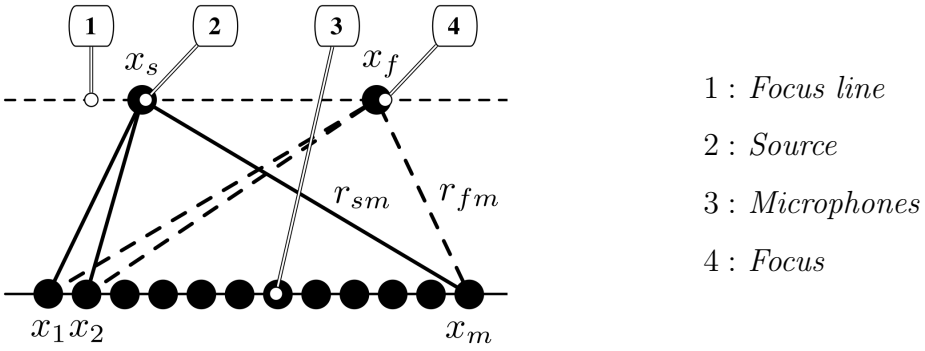

Figure 7.6.: Sound source and assumed focus position leading to time differences of acoustic signals [67]

For spherical waves, the time signal of each microphone gets evaluated for each assumed focus position x_f, using the emission time t_f as a trigger. Therefore, the time signal has to be evaluated using the delayed time t_m, since each microphone position is different with:

$$t_m = t_f + t_{fm} \tag{7.4}$$

The focused signal of the acoustic antenna as a function of the assumed focus position,

can be calculated out of summarising all time-delayed microphone signals with:

$$p(x_f, t_f) = \frac{1}{M} \sum_{m=1}^{M} \frac{P - m(t_f + t_{fm}) w_m r_{fm}}{r_{ref}} \tag{7.5}$$

Here, w_m is the weighting factor for which the following constraint holds:

$$\sum_{m=1}^{M} w_m = M \tag{7.6}$$

In this measurement setup, w_m can be assumed to be 1. In equation (7.5), the time dependent function is presented. This is not of interest in this dissertation but its RMS value $\overline{p^2(x_f)}$ is.

Unlike the general demanded sampling frequency, acoustic antennas require the sampling frequency to be at least 4 times the highest frequency range to assure a high signal to noise ratio.

$$f_b > 4 f_h \tag{7.7}$$

Using the digitizer card NI PXI-6250 is sufficient for a measurement system operating at $300\,kHz$ as the highest frequency.

To avoid so called grid-lobes, the ratio of the length of the array and the distance to the microphones has to be high:

$$\frac{l_r}{r_{ds}} > 1 \tag{7.8}$$

The required microphone distance between each other has to be at least: [67]

$$\frac{f_h \Delta x}{c_{lf}} = 0,5 \tag{7.9}$$

With:

c_{lf}	=	Sound velocity of fluid	$^{m}/_{s}$
f_b	=	Bandwidth frequency	Hz
f_h	=	Highest frequency	Hz
t_m	=	Delayed time	s
t_f	=	Emission time	s
l_r	=	Length of array	m
r_{ds}	=	Distance from source to array	m
t_{fm}	=	Time from focus to microphone position	s
r_{fm}	=	Distance between focus and microphone	m
r_{ref}	=	Reference distance	m
w_m	=	Weighting factor	1
tr_d	=	Rising time of digitizer	s
Δx	=	Distance of microphones to each other	m

Therefore, in this apparatus, the distance between the microphones has to be 0,5 mm for a measurement with 100 kHz and a sound speed velocity in Decafluorobutane with 100 m/s. Since no microphone or transducer exists which would be able to be small enough to form an array, only one transducer will be used which moves across a straight line. A measurement will be conducted for each assumed microphone position. The signal will be stored, therefore it can be summed up according to equation (7.5) at the end of all measurements. This increases measurement time. A measurement with 300 kHz is only possible when a measurement step of every 0,17 mm is conducted. This requires an array transducer package which, as an assembly, consists of many small ultrasonic transducers. No standard ultrasonic transducer is perfectly suitable for the above application. However, they can be customised to a 1mm transducer with a specially designed focus. If they are stacked next to each other on parallel lines, it would give a resolution required. The results of each of the transducers on the array

have to be compared to determine which transducer gives the shortest time at the highest pressure amplitude. Since the arrays are on different heights, the transducer box may have to be shifted to different heights during the measurement. Figure 7.7 shows the proposed transducer.

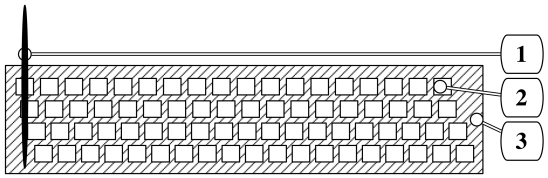

1 : *Focus shape*

2 : *Transducer*

3 : *Transducer Box*

Figure 7.7.: Proposed transducer box design to ensure a measurement every 0,17 mm

Once the basic measurement system proves that it is able to measure the ultrasonic parameters, the PXI System allows the development of an automatable measurement system without manually moving the transducers to the next measurement position.

7.6. Summary

In this chapter, the measurement hardware was selected to enable a modulable measurement system. It consists of:

Product	Manufacturer	Type	Information
2x Transducer	Sonotec	Sonoscale As 50,120,300	Appendix B
Transducer array	Ultran	Multi array element	
Power amplifier	OPTEL	OpLabBox	Appendix C
Pusle generating module	OPTEL	OPGUD HV	Appendix D
Oscilloscope-Chassis	NI	PXI-1033	Appendix E
Oscilloscope-A/D converter	NI	PXI-6250	Appendix F

Table 7.2.: Selected hardware for the measurement system

The transversal measurement from Subsection 5.4.4 requires acoustic antennas. However, it is shown that an array of transducers is not sufficient because the distance from one transducer to another is required to be too small. An acoustic antenna measurement can only be conducted taking out the same measurement for multiple transducer positions strung on an array.

8 Construction of the Test Rig

8.1. Introduction

The test rig has to be constructed to account for the measurements of all ultrasonic parameters, namely:

- The longitudinal wave velocity,
- All approaches for the transversal wave velocity, and
- The decrease in pressure amplitude.

Furthermore, the test rig should be gas tight and enable the re-use of the coupling fluid. Specimen conditioning should ensure that they are interspersed only with the respective coupling fluid which is going to be used.

8.2. Holders

The specimen holders are designed to influence the specimens as little as possible to not be in danger of effecting the material's properties. Therefore, needles are used to connect the specimen to the holder. Adjustments for the specimen holder can be made, to ensure that the specimen is centered to the slider. The slider connects the specimen holder to the measurement box. The centering adjustment is dependent on the specimen thickness and is important for the measurements of the transversal wave velocity presented in Chapter 5.4. Several holders have been constructed to

accommodate different specimen sizes: $50 \cdot 50\,mm$, $100 \cdot 100\,mm$ and $200 \cdot 200\,mm$. The Figure 8.1 shows the available specimen holder configurations:

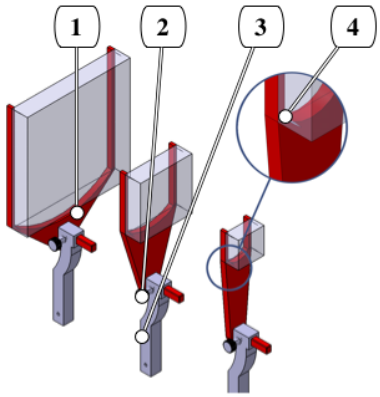

1 : *Specimen holder* $200 \cdot 200\,mm$

2 : *Adjustment screw*

3 : *Specimen holder neck*

4 : *Needle*

Figure 8.1.: 3D model of specimen holders

The holders for the ultrasonic transducers need to have the same center height as the specimen. They enable the use of different transducers without replacing the complete transducer holders. The holders for the transducers are presented in Figure 8.2.

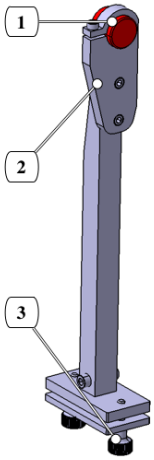

1 : *Ultrasonic transducer*

2 : *Transducer clamp*

3 : *Transducer holder neck*

4 : *Slider*

Figure 8.2.: 3D Model of transducer holders

8.3. Measurement Chamber

The measurement chamber is constructed as a scaled down version of free field measurement chambers used in the audible frequency range. This is done to avoid standing waves and reflections from walls of the measurement chamber. Unfortunately, no information about measurement chambers restricting reflected waves could be found in the ultrasonic range. Therefore, the guidelines for the audible frequency range have been applied here. All walls are covered with BASF Basotect®melamine foam, which was found to be useful in Section 6.5, due to its high absorption properties. The walls will be made out of PMMA because of its damping properties. This restricts radiated ultrasonic waves out of the measurement chamber. The outer dimensions of the measurement chamber are $1 \cdot 1 \cdot 0,8\,m$.

Special coupling gases in Section 6.3 are used for the transversal measurements in Section 5.4, which are heavier than air. Therefore, an outlet at the bottom side of the measurement chamber is constructed for re-use and changes between coupling fluids. This also accounts for the global warming potential of the coupling gases.

The transducers and the specimen holders are mounted upside down on a top plate. It can pick up sliders to change the distances and angles the measurements are conducted with. Two exchangeable top plates are used. The first is utilised to determine the longitudinal wave velocity with the approach in Section 5.3 and the pressure decrease with the approach in Section 5.5. The second plate is used to measure the transversal velocity with all approaches carried out in Section 5.4. The top plate of the measurement chamber is covered to reduce the sound, which dissipates into the surroundings through holes in the top plates. All panels of the measurement chamber will be glued and screwed together. This ensures a gas tight measurement chamber. The Figure 8.3 shows the whole measurement box as a 3D model. Here, the damping of the walls is hidden:

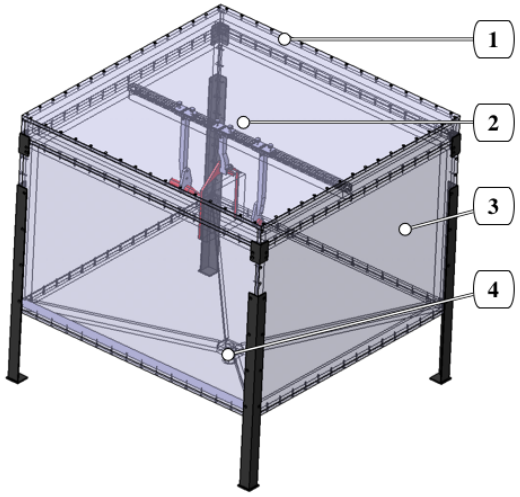

1 : *Chamber cover*

2 : *Top plate*

3 : *Measurement chamber*

4 : *Gas outlet*

Figure 8.3.: 3D Model of the measurement chamber

8.4. Possible Measurement Configurations

Lifting the cover of the measurement box allows adjustments on the sliders for various distance and angle settings. Two top plates can be exchanged for either the measurements of the longitudinal wave velocity and decrease in pressure amplitude, or for the transversal wave velocity, as shown in Figure 8.4.

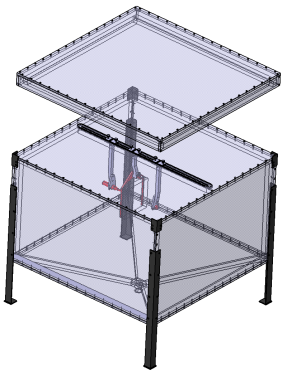

Figure 8.4.: Accessing the top plate through the measurement cover

The distance scales on the top plate for longitudinal velocity/loss factor measurements allow a resolution up to 0,125 mm, to ensure a measurement with different distance

settings. The measurements are described in Section 5.3 and 5.5. The Figure 8.5 shows the mounted transducers and the specimen on the top plate. The picture has been taken from the inside of the damped measurement box, which is viewed from the bottom.

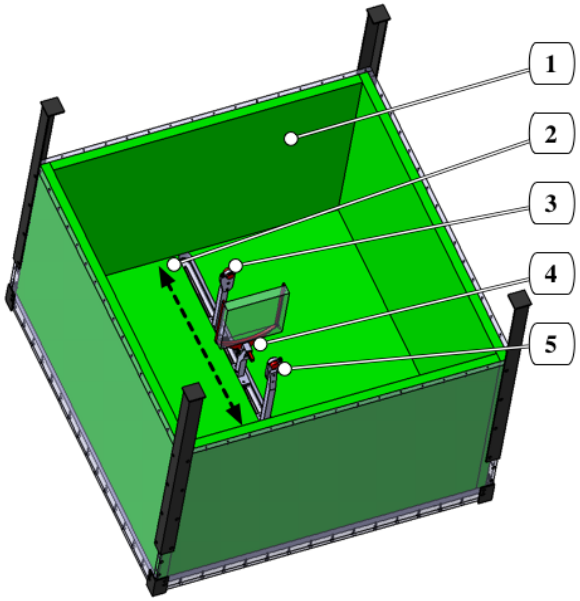

1 : *Damping of chamber*

2 : *Adjustments of transducers and specimen*

3 : *Emitter*

4 : *Specimen*

5 : *Receiver*

Figure 8.5.: 3D Model of longitudinal wave velocity and loss factor measurement

The top plate of the transversal velocity measurements can accommodate transducers for all measurements of the transversal wave described in Section 5.4. The Figure 8.6 shows the top plate configuration for the critical angle measurement described in Subsection 5.4.2. Using other orbits for the ultrasonic transducers, allows different distance settings. The angle resolution to turn the specimen is up to $0,25\,°$, the smallest angle adjustment is limited to $10\,°$.

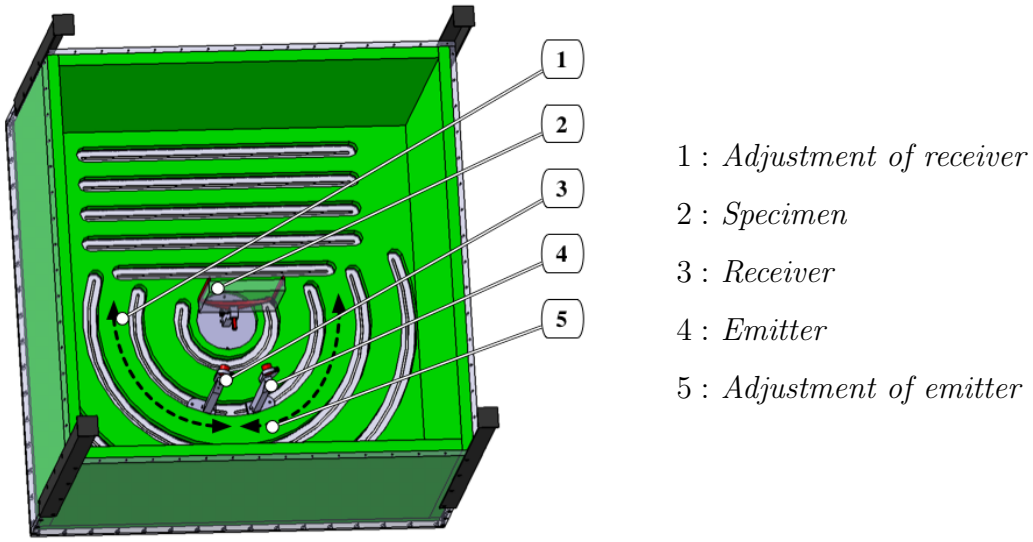

Figure 8.6.: 3D Model of transversal wave velocity, reflection measurement

The Figure 8.7, shows the model for the refraction angle measurement, as well as the measurement using shifted wave patterns, described in Subsection 5.4.4 and 5.4.3. Using other orbits for the ultrasonic emitter and straight lines for the receiver, allows different distance settings. The angle resolution to turn the specimen is up to $0,25°$. The resolution of the movement of the receiver to ensure a measurement proposed in Subsection 5.4.4 is up to $0,125\,mm$. This is sufficient for $300\,kHz$, as described in Section 7.5. For the measurement with shifting wave patterns, described in Subsection 5.4.3, only the transducer is moved inside the transducer holder clamp. For an exact adjustment, a micrometer screw can be used.

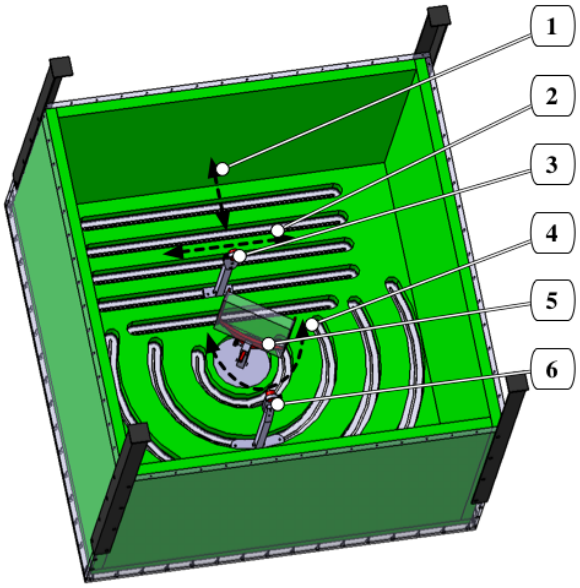

1 : *Adjustment of receiver (shifting wave patterns)*

2 : *Adjustment of receiver (refraction angle)*

2 : *Receiver*

3 : *Adjustment of specimen*

4 : *Specimen*

5 : *Emitter*

Figure 8.7.: 3D Model of transversal velocity refraction and shifting wave patterns measurement

8.5. Conditioning of Specimens

The specimens are within the measurement process filled by a coupling fluid, which is a gas such as Sulfurhexafluid or Decafluorobutane. It must be made certain that the specimen is only filled with the respective coupling fluid. To ensure this condition, the specimens will be filled with coupling fluid after they have been attached in the measurement chamber. This is done directly out of the gas bottle, which is under pressure, by using a cone. If air is used as a coupling fluid, a compressor ensures that the specimen is only filled with air. Several adapters enable the use of the same cone can for different specimen sizes.

The cone and its application with the specimen mounted on the holder, can be seen in Figure 8.8.

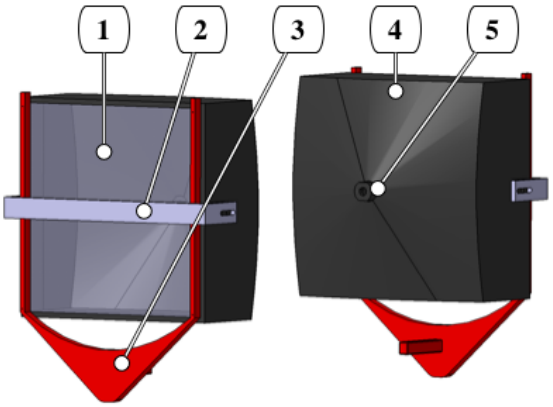

1 : *Specimen*

2 : *Cone holder*

3 : *Specimen holder*

4 : *Cone*

5 : *Attachment of hose*

Figure 8.8.: 3D Model of the cone, ensuring the conditioning of specimens with the coupling fluid

8.6. Summary

The aim of this chapter was to construct a test rig to accommodate all possible ultrasonic measurements. This included the longitudinal wave velocity as well as all the transversal wave velocity measurement approaches and the determination of the amplitude decrease. It was addressed using two exchangeable top plates. One top plate for the longitudinal wave velocity measurement and decrease in pressure amplitude, and another top plate for all transversal wave velocity measurements. The transducer holders are suspended upside down on the top plate. The plates allow various distance and angle settings to conduct the measurements.

A cover for the measurement box restricts transmitted sound energy through the holes in the top plates. An outlet at the bottom of the measurement chamber allows the exchange and re-use of the coupling fluid, in order to account for their global warming potential.

Specimen conditioning is possible using a cone and the pressure difference of the gas bottle to the ambient air. If the specimen has to be interspersed with air, a compressor should be used.

9 Summary

9.1. Introduction

Chapter 9 will provide an overview of the study. Furthermore, the main findings will be discussed and the contribution of the study will be provided. In conclusion, the limitations of this dissertation and possibilities for future research will be given.

9.2. Overview of the Research

Damping materials for air-borne sound are widely used to influence the transfer path between sound source and the receiver. This leads to a reduction of noise exposure. In automotive applications, simulation techniques are used to save resources as well as engineering time. Simulations of the acoustic behaviour of damping materials are mostly based on Biot's theory. Biot's theory has proven to be able to sufficiently simulate the acoustics of damping materials. However, to date, simulations of damping materials led to insufficient results because the determination of the structural Biot parameters, Young's modulus and loss factor, have been inconclusive.

The primary objective was to propose a new measurement system for the structural Biot parameters of damping materials used to absorb air-borne sound energy i.e. foams and nonwoven materials. The new measurement system should be able to determine the Young's modulus and loss factor more precisely than commonly used measurement systems. To achieve the primary objective of the study, the secondary objectives were

defined:

1. To undertake studies of the structure and general behaviour of damping materials i.e. foams and nonwoven materials.
2. To study commonly used apparatuses to measure structural Biot parameters of damping materials.
3. To conduct research about measurement issues of commonly used measurement systems.
4. To propose a new measurement concept and formulas, which circumvents the measurement errors in commonly used measurement systems.
5. To set up the first steps in order to test and validate the new measurement principle in the future. I.e. to design and select hardware components and to construct a test rig for the measurement system.

A comprehensive literature review of damping materials, along with commonly used apparatuses for structural Biot parameters, was conducted. Furthermore, ultrasonics have been investigated to be useful in determining the Young's modulus and loss factor. Therefore, ultrasonic approaches to measure the aforementioned parameters have been reviewed.

Chapter 2 focused on the fundamentals of the study. Biot's model was briefly presented, along with the acoustic, and structural Biot parameters. In this chapter, the section discussing damping materials provided knowledge on their general structure and the complex behaviour of damping materials. An important finding from this chapter is that foams may be considered as almost homogeneous and isotropic, whereas nonwoven materials are polytrophic and inhomogeneous materials. The sensitivity of damping materials for unknown stresses and compression in a commonly used measurement apparatus was reported.

Chapter 3 concentrated on current measurement techniques for the Young's modulus and loss factor, which are all based on mechanical transfer function systems. It was

shown that these measurement approaches lead to unknown stresses and compression during testing. Several correctional methods exist, which only account for an isotropic and homogeneous medium. Therefore, a foam might be able to be measured in these apparatuses with less errors than a nonwoven material. Although no uncorrected validation was given in any of the approaches. In particular, for a nonwoven material, other measurement approaches have to be investigated. Therefore, in chapters two and three, the first, second and third secondary research objectives of this study were achieved.

Chapter 4 showed why ultrasonics may lead to a better parameter estimation than mechanical transfer function systems. Furthermore it described the theoretical background of the new ultrasonic based measurement system. The final equations linking structural Biot parameters to measurable ultrasonic parameters, have been derived from general wave theories. These equations have been corrected for a porous viscoelastic material. They have previously been used in medical techniques, measuring bones. The chapter shows that several ultrasonic parameters will have to be investigated in order to calculate structural parameters of damping materials, namely:

- The longitudinal wave velocity and the transversal wave velocity for the Young's modulus measurement, and
- The decrease in longitudinal wave amplitude through the specimen, in order to investigate the loss factor.

Furthermore, since the transversal wave velocity has to be measured, the ultrasonic approach will also lead to the Poisson's ratio. General parameters, without using ultrasonics, will also have to be investigated as well.

Chapter 5 described how the general parameters can be determined with well known approaches. It also showed how the ultrasonic parameters can be evaluated for damping materials. A transmission measurement using the phase velocity, can be conducted for the longitudinal wave velocity. The decrease in longitudinal wave amplitude, through the specimen, can be measured using transmission measurements. Refraction and

reflection laws can be used for the investigation of the measurement of the transversal wave velocity. However, known approaches require the sound speed of the longitudinal and transversal wave in the solid, to be less than in the fluid. To account for this problem, a new approach was investigated in Subsection 5.4.4, which only requires the longitudinal wave velocity to be slower in the fluid than in the solid.

Chapter 6, further addressed the problem of the sound speed in the fluid compared to the one in the solid. A prediction of the sound speed in the solid was given combining ultrasonic equations and known specimen parameters. It was shown that a special gas has to be used in order to measure damping materials with transversal wave velocity measurements presented in Section 5.4. This coupling fluid was found to be Sulfurhexafluorid or Decafluorobutane, however very heavy specimens such as PET nonwoven materials might not be able to be measured as their sound velocity in the specimen is too slow. This can not be stated with certainty since the inner sound velocity is also dependent on other parameters, Poisson's ratio, porosity, Young's and shear modulus. The respective chapter also calculated a recommended frequency range for the test rig and gave material recommendations for the measurement chamber. This will lead to a poorly reflecting behaviour and also restricts transmitted sound waves. The materials have been found to be a Basotect ®melamine foam from BASF as a damping material and PMMA for the walls of the measurement chamber. Consequently, in Chapter 5 and 6, the fourth secondary objective could be attained.

Chapter 7 described a sufficient selection of the measurement hardware and their functionality. The test rig was constructed in Chapter 8. The test rig and the hardware ensures that the ultrasonic measurements of the longitudinal wave velocity, decrease in pressure amplitude in the specimen and all transversal wave velocity approaches can be measured in the future. The test rig was constructed following miniature free field measurement chambers in acoustics to avoid standing waves and the measurement of reflected waves from the measurement wall. The test rig also includes an outlet at the bottom side of the chamber to account for the global warming potential of investigated coupling fluids. The fifth and final secondary objective was therefore achieved

in Chapter 7 and 8

The hardware was selected as a modulable system, which consists of:

- Two transducers from Sonotec (Emitter, Receiver) to emit and receive an ultrasonic pulse in the frequency range of 50-300 kHz,
- A pulse generating module from Optel to power the emitter,
- A power amplifier from Optel to amplify and condition the signal from the receiver, and
- A modulable oscilloscope from National Instruments with integrated filters and calculations for evaluation.

9.3. Main Findings

The findings of this study show that Biot's theory is able to simulate the acoustic behaviour of damping materials, see Section 2.2, when structural and acoustic parameters of damping materials are given. Chapter 3 states, that mechanical transfer functions compress the damping materials during the measurement, which leads to unknown stresses and false measurement results of structural Biot parameters. Methods to correct them only account for an isotropic and homogeneous foam, but not for nonwoven materials. Nonwoven materials can be characterised as a polytrophic, inhomogeneous material, as reported in Subsection 2.3.1. Furthermore, the only validation given on mechanical transfer function methods, had to be corrected. Hence, the accuracy of the mechanical transfer functions cannot be proven, even for homogeneous and isotropic materials.

The new measurement system based on ultrasonics will be able to evaluate the Young's modulus, loss factor and Poisson's ratio. Hereby, no compression will occur. The previously described problems with mechanical transfer function systems can therefore be circumvented. The following parameters have to be measured in an ultrasonic

measurement system in order to determine the structural Biot parameters, as can be seen in Chapter 4:

- Longitudinal wave velocity inside the specimen,
- Transversal wave velocity inside the specimen, and
- Decrease in pressure amplitude through the specimen.

The longitudinal wave velocity and the decrease in pressure amplitude can be measured with an ultrasonic transmission measurement, refer to Section 5.3 and Section 5.5. The transversal wave velocity requires the sound speed of the two waves in the solid to be higher than in the fluid, see Subsection 5.4.2 and 5.4.3. This can be critical for damping materials, as described in Section 6.2. The problem was partially solved with a special coupling fluid. Sulfurhexafluorid and Decafluorobutane have been recommended for that purpose in Section 6.3. In order to further address the problem, a new approach measuring the transversal wave velocity was proposed in Subsection 5.4.4. Given these solutions, only the heavy framed PET nonwoven materials may not be measured using the ultrasonic measurement system in this dissertation, because their inner sound speed velocity is expected to be very low. However, the inner sound speed velocity is dependent on other parameters such as Poisson's ratio, porosity, Young's modulus and shear modulus. Therefore, the transversal wave velocity of PET foams may be able to be measured as well.

In order for the measurement system to work with most damping materials, it is recommended to start measurements at $50\,kHz$, see Section 6.4. The highest frequency is limited due to frequency dependent attenuation in the fluid to be $300\,Khz$, see Section 7.2. A poorly reflecting measurement chamber is important for not being in danger of measuring relfected waves. The measurement chamber will furthermore restrict transmitted waves in order to address the problem of high sound energy, which might damage the ears of users. Both demands can be achieved using BASF Basotect®melamine foams as a damping material for the walls of the measurement chamber and PMMA as a wall material, as it was investigated in Chapter 6.

A construction of the test rig, derived from free field measurement chambers, ensures that all measurements using ultrasonics can be tested. The test rig also included a cycle to account for the global warming potential of the coupling fluids.

9.4. Contributions of the Study

The study has contributed towards Young's modulus and loss factor measurements of damping materials for air-borne sound. This can be extended to structural parameter analysis of porous viscoelastic materials in general.

It has been shown why mechanical transfer functions have to produce errors for damping materials especially for rather inhomogeneous, polytrophic and also dispersive materials.

The study made a significant contribution towards ultrasonic measurements of porous viscoelastic materials in the Young's modulus range of damping materials, approximately 50000-200000 $^{N}/_{m^2}$, where known noncontact transversal wave velocity measurement approaches won't lead to sufficient measurement results. Transversal wave velocity measurements require the sound speed in the solid to be higher than in the fluid. This cannot be fullfilled with known measurement approaches. This problem was addressed using a new approach to measure the transversal wave velocity in combination with a special coupling fluid.

As a result, the use of ultrasonics may expand into the lower Young's modulus range of porous viscoelastic materials in future and provide better measurement results than mechanical transfer function systems.

9.5. Limitations of the Study and Recommendations for Future Research

Although this study attempted to make a significant contribution in order to solve the measurement errors with existing systems to measure the Young's modulus and loss factor of existing systems, several limitations were encountered. Although this study has investigated an ultrasonic measurement approach, which does not lead to unknown stresses resulting in measurement errors, it has also revealed opportunities for future research. The following limitations and possibilities will therefore be highlighted.

One limitation of this study is the strong focus on ultrasonic techniques to reveal the structural Biot parameters. Although this approach, with its adaptions, attempts to provide better measurement results than mechanical systems, other approaches may also be sufficient. Another limitation can be found, since the transversal wave velocity of materials with very heavy frames may not be able to be measured with the approaches proposed in this dissertation.

Both limitations should be considered in future research. In this study, no testing of the measurement system as well as validation of the measurement system is given. To address this in future, the research can be continued with the following steps:

- Assembling the measurement system,
- Programing the evaluation software using LabVIEW,
- Testing the specimens with the proposed approaches in this study, to determine the longitudinal wave velocity, decrease of pressure amplitude in the specimen and transversal wave velocity,
- Compare the measurement results of Young's modulus and loss factor with mechanical transfer function systems, and
- Validate the measurement system using simulations based on Biot's theory, which used the structural Biot parameters acquired from the ultrasonic measurement

system proposed in this dissertation. Furthermore, these results can be compared with Biot's simulations, which gathered the material parameters out of mechanical transfer function systems.

Bibliography

[1] Chemical search engine. `http://www.chemicalbook.com`, 2013.

[2] Achenbach, J. *Wave Propagation in Elastic Solids.* North Holland Publishing, 1973.

[3] Allard, J., and Atalla, N. *Propagation of Sound in Porous Media: Modelling Sound Absorbing Materials.* Wiley, 2009.

[4] Allard, J., Castagnede, B., and Henry, M. Evaluation of the tortuosity in acoustic porous materials saturated by air. *Review of Scientific Instruments 65* (1994), 754–755.

[5] Allard, J., Depollier, C., Guignourd, C., and Rebillard, P. Effect of a resonance of the frame on the surface impedance of glass wool of high density and stiffness. *Journal of the Acoustical Society of America 89* (1991), 999–1001.

[6] Anderson, C., Bauer, A., and Holland, M. Inverse problems in cancellous bone: Estimation of the ultrasonic properties of fast and slow waves using Bayesian probability theory. *Journal of the Acoustical Society of America 128* (2010), 2940–2948.

[7] Antich, P. Ultrasound critical-angle reflectometry (UCR): a new modality for functional elastomeric imaging. *Physics in Medicine and Biology 42* (1997), 1763–1777.

[8] Antich, P., Dowdey, J., and Murry, R. Method and apparatus for analysing material properties using reflected ultrasound, 1991.

[9] Atalla, Y., Raymon, P., and Franck, S. Evolutionary strategy algorithm for a complete characterization of porous materials using a standing wave tube. *Journal of the Acoustical Society of America 108* (2000), 2519.

[10] Australian Government Department of Health. National industrial chemicals notification and assessment scheme, full public report, perfluorobutane. `http://www.nicnas.gov.au/publications/CAR/new/NA/NAFULLR/NA0300FR/NA317FR.pdf`, July 1996.

[11] Autoneum Holding AG. Presentation of Autoneum Measurement System ELWIS-S. Describtion ELWIS-S.

[12] Bär, R., and Walti, A. Über die Bestimmung der Poisson'schen Elastizitätskonstante mit Hilfe von Ultraschallwellen. *Helvetica Physica Acta 7* (1934), 658–659.

[13] BASF. Presentation Basotect®. `http://www.glasscellisofab.com/sheets/melamine/data_sheets/Basotect%20english%202.pdf`, 2000.

[14] Becker, U. Vorlesung Fahrzeugakustik Teil 4: Grundlagen der Laborakustik. Lecture skript, Ostfalia, Fakultät Fahzeugtechnik, 2011.

[15] Biot, M. Theory of propagation of elastic waves in fluid-saturated porous solid. 1. lower frequency range. *Journal of the Acoustical Society of America 28* (1956), 168–178.

[16] Biot, M. Theory of propagation of elastic waves in fluid-saturated porous solid. 2. higher frequency range. *Journal of the Acoustical Society of America 28* (1956), 179–191.

[17] Bourbie, T. *Acoustics of Porous Media.* Gulf Publishing, 1987.

[18] Brown, R. Connection between the formation factor for electrical resistivity and fluid-solid coupling factors for acoustic wave in fluid-filled porous media. *Geophysics 45* (1980), 1269–1275.

[19] Champoux, Y., and Allard, J. Dynamic tortuosity and bulk modulus in air saturated porous media. *Journal of Applied Physics 70* (1991), 1975–1979.

[20] Champoux, Y., Stinson, M., and Daigle, G. Air-based system for the measurement of porosity. *Journal of the Acoustical Society of America 89* (1991), 910–916.

[21] Chen, Q., and Payne, P. Industrial applications of piezoelectric polymer transducers. *Measurement Science and Technology 6* (1995), 249–267.

[22] Cheng, J. Maurice Anthony Biot. `http://www.olemiss.edu/sciencenet/poronet/piobiotbio.html`, 2013.

[23] Craggs, A., and Hildebrandt, J. Effective densities and resistivities for acoustical propagation in narrow tubes. *Journal of Sound and Vibration 176* (1984), 321–331.

[24] Dobrucki, A., Żółtogórski, B., Prunchnicki, P., and Bolkejeko, R. Sound- absorbing and insulating enclosures for ultrasonic range. *Archives of Acoustics 35* (2010), 157–164.

[25] Droin, P., Berger, G., and Laugier, P. Velocity dispersion of acoustic waves in cancellous bone. *IEEE Transactions on Ultrasonics, Ferroelectrics and Frequency Control 45* (1998), 581–592.

[26] Environmental Protection Agency United. Overview of greenhouse gases. `http://epa.gov/climatechange/ghgemissions/gases/fgases.html`, 2013.

[27] Fasold, W., Sonntag, E., and Winkler, H. *Bau- und Raumakustik*. VEB-Verlag für Bauwesen, 1987.

[28] Fellah, Z. Ultrasonic wave propagation in human cancellous bone: Application of biot theory. *Journal of the Acoustical Society of America 116* (2004), 61–73.

[29] Fellah, Z., and Depollier, C. Transient acoustic wave propagation in rigid porous media: a time domain approach. *Journal of the Acoustical Society of America 107* (2000), 683–688.

[30] Ferry, J. *Viscoelastic Properties of Polymers.* Wiley, 1961.

[31] Fraunhofer Institut Techno- und Wirtschaftsmathematik. Simulation und Messungen mittels Ultraschall an porösen Absorbern, Ergebnisse zur MEF, Workshop Dämmstoffe und Isolationsmaterialien. `http://www.itwm.fraunhofer.de/fileadmin/ITWM-Media/Abteilungen/BV/Pdf/MEF_poroese_Absorber_Spies-Rieder_230109.pdf`, 2008.

[32] Fuchs, H., Zha, X., and Babuke, G. *Schallabsorber und Schalldämpfer: Innovative Akustik-Prüfstände.* Springer, 2004.

[33] Garibaldi, L., and Onah, H. *Viscoelastic Material Damping Technology.* Becchis Osiride, 1996.

[34] Gibson, L., and Ashby, M. *Cellular solids: structure and properties.* Cambridge University Press, 1988.

[35] Greaves, G., Greer, A., Lakes, R., and Rouxel, T. Poisson's ratio and modern materials. *Nature Materials 10* (2011), 1129–1140.

[36] Haire, T., and Langton, C. Biot theory: a review of its application to ultrasound propagation through cancellous bone. *Bone 24* (1999), 291–295.

[37] Hartmann, B., and Jarzynski, J. Ultrasonic hysteresis absorption in polymers. *Journal of Applied Physics 43* (1972), 4303–4312.

[38] Henn, H., Sinambari, G., and Fallen, M. *Ingenieurakustik.* Vieweg Teubner, 2008.

[39] Henry, M. *Measurement of porous materials parameters.* PhD thesis, University du Maine, Le Mans, 1997.

[40] Herrlich, N., Kunz, J., and Land, W. *Kunststoffpraxis: Eigenschaften.* WEKA MEDIA GmbH und Co. KG, 2004.

[41] Hosokawa, A., and Otani, T. Ultrasonic wave propagation in bovine cancellous bone. *Journal of the Acoustical Society of America 101* (1997), 558–562.

[42] Hugh, J. M. *Ultrasound Technique for the Dynamic Mechanical Analysis (DMA) of Polymers.* PhD thesis, Fakultät Prozesswissenschaften, TU Berlin, 2007.

[43] Hughes, E., Leighton, T., Petley, G., and White, P. Ultrasonic propagation in cancellous bone: A new stratified model. *Ultrasound in Medicine and Biology 25* (1999), 811–821.

[44] IFA Institut für Arbeitsschutz der Deutschen Unfallversicherung. Gestis Stoffdatenbank Eintrag Melamin. `http://gestis.itrust.de/nxt/gateway.dll/gestis_de/013360.xml?f=templates$fn=default.htm$3.0`, 2013.

[45] Ingard, U. *Notes on Sound Absorption Technology.* Noise Control Foundation, 1994.

[46] Institut ITWN, Abteilung für Strömungs und Materialsimulation Fraunhofer. Jahresbericht 2008. `http://www.itwm.fraunhofer.de/fileadmin/ITWM-Media/Zentral/Pdf/Jahresberichte/jb2008/jb2008_sms_de_12.5.pdf`, 2008.

[47] Acoustics-measurement of sound absorption in a reverberation room, iso 354:2003, 2003.

[48] Jeong. Experimental analysis of porosity-induced ultrasonic attenuation and velocity change in carbon composites. *Ultrasonics 33* (1995), 192–203.

[49] Johnson, D. *Recent developments in the acoustic properties of porous media.* North Holland Publishing, 1986.

[50] Johnson, D., Koplik, J., and Dashen, R. Theory of dynamic permeability and tortuosity in fluid-saturated porous media. *Journal of Fluid Mechanics 176* (1987), 379–402.

[51] Kuhn, W., and Grün, F. Beziehungen zwischen elastischen Konstanten und Dehnungsdoppelbrechung hochelastischer Stoffe. *Colloid and Polymer Science 101* (1942), 248–271.

[52] Kuttruff, H. *Ultrasonics Fundamentals and Applications.* Elsevier Applied Science, 1991.

[53] Langois, C., Panneton, R., and Atalla, N. Polynominal relations for quasi-static mechanical characterization of isotropic poroelastic materials. *Journal of the Acoustical Society of America 110* (2001), 3032–3040.

[54] Laugier, P., Giat, P., Droin, P., Saied, A., and Berger, G. Ultrasound images of the os calcis: A new method of assessment of bone status. *IEEE Ultrasound Symposium 2* (1993), 989–992.

[55] Laugier, P., and Haïat, G. *Bone Quantitative Ultrasound.* Springer, 2011.

[56] Lauriks, W., Cops, A., Allard, J., Depollier, C., and Rebillard, P. Modelisation at oblique incidence of layered porous materials with impervious screens. *Journal of the Acoustical Society of America 87* (1990), 1200–1206.

[57] Lauriks, W., Thoen, J., van Asbroeck, I., Lowet, G., and van der Perre, G. Propagation of ultrasonic pulses through trabecular bone. *Journal de Physique IV 4* (1994), 1255–1258.

[58] Leclaire, P., Kelder, L., Lauriks, W., Glorieux, C., and Thoen, J. Determinmedia of the viscous characteristic length in air-filled porous materials by ultrasonic attenuation measurements. *Journal of the Acoustical Society of America 99* (1996), 1944–1948.

[59] Lee, K., and Yoon, S. Comparison of acoustic characteristic predicted by Biot's theory and the modified Biot-Attenborough model in cancellous bone. *Journal of Biomechanics 39* (2006), 346–368.

[60] Maeda, Y. Ultrasonic studies of high polymers. *Journal of Polymer Science 18* (1955), 87–103.

[61] Mariez, E., Sahraoul, S., and Allard, J. Elastic constants of polyurethane foam's skeleton for biot model. In *Internoise* (1996), pp. 951–954.

[62] Marutyan, K., Anderson, C., Wear, K., Holland, M., Miller, J., and

Bretthorst, G. Parameter estimation in ultrasonic measurement on trabecular bone. *AIP Conference Proceedings 954* (2009), 329–336.

[63] Marutyan, K., Holland, M., and Miller, J. Anomalous negative dispersion in bone can result from the interference of fast and slow waves. *Journal of the Acoustical Society of America 120* (2006), 55–61.

[64] McSkimin, H. Ultrasound method for measuring the mechanical properties of liquids and solids. *Physical Acoustics 1* (1964), 271–417.

[65] Mechel, F. *Schallabsorber Band 2 Innere Schallfelder und Strukturen*. S. Hirzel, 1995.

[66] Merkulova, V. Accuracy of the pulse method for measuring the attenuation and velocity of ultrasound. *Sov. Phys. Acoustics 12* (1967), 411–414.

[67] Möser, M. *Messtechnik der Akustik*. Springer, 2010.

[68] Müller, G., and Möser, M. *Taschenbuch der technischen Akustik*. Springer, 2004.

[69] Na, Y., Lancester, J., Casali, J., and Cho, G. Sound absorbing coefficients of micro-fiber fabrics by reverberation room method. *Textile Research Journal 77* (2007), 330–335.

[70] National Institute of Standards and Technology (NIST). NIST Standard Reference Database 69. `http://webbook.nist.gov/chemistry/`, Mai 2013.

[71] National Instruments. 10 wichtige Überlegungen bei der Auswahl eines Digitizers/Oszilloskops. `http://www.ni.com/white-paper/4333/de`, 2008.

[72] National Instruments. Pc-based ultrasonic test system basics. `http://www.ni.com/white-paper/3766/en`, 2013.

[73] Nelson, A., Hoffmann, J., Anderson, C., and Holland, M. Determining attenuation properties of interfering fast and slow ultrasonic waves in cancellous bone. *Journal of the Acoustical Society of America 130* (2011), 2233–2340.

[74] Nicholson, P., Lowet, C., Langton, C., Dequeker, J., and van der Perre, G. A comparison of time-domain and frequency-domain approaches to ultrasonic velocity measurement in trabecular bone. *Physics in Medicine and Biology 41* (1996), 2421–2435.

[75] Ogam, E., Fellah, Z., Sebaa, N., and Groby, J.-P. Non-ambiguous recovery of biot poroelastic parameters of cellular panels using ultrasonic waves. *Journal of Sound and Vibration 330* (2011), 1074–1090.

[76] Pakula, M. Application of Biot's theory to ultrasonic characterization of human cancellous bones: Determination of structural, material and mechanical properties. *Journal of the Acoustical Society of America 123* (2008), 2415–2423.

[77] Sadowski, J. *Architectural Acoustics, Akustyka architektoniczna.* PWN Warszawa-Pozan, 1976.

[78] Sagartzazu, X., Hervella, L., and Pagalday, J. Review in sound absorbing materials. *Archives of Computational Methods in Engineering 15* (2008), 311–342.

[79] Schultz, L., and Grün, F. Physikalische Werkstoffeigenschaften- Grundlagen der mechanischen Eigenschaften. `http://www.ifw-dresden.de/userfiles/groups/imw_folder/lectures/Physikalische_Werkstoffeigenschaften/c10-meche.pdf`, 2003.

[80] Sebaa, N., Fellah, Z., Fellah, M., Ogam, E., Wirgin, A., Mitri, F., Depollier, C., and Lauriks, W. Ultrasonic characterisation of human cancellous bone. *Journal of the Acoustical Society of America 120* (2006), 1816–1824.

[81] Sebaa, N., Fellah, Z., Lauriks, W., and Depollier, C. Application of fractional calculus to ultrasonic wave propagation in human cancellous bone. *Signal Processing 86* (2006), 2668–2677.

[82] Sim, S., and Kim, K. A method to determine the complex modulus and poisson's ratio of viscoelastic materials for FEM applications. *Journal of Sound and Vibration 141* (1990), 71–82.

[83] Simon, L., Wilkens, V., Fedtke, T., and Beyer, M. Ignition of dust-air atmospheres by ultrasonic waves. In *Fundamentals of Explosion Protection* (2012).

[84] Solvey Special Chemicals. Sulphur Hexafluoride. `http://www.glasscellisofab.com/sheets/melamine/data_sheets/Basotect%20english%202.pdf`, 2007.

[85] Strelitzki, R., and Evans, J. On the measurement of the velocity of ultrasound in the os calcis using short pulses. *European Journal of Ultrasound 4* (1996), 205–213.

[86] Szabo, T. Causal theories and data for acoustic attenuation obeying a frequency power law. *Journal of the Acoustical Society of America 97* (1995), 14–24.

[87] Thieme Chemistry. Chemical Encyclopaedia. `http://www.roempp.com/prod3/`, 2013.

[88] Virgan, T., Kelders, L., Lauriks, W., Leclaire, P., and Johansen, T. Prediction and measurements of the influence of boundary conditions in a standing wave tube. *Acta Acustica united with Acustica 83* (1997), 419–423.

[89] Waterman, H. Determination of the complex moduli of viscoelastic materials with the ultrasonic pulse method (part 1). *Kolloid-Zeitschrift und Zeitschrift für Polymere 192* (1963), 1–8.

[90] Waterman, H. Determination of the complex moduli of viscoelastic materials with the ultrasonic pulse method (part 2). *Kolloid-Zeitschrift und Zeitschrift für Polymere 192* (1963), 9–16.

[91] Waters, K., and Hoffmeister, B. Kramers-Kronig analysis of attenuation and dispersion in trabecular bone. *Journal of the Acoustical Society of America 118* (2005), 581–592.

[92] Wear, K. The effects of frequency-dependent attenuation and dispersion on sound speed measurement: Application in human trabecular bone. *IEEE Transactions on Ultrasonics, Ferroelectrics and Frequency Control 47* (2000), 265–273.

[93] Wear, K. Measurement of phase velocity and group velocity in human calcaneus. *Ultrasound in Medicine and Biology 26* (2000), 641–646.

[94] Wear, K. Frequency dependence of average phase shift from human calcaneus in vitro. *Journal of the Acoustical Society of America 126* (2009), 3291–3300.

Appendices

A Computet Gases as a Coupling Fluid

- Octafluoropropane R218
- 1,1,1,2,3,3,3-Heptafluoropropane (R227ea)
- 1,1,1,2,3,3-Hexafluoropropane (R236ea)
- 1,1,1,3,3,3-Hexafluoropropane (R236fa)
- 1,1,2,2,3-Pentafluoropropane (R245ca)
- 1,1,1,3,3-Pentafluoropropane (R245fa)
- Octafluorocyclobutane (RC318)
- Ethane, 1,1-difluoro- (R152a)
- Ethane, 1,1,1-trifluoro- (R143a)
- 1-Chloro-1,1-difluoroethane (R142b)
- 1,1-Dichloro-1-fluoroethane (R141b)
- Ethane, 1,1,1,2-tetrafluoro- (R134a)
- Ethane, pentafluoro- (R125)
- Ethane, 1-chloro-1,2,2,2-tetrafluoro- (R124)
- Ethane, 2,2-dichloro-1,1,1-trifluoro- (R123)

- Hexafluoroethane (R116)
- Chloropentafluoroethane (R115)
- 1,2-Dichloro-1,1,2,2-tetrafluoroethane (R114)
- Fluoromethane (R41)
- Methane, difluoro- (R32)
- Trifluoromethane (R23)
- Methane, chlorodifluoro- (R22)
- Dichlorofluoromethane (R21)
- Tetrafluoromethane (R14)
- Chlorotrifluoromethane (R13)
- Dichlorodifluoromethane (R12)
- Trichlorofluoromethane (R11)
- Decafluorobutane
- Dodecafluoropentane
- Sulfur dioxide
- Hydrogen sulfide
- Sulfur hexafluoride
- Carbonyl sulfide
- Nitrogen trifluoride
- Ammonia
- Xenon
- Krypton
- Argon

- Neon
- 2,2-Dimethylpropane
- 2-Methylbutane
- Pentane
- Isobutane
- Butane
- Cyclopropane
- Propyne
- Propene
- Propane
- Ethene
- Ethane
- Dinitrogen monoxide
- Carbon dioxide
- Fluorine
- Oxygen

B Data Sheets of Transducers

Luftultraschallwandler

SONOTEC

SONOSCALE AS50

Bestellnummer: 100010210

Schallfeld

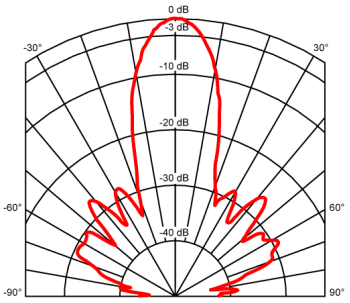

Technische Daten

Betriebsfrequenz:	50 kHz ± 4 %
Öffnungswinkel: bei -3 dB Abfall	12° ± 2°
Minimale Sendeempfindlichkeit: bei opt. Sendefrequenz	102 dB re 1 µPa/V bei 1 m
Minimale Empfangsempfindlichkeit: bei opt. Empfangsfrequenz	-160 dB re 1 V/µPa
Betriebstemperatur:	-40 °C bis +90 °C
Max. Anregungsspannung: 2% Tonsignal pro Arbeitszyklus	1500 V_{pp}
Kapazität: bei 1 kHz	4700 pF ± 500 pF
Abmessungen:	Ø 57 mm x 51 mm
Gewicht:	150 g
Gehäuse:	POM
Akustisches Fenster:	gefülltes Epoxidharz

Sende- und Empfangsempfindlichkeit

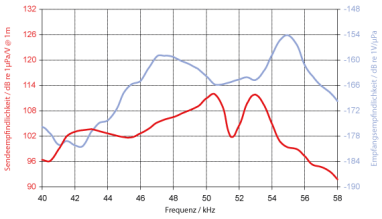

Impedanzmagnitude und Phase

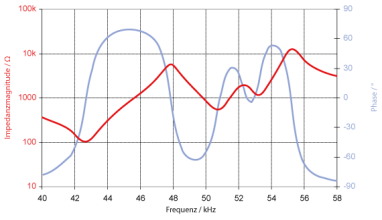

SONOTEC Ultraschallsensorik Halle GmbH
Nauendorfer Str. 2
D-06112 Halle (Saale)

Tel.: +49 (0)345 / 133 17- 0
sonotec@sonotec.de
www.sonotec.de

SONOSCALE AS120

Bestellnummer: 100010205

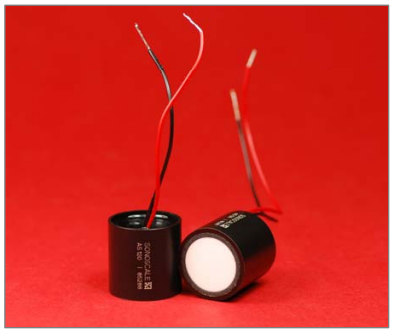

Schallfeld

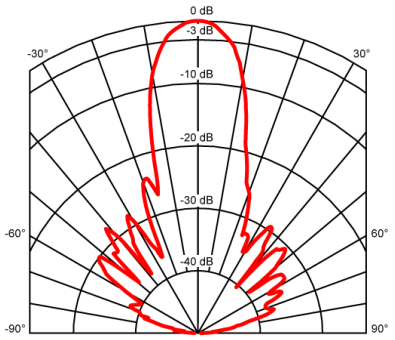

Technische Daten

Betriebsfrequenz:	125 kHz ± 4 %
Öffnungswinkel: bei -3 dB Abfall	15° ± 2°
Minimale Sendeempfindlichkeit: bei opt. Sendefrequenz	106 dB re 1 µPa/V bei 1 m
Minimale Empfangsempfindlichkeit: bei opt. Empfangsfrequenz	-169 dB re 1 V/µPa
Betriebstemperatur:	-40 °C bis +90 °C
Max. Anregungsspannung: 2% Tonsignal pro Arbeitszyklus	800 V_{pp}
Kapazität: bei 1 kHz	880 pF ± 200 pF
Abmessungen:	Ø 25 mm x 25 mm
Gewicht:	15 g
Gehäuse:	POM
Akustisches Fenster:	gefülltes Epoxidharz

Sende- und Empfangsempfindlichkeit

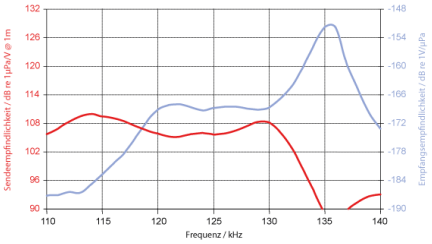

Impedanzmagnitude und -phase

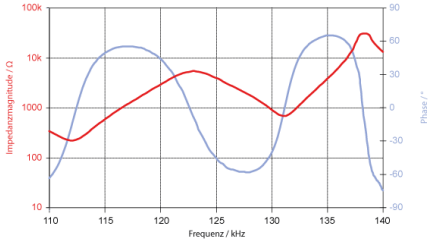

SONOTEC Ultraschallsensorik Halle GmbH
Nauendorfer Str. 2
D-06112 Halle (Saale)

Tel.: +49 (0)345 / 133 17- 0
sonotec@sonotec.de
www.sonotec.de

SONOSCALE AS300

Bestellnummer: 100010206

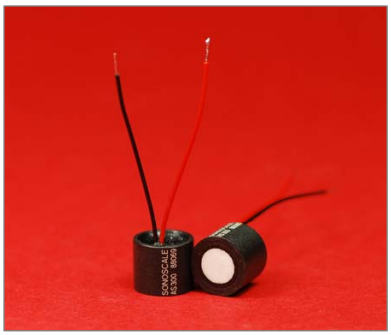

Schallfeld

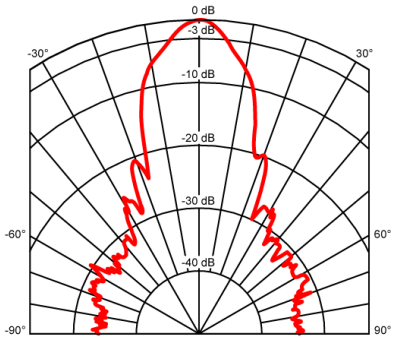

Technische Daten

Betriebsfrequenz:	300 kHz ± 4 %
Öffnungswinkel: bei -3 dB Abfall	10° ± 2°
Minimale Sendeempfindlichkeit: bei opt. Sendefrequenz	95 dB re 1 µPa/V bei 1 m
Minimale Empfangsempfindlichkeit: bei opt. Empfangsfrequenz	-180 dB re 1 V/µPa
Betriebstemperatur:	-40 °C bis +90 °C
Max. Anregungsspannung: 2% Tonsignal pro Arbeitszyklus	400 V_{pp}
Kapazität: bei 1 kHz	450 pF ± 100 pF
Abmessungen:	Ø 12 mm x 10 mm
Gewicht:	2 g
Gehäuse:	POM GF
Akustisches Fenster:	gefülltes Epoxidharz

Sende- und Empfangsempfindlichkeit

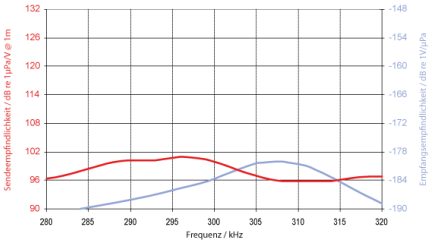

Impedanzmagnitude und -phase

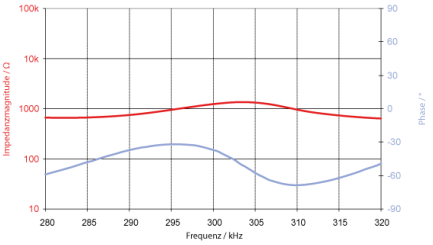

SONOTEC Ultraschallsensorik Halle GmbH
Nauendorfer Str. 2
D-06112 Halle (Saale)

Tel.: +49 (0)345 / 133 17- 0
sonotec@sonotec.de
www.sonotec.de

C Data Sheet of Power Amplifier

Przedsiębiorstwo Badawczo-Produkcyjne OPTEL Spółka z o.o.
ul. Morelowskiego 30 PL-52-429 Wrocław
phone: +48 71 329 68 53 fax: +48 71 329 68 52 NIP: 898-10-47-033
Research & Development / Ultrasonic Technology / Fingerprint recognition

OPLabBox
Ultrasonic Pulser & Receiver with Bandpass Amplifier

Description

OPLabBox is particularly well suited for ultrasonic measurements. Wide bandwidth amplifier with switched bandpass filter and integrated pulser makes these device suitable for variety of ultrasonic applications. It is designed to work as an self sufficient scope adapter, however it can be used as expansion box to other signal processing devices. Together with our ultrasonic testing devices (OPCARD or OPBOX) enables to implement complete ultrasonic system with full hardware and software support.

Specifications:

Power supply:
- Supply Voltage: 9...12V DC
- Power: max 3.5W

Size (LxWxD):
200x110x43 [mm] 7.9x4.3x1.7 [inch]

Analog parameters:

- Input channels: 2 (switched): send & receive and receive
- Input range: 275mVpp
- Input impedance: 50 ohms
- Bandwidth [-3dB]: 40kHz to 22MHz
- High Pass Filter [Hz] (switched): 40k, 57k, 65k, 100k, 210k, 320k, 400k, 1.0M, 1.6M, 3.7M, 5.6M
- Low Pass Filter [Hz] (switched): 400k, 560k, 770k, 1.25M, 2.0M, 4.75M, 5.5M, 8.5M, 11M, 16M, 22M
- Input amplifier gain: 0 to 92dB full range: 0 to 68dB fluently regulated, +0 or +24dB switched post amplifer.
- Output range: 1.125Vpp

- Trigger: Internal (regulated) or external (max 20 kHz)

- Pulser: Step pulser, 0V 360V fluently regulated, <40ns edge falling time

General Description:

OPLabBox is an wide bandwidth (40kHz to 22MHz) amplifier with switched bandpass filter and integrated step pulser.
Amplifier range is 0dB up to 92dB controlled by two knob (coarse and fine) and +24dB post amplifier switch.
It's possible to control gain by voltage via CONTROL connector.
Filter section has two 11 position switches which separately control low and high pass filter. Integrated pulser can be triggered internally (by Pulse Repetition knob) or externally by TTL signal. Output voltage is controlled by Pulse Voltage knob in range 0 to 360V (without load). It's possible to control pulse voltage via CONTROL connector.

Customize:
Optionally, it is possible to make hardware versions for the special needs of the user.

Karta katalogowa OpLabBox

D Data Sheet of Ultrasonic Pulse Generating Module

Przedsiębiorstwo Badawczo-Produkcyjne OPTEL Spółka z o.o.
ul. Morelowskiego 30 PL-52-429 Wrocław
phone: +48 71 329 68 53 fax: +48 71 329 68 52 NIP: 898-10-47-033
Research & Development / Ultrasonic Technology / Fingerprint recognition

OPGUD-01 Pulser&Receiver

The basic version of our pulser&receiver circuit have the size of a matchbox and integrated amplifier. It is powered directly from our oscilloscope card and enable the adjustment of the transmitter voltage directly from a PC. This device is intended for use with our OPKUD card or OPBOX.

Specifications:

Pulser: Step pulser, 50V -360V in 8 levels (the voltage depends on the used transducer), 20ns edge falling time, separate,

Amplifier: 40dB

Size: 40x85x25mm

Features:

Pulser circuit waveforms: The rising edge of the Trigger signal (described as Trig Inp) initiates the transducer charging process which takes about 3us. After this time a transistor switch which discharges the transducer is turned on (discharge time is about 20ns, but it can be longer, if the capacitance of the transducer is too large; the limit is reached, if the transducer is made from the standard ceramics, is 0.1 mm thick and has 8 mm
diameter).

Comments:

Because of the very low output impedance of the device (<1 Ohm) and short discharge time the pulse generated with thisdevice could be concerned as a real pulse answer for the most transducers. Transducers with a parallel matching inductance should not be used, since they do not allow the transducer to be pre-charged (the inductance causes a short-circuit).

Signal form

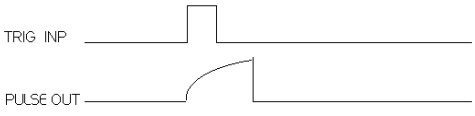

Google™ Custom Search

E Data Sheet of Oscilloscope-Chassis

Last Revised: 2012-12-11 09:57:40.0

PXI Chassis With Integrated MXI-Express Remote Controller

NI PXI-1033

- High-value chassis for remote control applications
- Controlled from either a PCI Express desktop host or an ExpressCard laptop host
- MXI-Express remote controller achieves up to 110 MB/s sustained throughput
- Rugged, compact chassis accepts up to 5 peripheral modules
- Optional handle and feet kit
- Operating temperature range from 0 to 50 °C
- Accepts 3U PXI and CompactPCI modules
- Optional rack-mount kit
- Acoustic noise as low as 38 dBA

Overview

The NI PXI-1033 chassis kits consist of a high-value chassis designed with an integrated controller for remote control applications, either a host PCI Express board for desktops or a host ExpressCard for laptops, and a cable. The PXI-1033 provides a transparent remote link with up to 110 MB/s sustained throughput. It offers five peripheral slots for I/O modules and features compact, rugged packaging as well as quiet operation, which makes it ideal for both portable and desktop ATE systems.

Back to Top

Application and Technology

Lightweight and Quiet Portable System

The PXI-1033 compact, rugged, and portable chassis weighs less than 12 lb, making it ideal for portable applications. It features an AUTO/HIGH fan-speed selector that provides a HIGH fan setting to maximize cooling and AUTO fan setting to minimize acoustic emissions. When set to AUTO, the PXI-1033 chassis monitors air intake temperature and adjusts fan speed accordingly. When set to AUTO in an environment with ambient temperatures of 25 °C, the sound pressure level measured at the operator interface is only 37.4 dBA.

PXI Timing and Synchronization

The PXI-1033 includes a 10 MHz reference clock supplied independently to each peripheral slot with a maximum slot-to-slot skew of 250 ps. For triggering and handshaking needs, the PXI-1033 offers the PXI trigger bus.

Back to Top

Ordering Information

For a complete list of accessories, visit the product page on ni.com.

Products	Part Number	Recommended Accessories	Part Number
NI-PXI 1033			
PXI-103x and PXIe-107x Side handle and rubber feet kit	781482-01	No accessories required.	
PXI-103x and PXIe-107x Rack Mount Kit	778948-01	No accessories required.	

Support and Services

System Assurance Programs

NI system assurance programs are designed to make it even easier for you to own an NI system. These programs include configuration and deployment services for your NI PXI, CompactRIO, or Compact FieldPoint system. The NI Basic System Assurance Program provides a simple integration test and ensures that your system is delivered completely assembled in one box. When you configure your system with the NI Standard System Assurance Program, you can select from available NI system driver sets and application development environments to create customized, reorderable software configurations. Your system arrives fully assembled and tested in one box with your software preinstalled. When you order your system with the standard program, you also receive system-specific documentation including a bill of materials, an integration test report, a recommended maintenance plan, and frequently asked question documents. Finally, the standard program reduces the total cost of owning an NI system by providing three years of warranty coverage and calibration service. Use the online product advisors at ni.com/advisor to find a system assurance program to meet your needs.

Calibration

NI measurement hardware is calibrated to ensure measurement accuracy and verify that the device meets its published specifications. To ensure the ongoing accuracy of your measurement hardware, NI offers basic or detailed recalibration service that provides ongoing ISO 9001 audit compliance and confidence in your measurements. To learn more about NI calibration services or to locate a qualified service center near you, contact your local sales office or visit ni.com/calibration.

Technical Support

Get answers to your technical questions using the following National Instruments resources.

Support - Visit ni.com/support to access the NI KnowledgeBase, example programs, and tutorials or to contact our applications engineers who are located in NI sales offices around the world and speak the local language.
Discussion Forums - Visit forums.ni.com for a diverse set of discussion boards on topics you care about.
Online Community - Visit community.ni.com to find, contribute, or collaborate on customer-contributed technical content with users like you.

Repair

While you may never need your hardware repaired, NI understands that unexpected events may lead to necessary repairs. NI offers repair services performed by highly trained technicians who quickly return your device with the guarantee that it will perform to factory specifications. For more information, visit ni.com/repair.

Training and Certifications

The NI training and certification program delivers the fastest, most certain route to increased proficiency and productivity using NI software and hardware. Training builds the skills to more efficiently develop robust, maintainable applications, while certification validates your knowledge and ability.

Classroom training in cities worldwide - the most comprehensive hands-on training taught by engineers.
On-site training at your facility - an excellent option to train multiple employees at the same time.
Online instructor-led training - lower-cost, remote training if classroom or on-site courses are not possible.
Course kits - lowest-cost, self-paced training that you can use as reference guides.
Training memberships and training credits - to buy now and schedule training later.

Visit ni.com/training for more information.

Extended Warranty

NI offers options for extending the standard product warranty to meet the life-cycle requirements of your project. In addition, because NI understands that your requirements may change, the extended warranty is flexible in length and easily renewed. For more information, visit ni.com/warranty.

OEM

NI offers design-in consulting and product integration assistance if you need NI products for OEM applications. For information about special pricing and services for OEM customers, visit ni.com/oem.

Alliance

Our Professional Services Team is comprised of NI applications engineers, NI Consulting Services, and a worldwide National Instruments Alliance Partner program of more than 700 independent consultants and integrators. Services range from start-up assistance to turnkey system integration. Visit ni.com/alliance.

Back to Top

Detailed Specifications

Caution If the PXI-1033 chassis is used in a manner inconsistent with the instructions or specifications listed by National Instruments, the protective features of the chassis may be impaired.

Note Specifications are subject to change without notice.

This appendix contains specifications for the PXI-1033 chassis.

Electrical	
AC Input	
Input voltage range	100–240 VAC
Operating voltage range [1]	90–264 VAC

Input frequency	50/60 Hz
Operating frequency range [1]	47–63 Hz
Input current rating	4–2 A
Efficiency	>70% at full load, normal input voltage
Power disconnect	The AC power cable provides main power disconnect. The front-panel power switch controls the internal chassis power supply that provides DC power to the CompactPCI/PXI backplane.
DC Output	

DC current capacity (I_{MP})	
Voltage	**0–50 °C**
+3.3 V	10 A
+5 V	15 A
+12 V	2.5 A
–12 V	0.8 A

Over-current protection	All outputs protected from short circuit

Over-voltage protection		
Over-voltage at	**Active Range**	
	Minimum	**Maximum**
+3.3 V	3.76 V	4.3 V
+5 V	5.74 V	7.0 V
+12 V	13.4 V	15.6 V

Chassis Cooling	
Per slot cooling capacity	25 W
Slot airflow direction	P1 to P2, bottom of module to top of module
Module cooling	
System	Forced air circulation (positive pressurization) through a High Flow fan with HIGH/AUTO speed selector
Intake	Bottom of chassis
Exhaust	Along rear, right side, and top of chassis
Power supply cooling	
System	Forced air circulation through integrated fan
Intake	Front side of chassis
Exhaust	Rear side of chassis
Environmental	
Maximum altitude	2,000 m (800 mbar) (at 25 °C ambient)
Measurement Category	II
Pollution Degree	2
For indoor use only.	
Operating Environment	
Ambient temperature range	0 to 50 °C (Tested in accordance with IEC-60068-2-1 and IEC-60068-2-2. Meets MIL-PRF-28800F Class 3 low temperature limit and high temperature limit.)
Relative humidity range	20 to 80%, noncondensing (Tested in accordance with IEC-60068-2-56.)
Storage Environment	
Ambient temperature range	–40 to 85 °C (Tested in accordance with IEC-60068-2-1 and IEC-60068-2-2. Meets MIL-PRF-28800F Class 3 limits.)
Relative humidity range	10 to 95%, noncondensing (Tested in accordance with IEC-60068-2-56.)

Shock and Vibration	
Operational shock	20 g peak, half-sine, 11 ms pulse (Tested in accordance with IEC-60068-2-27. Meets MIL-PRF-28800F Class 2 limits.)
Random Vibration	
Operating	5 to 500 Hz, 0.3 g_{rms}
Nonoperating	5 to 500 Hz, 2.4 g_{rms} (Tested in accordance with IEC-60068-2-64. Nonoperating test profile exceeds the requirements of MIL-PRF-28800F, Class 3.)

Acoustic Emissions	
Sound Pressure Level (at Operator Position)	
(Tested in accordance with ISO 7779. Meets MIL-PRF-28800F requirements.)	
PXI-1033	
Auto fan (at 25 °C ambient)	37.4 dBA
High fan	51.5 dBA
Sound Power	
(Tested in accordance with ISO 7779.)	
PXI-1033	
Auto fan (at 25 °C ambient)	43.8 dBA
High fan	60.9 dBA

Safety Standards

This product is designed to meet the requirements of the following standards of safety for electrical equipment for measurement, control, and laboratory use:
IEC 61010-1, EN 61010-1
UL 61010-1, CAN/CSA-C22.2 No. 61010-1

Note For UL and other safety certifications, refer to the product label, or visit ni.com/certification, search by model number or product line, and click the appropriate link in the Certification column.

Electromagnetic Compatibility

This product is designed to meet the requirements of the following standards of EMC for electrical equipment for measurement, control, and laboratory use:

EN 61326 EMC requirements; Minimum Immunity
EN 55011 Emissions; Group 1, Class A
CE, C-Tick, ICES, and FCC Part 15 Emissions; Class A

Note For EMC compliance, operate this device according to printed documentation.

CE Compliance

This product meets the essential requirements of applicable European Directives, as amended for CE marking, as follows:

Low-Voltage Directive (safety)	73/23/EEC
Electromagnetic Compatibility Directive (EMC)	89/336/EEC

Note Refer to the Declaration of Conformity (DoC) for this product for any additional regulatory compliance information. To obtain the DoC for this product, visit ni.com/certification, search by model number or product line, and click the appropriate link in the Certification column.

Waste Electrical and Electronic Equipment (WEEE)

EU Customers At the end of the product life cycle, all products *must* be sent to a WEEE recycling center. For more information about WEEE recycling centers, National Instruments WEEE initiatives, and compliance with WEEE Directive 2002/96/EC on Waste Electrical and Electronic Equipment, visit ni.com/environment/weee.htm.

Backplane

Size	3U-sized; integrated controller and 5 peripheral slots. Compliant with IEEE 1101.10 mechanical packaging. *PXI Hardware Specification, Revision 2.2* compliant. Accepts both PXI and CompactPCI 3U modules.
V(I/O) [2]	+5 V
Backplane bare-board material	UL 94 V-0 recognized
Backplane connectors	Conform to IEC 917 and IEC 1076-4-101, and are UL 94 V-0 rated

10 MHz System Reference Clock (10 MHz REF)	
Maximum clock skew between slots	250 ps
Built-in 10 MHz clock	
Accuracy	±25 ppm (guaranteed over the operating temperature range)

Mechanical	
Overall dimensions (standard chassis)	
Height	177 mm (6.97 in.)

Note 12.7 mm (0.50 in.) is added to height when feet are installed.

Width	257.1 mm (10.12 in.)
Depth	212.8 mm (8.38 in.)
Weight	5 kg (11.0 lbs)
Chassis materials	Sheet Aluminum, Extruded Aluminum, Cold Rolled Steel, Nylon
Finish	Clear Chromate Conversion Coat on Aluminum, Electrodeposited Nickel Plate Plate on Cold Rolled Steel, Polyester Urethane Powder Paint

The following two figures show the PXI-1033 dimensions. The holes shown are for the installation of the optional rack-mount kits as shown in the third figure. Notice that the front and rear rack mounting holes (size M4) are symmetrical.

PXI-1033 Dimensions (Front and Side) in Inches (mm)

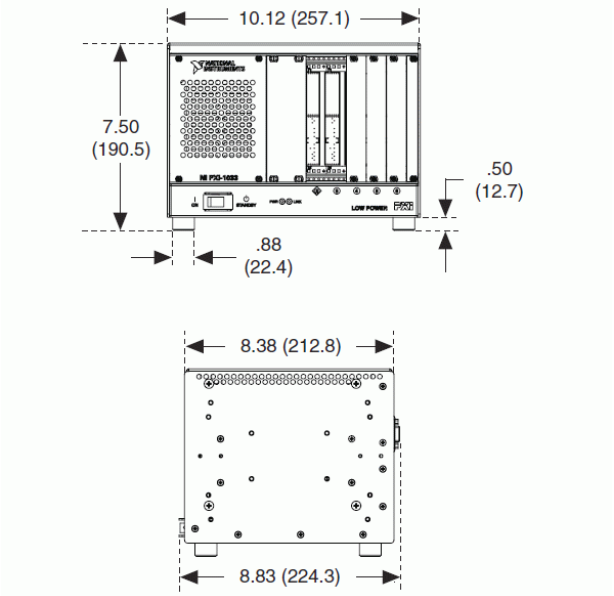

PXI-1033 Dimensions (Bottom) in Inches (mm)

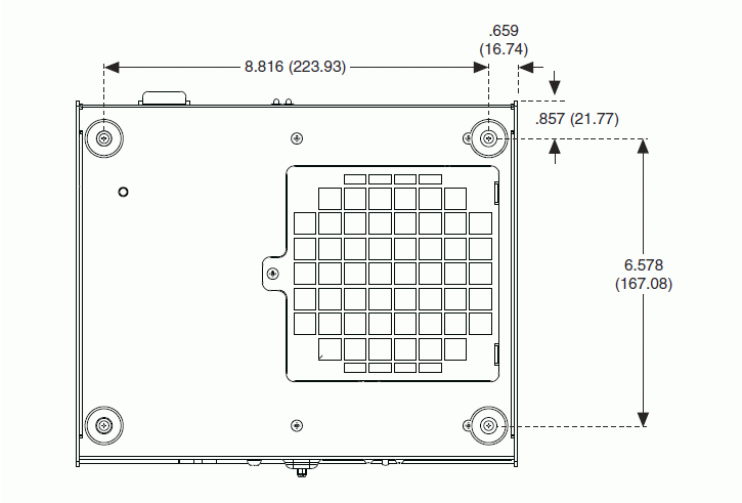

The following figure shows the PXI-1033 rack mount kit components.

PXI-1033 Rack Mount Kit Components

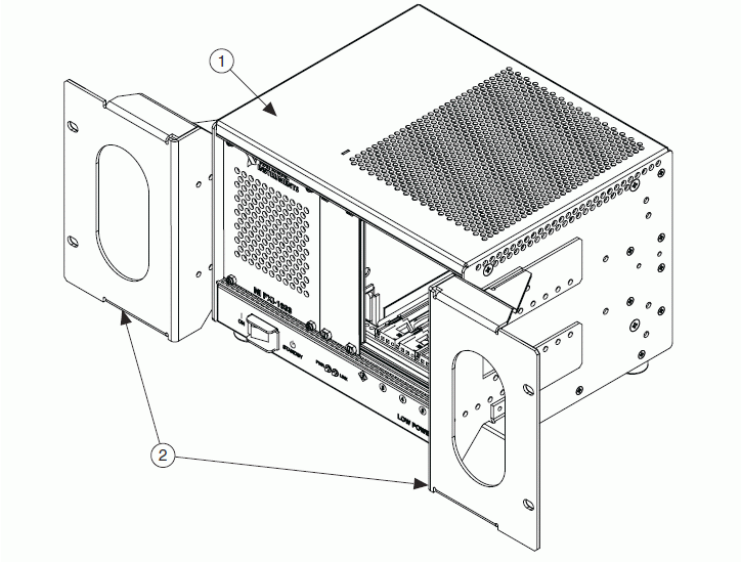

1 PXI-1033 Chassis	2 Rack Mount Kit

[1] The operating range is guaranteed by design.
[2] V(I/O) is connected to the +5 V DC power plane, so the same specifications apply to V(I/O) and +5 V.

Back to Top

F Data Sheet of A/D converter

Last Revised: 2011-10-21 10:32:43.0

High-Speed M Series Multifunction Data Acquisition - 16-Bit, up to 1.25 MS/s, up to 80 Analog Inputs

- 16, 32, or 80 analog inputs at 16 bits, 1.25 MS/s (1 MS/s scanning, NI 6255 specified at 750 kS/s scanning)
- Up to 4 analog outputs at 16 bits, 2.8 MS/s (2 µs full-scale settling)
- 7 programmable input ranges (±100 mV to ±10 V) per channel
- Up to 48 TTL/CMOS digital I/O lines (up to 32 hardware-timed at 10 MHz)
- Two 32-bit, 80 MHz counter/timers
- Analog and digital triggering
- X1, X2, or X4 quadrature encoder inputs
- 2-year calibration interval

Overview

NI M Series high-speed multifunction data acquisition (DAQ) devices are optimized for superior accuracy at fast sampling rates. These devices have NI-MCal calibration technology for improved measurement accuracy and six DMA channels for high-speed data throughput. They have an onboard NI-PGIA 2 amplifier designed for fast settling times at high scanning rates, ensuring 16-bit accuracy even when measuring all channels at maximum speeds. All high-speed devices have a minimum of 16 analog inputs, 24 digital I/O lines, seven programmable input ranges, analog and digital triggering, two counter/timers, and an extended two-year calibration interval.

NI recommends high-accuracy M Series devices (NI 628x) for 5X more measurement sensitivity or industrial M Series devices (NI 623x) for 60 VDC isolation and superior noise rejection.

See the NI USB-625x data sheet for information specific to USB M Series devices.

Back to Top

Requirements and Compatibility

OS Information
Linux®
Mac OS X
Windows 2000/XP
Windows 7
Windows Vista x64/x86

Driver Information
NI-DAQmx
NI-DAQmx Base

Software Compatibility
ANSI C/C++
LabVIEW
LabWindows/CVI
SignalExpress
Visual Basic
Visual C#
Visual Studio .NET

Back to Top

Comparison Tables

Family	Bus	Analog Inputs	AI Resolution (bits)	Analog Outputs	AO Resolution	Max Update Rate (MS/s)	AO Range (V)	Digital I/O	Correlated (clocked) DIO
NI 6250	PCI, PXI	16	16	0	-	-	-	24	8, up to 10 MHz
NI 6251	PCI, PCI Express, PXI, PXI Express, USB	16	16	2	16	2.8	±10, ±5, ±ext ref	24	8, up to 10 MHz
NI 6254	PCI, PXI	32	16	0	-	-	-	48	32, up to 10 MHz

Family	Bus	Analog Inputs	AI Resolution (bits)	Analog Outputs	AO Resolution	Max Update Rate (MS/s)	AO Range (V)	Digital I/O	Correlated (clocked) DIO
NI 6255	PCI, PXI, USB	80	16	2	16	2.8	±10, ±5, ±ext ref	24	8, up to 10 MHz
NI 6259	PCI, PCI Express, PXI, PXI Express, USB	32	16	4	16	2.8	±10, ±5, ±ext ref	48	32, up to 10 MHz

Back to Top

Application and Technology

M Series for Test

For test, you can use M Series high-speed analog inputs and 10 MHz digital lines with NI signal conditioning for applications including electronics test, component characterization, and sensor measurements. High-speed M Series devices are compatible with NI SCC and SCXI signal conditioning platforms, which provide amplification, filtering, and power for virtually every type of sensor. These platforms also are compliant with IEEE 1451.4 smart transducer electronic data sheet (TEDS) sensors, which provide digital storage for sensor data sheet information.

M Series for Control

M Series digital lines can drive 24 mA for relay and actuator control. By clocking the digital lines as fast as 10 MHz, you can use these lines for pulse-width modulation (PWM) to control valves, motors, fans, lamps, and pumps. With four waveform analog outputs, two 80 MHz counter/timers, and six DMA channels, M Series devices can execute multiple control loops simultaneously. High-speed M Series devices also have direct support for quadrature encoder measurements, protected digital lines, and digital debounce filters for control applications. With up to 80 analog inputs, 32 clocked digital lines, and four analog outputs, you can execute multiple control loops with a single device. For higher-count control loops, you can use M Series devices in conjunction and tightly synchronized with National Instruments analog output devices for 64 or more loops. With the NI SoftMotion Development Module for LabVIEW, you can create a complete custom motion controller with M Series devices.

M Series for Design

You can use the wide range of I/O – from 80 analog inputs to 48 digital lines – to measure and verify prototype designs. M Series devices and NI LabVIEW SignalExpress interactive measurement software deliver benchtop measurements to the PC. With LabVIEW SignalExpress interactive configuration-based steps, you can quickly create design verification tests. The fast acquisition and generation rates of high-speed M Series devices along with LabVIEW SignalExpress provide on-the-fly design analysis. You can convert your tested and verified LabVIEW SignalExpress projects to LabVIEW applications for immediate M Series DAQ use, thus bridging the gap between test, control, and design applications.

M Series Performance on PCI Express

National Instruments was the first company to empower engineers and scientists to use the PCI Express and PXI Express buses for data acquisition. PCI Express M Series boards contain six DMA channels to maximize data throughput without using PC processing time. The PCI Express bus delivers the highest bandwidth compared to any other PC bus, and it eliminates throughput bottlenecks by providing 250 MB/s per-direction bandwidth across the x1 (“by one”) lane for increased data transfer. Each slot allocates dedicated bandwidth, meaning that multiple PCI Express boards do not share bandwidth for data transfer. With this improvement over the shared-bandwidth PCI architecture, all onboard I/O runs simultaneously while data is transferred to and from PC memory across the bus. The PXI Express specifications integrate PCI Express signaling into the PXI Standard, which increases backplane bandwidth from 132 MB/s to 6 GB/s, a 45 times improvement. Both PCI Express and PXI Express facilitate a smooth transition to new hardware by providing complete backward compatibility to software written for applications that use PCI or PXI, respectively.

Hybrid-Slot-Compatible PXI Modules

PXI M Series modules are hybrid-slot-compatible so that you can use them in both PXI slots and the hybrid slots found in new PXI Express chassis. The PXI Systems Alliance specifies that hybrid-slot-compatible PXI modules use modified slot connectors to mechanically fit in both PXI slots and hybrid slots. This mechanical change:

Provides compatibility with past, current, and future PXI chassis
Maintains existing product specifications
Requires no software changes (application or driver)
Maintains speed and capability of all PXI communication (PXI Express signaling is not provided)

However, hybrid-slot-compatible PXI modules do not include the pins used to implement PXI local bus communication, which is used for backplane SCXI control from the right-most PXI slot in PXI/SCXI combination chassis (PXI-1010, PXI-1011, PXI-1050, and PXI-1052). For these applications, NI provides unmodified PXI M Series modules that maintain the required local bus capabilities. Refer to the SCXI Control of PXI/SCXI Combination Chassis section in the Ordering Information section for part numbers.

Industrial Data Acquisition

When you need performance and accuracy from a data acquisition device in an electrically noisy or harsh environment, consider National Instruments industrial M Series devices (NI 623x). NI industrial DAQ devices offer a set of high-reliability features, including isolation, ±20 mA current I/O, 24 V digital logic levels, and digital debounce filters. Isolation prevents ground loops, rejects high common-mode voltages, and protects users and equipment from high-voltage transients. Four to 20 mA current loops are immune to most sources of electrical noise and voltage (IR) drops along extensive cable lengths. Sourcing or sinking 24 V digital I/O interfaces directly with pumps, valves, relays, and other industry-standard sensors and actuators, and programmable debounce filters remove glitches and spikes from switches and relays connected to digital input lines.

Simultaneous and Intelligent Data Acquisition

When you need to obtain performance from a data acquisition device beyond the capabilities of a multifunction data acquisition device, National Instruments provides simultaneous sampling with NI S Series and intelligent data acquisition with NI R Series. The S Series architecture dedicates an analog-to-digital converter (ADC) per channel to provide higher aggregate sampling rates compared to multiplexed devices. S Series devices are ideal for applications including IF digitization, transient recording, ultrasound and sonar testing, and high-energy physics. R Series multifunction DAQ devices contain a field-programmable gate array (FPGA) that is reconfigurable using the LabVIEW FPGA Module.

They combine analog input, analog output, and digital I/O on a single device. You can customize these devices to develop capabilities such as complete control over the synchronization and timing of all signals and operations; user-defined onboard decision-making logic; and digital lines individually configurable as input, output, counter/timers, PWM, flexible encoder inputs, or user-defined communication protocols.

Recommended Accessories

Signal conditioning is required for sensor measurements or voltage inputs greater than 10 V. NI SCXI is a versatile, high-performance signal conditioning platform optimized for high-channel-count applications. NI SCC provides portable, flexible signal conditioning options on a per-channel basis. Visit **ni.com/sigcon** for resources on available NI signal conditioning.

Recommended Driver Software

National Instruments measurement services software, built around NI-DAQmx driver software, includes intuitive application programming interfaces, configuration tools, I/O assistants, and other tools designed to reduce system setup, configuration, and development time. National Instruments recommends using the latest version of NI-DAQmx driver software for application development in NI

LabVIEW, LabVIEW SignalExpress, LabWindows™/CVI, and Measurement Studio software. To obtain the latest version of NI-DAQmx, visit **ni.com/support/daq/versions**. NI measurement services software speeds up your development with features including the following:

A guide to create fast and accurate measurements with no programming using the DAQ Assistant
Automatic code generation to create your application in LabVIEW; LabWindows/CVI; LabVIEW SignalExpress; and C#, Visual Studio .NET, ANSI C/C++, or Visual Basic using Measurement Studio
Multithreaded streaming technology for 1,000 times performance improvements
Automatic timing, triggering, and synchronization routing to make advanced applications easy
Thousands of free software downloads available at **ni.com/zone** to jump-start your project
Software configuration of all digital I/O features without hardware switches/jumpers
Single programming interface for analog input, analog output, digital I/O, and counters on hundreds of multifunction data acquisition hardware devices

M Series devices are compatible with the following versions (or later) of NI application software – LabVIEW, LabWindows/CVI, or Measurement Studio versions 7.x; and LabVIEW SignalExpress 2.x.

Back to Top

Ordering Information

For a complete list of accessories, visit the product page on ni.com.

Products	Part Number	Recommended Accessories	Part Number
NI PCI-6250			
NI PCI-6250 Requires: 1 Cables , 1 Connector Blocks ;	779069-01	**Cables:** Shielded - SHC68-68-EPM Cable (2m) ***Also Available: [Unshielded]*	192061-02
		Connector Blocks: Spring-Screw_Terminals - SCB-68A ***Also Available: [BNC_Terminals, Custom]*	782536-01
NI PXI-6250			
NI PXI-6250 Requires: 1 Cable , 1 Connector Block ;	779116-01	**Cable:** Shielded - SHC68-68-EPM Cable (2m) ***Also Available: [Unshielded]*	192061-02
		Connector Block: Spring-Screw_Terminals - SCB-68A ***Also Available: [BNC_Terminals, Custom]*	782536-01
NI PCI-6251			
NI PCI-6251 Requires: 1 Cables , 1 Connector Blocks ;	779070-01	**Cables:** Shielded - SHC68-68-EPM Cable (2m) ***Also Available: [Unshielded]*	192061-02
		Connector Blocks: Spring-Screw_Terminals - SCB-68A ***Also Available: [BNC_Terminals, Custom]*	782536-01
NI PCIe-6251			
NI PCIe-6251 Requires: 1 Cables , 1 Connector Blocks ;	779512-01	**Cables:** Shielded - SHC68-68-EPM Cable (2m) ***Also Available: [Unshielded]*	192061-02
		Connector Blocks: Spring-Screw_Terminals - SCB-68A ***Also Available: [BNC_Terminals, Custom]*	782536-01
NI PXI-6251			
NI PXI-6251 Requires: 1 Cables , 1 Connector Block ;	779631-01	**Cables:** Shielded - SHC68-68-EPM Cable (2m) ***Also Available: [Unshielded]*	192061-02
		Connector Block: Spring-Screw_Terminals - SCB-68A ***Also Available: [BNC_Terminals, Custom]*	782536-01
NI PXIe-6251			
NI PXIe-6251 Requires: 1 Cables , 1 Connector Block ;	779777-01	**Cables:** Shielded - SHC68-68-EPM Cable (2m) ***Also Available: [Unshielded]*	192061-02
		Connector Block: Spring-Screw_Terminals - SCB-68A ***Also Available: [BNC_Terminals, Custom]*	782536-01
NI PCI-6254			
NI PCI-6254 Requires: 2 Cables , 2 Connector Blocks ;	779071-01	**Connector 0:**	
		Cables: Shielded - SHC68-68-EPM Cable (2m) ***Also Available: [Unshielded]*	192061-02
		Connector Blocks: Spring-Screw_Terminals - SCB-68A ***Also Available: [BNC_Terminals]*	782536-01
		Connector 1:	
		Cables: Shielded - SHC68-68-EPM Cable (2m) ***Also Available: [Unshielded]*	192061-02
		Connector Blocks: Spring-Screw_Terminals - SCB-68A ***Also Available: [BNC_Terminals]*	782536-01
NI PXI-6254			
NI PXI-6254 Requires: 1 Cables , 1 Connector Block ;	779118-01	**Connector 0:**	

		Cables: Shielded - SHC68-68-EPM Cable (2m) ***Also Available: [Unshielded]*	192061-02
		Connector Block: Spring-Screw_Terminals - SCB-68A ***Also Available: [BNC_Terminals]*	782536-01
		Connector 1:	
		Cables: Shielded - SHC68-68-EPM Cable (2m) ***Also Available: [Unshielded]*	192061-02
		Connector Block: Spring-Screw_Terminals - SCB-68A ***Also Available: [BNC_Terminals]*	782536-01
NI PCI-6255			
NI PCI-6255 Requires: 2 Cables , 2 Connector Block ;	779546-01	**Connector 0:**	
		Cables: Shielded - SHC68-68-EPM Cable (2m) ***Also Available: [Unshielded]*	192061-02
		Connector Block: Spring-Screw_Terminals - SCB-68A ***Also Available: [BNC_Terminals]*	782536-01
		Connector 1:	
		Cables: Shielded - SHC68-68-EPM Cable (2m) ***Also Available: [Unshielded]*	192061-02
		Connector Block: Spring-Screw_Terminals - SCB-68A ***Also Available: [BNC_Terminals]*	782536-01
NI PXI-6255			
NI PXI-6255 Requires: 1 Cables , 1 Connector Block ;	779547-01	**Connector 0:**	
		Cables: Shielded - SHC68-68-EPM Cable (2m) ***Also Available: [Unshielded]*	192061-02
		Connector Block: Spring-Screw_Terminals - SCB-68A ***Also Available: [BNC_Terminals, Custom]*	782536-01
		Connector 1:	
		Cables: Shielded - SHC68-68-EPM Cable (2m) ***Also Available: [Unshielded]*	192061-02
		Connector Block: Spring-Screw_Terminals - SCB-68A ***Also Available: [BNC_Terminals, Custom]*	782536-01
NI PCI-6259			
NI PCI-6259 Requires: 2 Cables , 2 Connector Blocks ;	779072-01	**Connector 0:**	
		Cables: Shielded - SHC68-68-EPM Cable (2m) ***Also Available: [Unshielded]*	192061-02
		Connector Blocks: Spring-Screw_Terminals - SCB-68A ***Also Available: [BNC_Terminals]*	782536-01
		Connector 1:	
		Cables: Shielded - SHC68-68-EPM Cable (2m) ***Also Available: [Unshielded]*	192061-02
		Connector Blocks: Spring-Screw_Terminals - SCB-68A ***Also Available: [BNC_Terminals]*	782536-01
NI PCIe-6259			
NI PCIe-6259 Requires: 2 Cables , 2 Connector Blocks ;	779513-01	**Connector 0:**	
		Cables: Shielded - SHC68-68-EPM Cable (2m) ***Also Available: [Unshielded]*	192061-02
		Connector Blocks: Spring-Screw_Terminals - SCB-68A ***Also Available: [BNC_Terminals]*	782536-01
		Connector 1:	
		Cables: Shielded - SHC68-68-EPM Cable (2m) ***Also Available: [Unshielded]*	192061-02
		Connector Blocks: Spring-Screw_Terminals - SCB-68A ***Also Available: [BNC_Terminals]*	782536-01
NI PXI-6259			
NI PXI-6259 Requires: 1 Cables , 1 Connector Block ;	779632-01	**Connector 0:**	
		Cables: Shielded - SHC68-68-EPM Cable (2m) ***Also Available: [Unshielded]*	192061-02
		Connector Block: Spring-Screw_Terminals - SCB-68A	782536-01

		***Also Available: [BNC_Terminals]*	
		Connector 1:	
		Cables: Shielded - SHC68-68-EPM Cable (2m) ***Also Available: [Unshielded]*	192061-02
		Connector Block: Spring-Screw_Terminals - SCB-68A ***Also Available: [BNC_Terminals]*	782536-01
NI PXIe-6259			
NI PXIe-6259 Requires: 1 Cables , 1 Connector Block ;	779778-01	**Connector 0:**	
		Cables: Shielded - SHC68-68-EPM Cable (2m) ***Also Available: [Unshielded]*	192061-02
		Connector Block: Spring-Screw_Terminals - SCB-68A ***Also Available: [BNC_Terminals]*	782536-01
		Connector 1:	
		Cables: Shielded - SHC68-68-EPM Cable (2m) ***Also Available: [Unshielded]*	192061-02
		Connector Block: Spring-Screw_Terminals - SCB-68A ***Also Available: [BNC_Terminals]*	782536-01

Back to Top

Software Recommendations

LabVIEW Professional Development System for Windows

Advanced software tools for large project development
Automatic code generation using DAQ Assistant and Instrument I/O Assistant
Tight integration with a wide range of hardware
Advanced measurement analysis and digital signal processing
Open connectivity with DLLs, ActiveX, and .NET objects
Capability to build DLLs, executables, and MSI installers

SignalExpress for Windows

Quickly configure projects without programming
Control over 400 PC-based and stand-alone instruments
Log data from more than 250 data acquisition devices
Perform basic signal processing, analysis, and file I/O
Scale your application with automatic LabVIEW code generation
Create custom reports or easily export data to LabVIEW, DIAdem or Microsoft Excel

NI LabWindows™/CVI for Windows

Real-time advanced 2D graphs and charts
Complete hardware compatibility with IVI, VISA, DAQ, GPIB, and serial
Analysis tools for array manipulation, signal processing statistics, and curve fitting
Simplified cross-platform communication with network variables
Measurement Studio .NET tools (included in LabWindows/CVI Full only)
The mark LabWindows is used under a license from Microsoft Corporation.

NI Measurement Studio Professional Edition

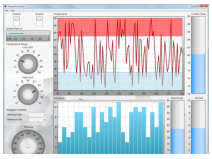

Customizable graphs and charts for WPF, Windows Forms, and ASP.NET Web Forms UI design
Analysis libraries for array operations, signal generation, windowing, filters, signal processing
Hardware integration support with native .NET data acquisition and instrument control libraries
Automatic code generation for all NI-DAQmx data acquisition hardware
Intelligent and efficient data-logging libraries for streaming measurement data to disk
Support for Microsoft Visual Studio .NET 2012/2010/2008

Back to Top

Support and Services

System Assurance Programs

NI system assurance programs are designed to make it even easier for you to own an NI system. These programs include configuration and deployment services for your NI PXI, CompactRIO, or Compact FieldPoint system. The NI Basic System Assurance Program provides a simple integration test and ensures that your system is delivered completely assembled in one box. When you configure your system with the NI Standard System Assurance Program, you can select from available NI system driver sets and application development environments to create customized, reorderable software configurations. Your system arrives fully assembled and tested in one box with your software preinstalled. When you order your system with the standard program, you also receive system-specific documentation including a bill of materials, an integration test report, a recommended maintenance plan, and frequently asked question documents. Finally, the standard program reduces the total cost of owning an NI system by providing three years of warranty coverage and calibration service. Use the online product advisors at ni.com/advisor to find a system assurance program to meet your needs.

Calibration

NI measurement hardware is calibrated to ensure measurement accuracy and verify that the device meets its published specifications. To ensure the ongoing accuracy of your measurement hardware, NI offers basic or detailed recalibration service that provides ongoing ISO 9001 audit compliance and confidence in your measurements. To learn more about NI calibration services or to locate a qualified service center near you, contact your local sales office or visit ni.com/calibration.

Technical Support

Get answers to your technical questions using the following National Instruments resources.

Support - Visit ni.com/support to access the NI KnowledgeBase, example programs, and tutorials or to contact our applications engineers who are located in NI sales offices around the world and speak the local language.
Discussion Forums - Visit forums.ni.com for a diverse set of discussion boards on topics you care about.
Online Community - Visit community.ni.com to find, contribute, or collaborate on customer-contributed technical content with users like you.

Repair

While you may never need your hardware repaired, NI understands that unexpected events may lead to necessary repairs. NI offers repair services performed by highly trained technicians who quickly return your device with the guarantee that it will perform to factory specifications. For more information, visit ni.com/repair.

Training and Certifications

The NI training and certification program delivers the fastest, most certain route to increased proficiency and productivity using NI software and hardware. Training builds the skills to more efficiently develop robust, maintainable applications, while certification validates your knowledge and ability.

Classroom training in cities worldwide - the most comprehensive hands-on training taught by engineers.
On-site training at your facility - an excellent option to train multiple employees at the same time.
Online instructor-led training - lower-cost, remote training if classroom or on-site courses are not possible.
Course kits - lowest-cost, self-paced training that you can use as reference guides.
Training memberships and training credits - to buy now and schedule training later.
Visit ni.com/training for more information.

Extended Warranty

NI offers options for extending the standard product warranty to meet the life-cycle requirements of your project. In addition, because NI understands that your requirements may change, the extended warranty is flexible in length and easily renewed. For more information, visit ni.com/warranty.

OEM

NI offers design-in consulting and product integration assistance if you need NI products for OEM applications. For information about special pricing and services for OEM customers, visit ni.com/oem.

Alliance

Our Professional Services Team is comprised of NI applications engineers, NI Consulting Services, and a worldwide National Instruments Alliance Partner program of more than 700 independent consultants and integrators. Services range from start-up assistance to turnkey system integration. Visit ni.com/alliance.

Back to Top

Detailed Specifications

Specifications listed below are typical at 25 °C unless otherwise noted. Refer to the *M Series User Manual* for more information about NI 625*x* devices.

Analog Input	
Number of channels	
NI 6250/6251	8 differential or 16 single ended
NI 6254/6259	16 differential or 32 single ended
NI 6255	40 differential or 80 single ended
ADC resolution	16 bits
DNL	No missing codes guaranteed
INL	Refer to the *AI Absolute Accuracy Table*
Sampling rate	
Maximum	
NI 6250/6251/6254/6259	1.25 MS/s single channel, 1.00 MS/s multi-channel (aggregate)
NI 6255	1.25 MS/s single channel 750 kS/s multi-channel (aggregate)
Minimum	No minimum
Timing accuracy	50 ppm of sample rate
Timing resolution	50 ns
Input coupling	DC
Input range	±10 V, ±5 V, ±2 V, ±1 V, ±0.5 V, ±0.2 V, ±0.1 V
Maximum working voltage for analog inputs (signal + common mode)	±11 V of AI GND
CMRR (DC to 60 Hz)	100 dB
Input impedance	

Device on	
AI+ to AI GND	>10 GΩ in parallel with 100 pF
AI- to AI GND	>10 GΩ in parallel with 100 pF
Device off	
AI+ to AI GND	820 Ω
AI- to AI GND	820 Ω
Input bias current	±100 pA
Crosstalk (at 100 kHz)	
Adjacent channels	-75 dB
Non-adjacent channels	-90 dB[1]
Small signal bandwidth (-3 dB)	1.7 MHz
Input FIFO size	4,095 samples
Scan list memory	4,095 entries
Data transfers	
PCI/PCIe/PXI/PXIe devices	DMA (scatter-gather), interrupts, programmed I/O
USB devices	USB Signal Stream, programmed I/O
Overvoltage protection (AI <0..79>, AI SENSE, AI SENSE 2)	
Device on	±25 V for up to four AI pins
Device off	±15 V for up to four AI pins
Input current during overvoltage condition	±20 mA max/AI pin

[1] For USB-6255 devices, channel AI <0..15> crosstalk to channel AI <64..79> is -67 dB; applies to channels with 64-channel separation, for example, AI (*x*) and AI (*x* + 64).

Settling Time for Multichannel Measurements

NI 6250/6251/6254/6259

Range	±60 ppm of Step (±4 LSB for Full Scale Step)	±15 ppm of Step (±1 LSB for Full Scale Step)
±10 V, ±5 V, ±2 V, ±1 V	1 µs	1.5 µs
±0.5 V	1.5 µs	2 µs
±0.2 V, ±0.1 V	2 µs	8 µs

NI 6255

Range	±60 ppm of Step (±4 LSB for Full Scale Step)	±15 ppm of Step (±1 LSB for Full Scale Step)
±10 V, ±5 V, ±2 V, ±1 V	1.3 µs	1.6 µs
±0.5 V	1.8 µs	2.5 µs
±0.2 V, ±0.1 V	3 µs	8 µs

Typical Performance Graphs

NI 6250/6251/6254/6259
Settling Error Versus Time for Different Source Impedances

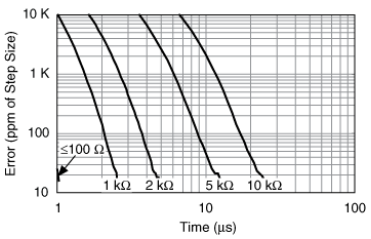

AI <0..79> Small Signal Bandwidth

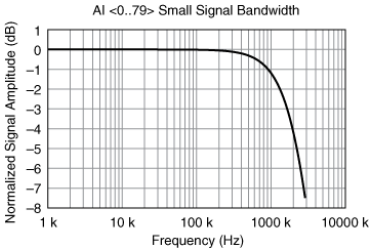

NI 6255
Settling Error Versus Time for Different Source Impedances

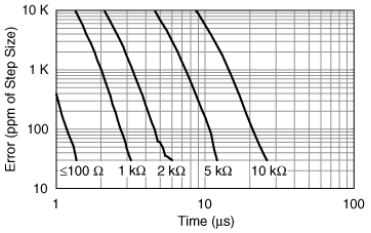

AI <0..79> CMRR

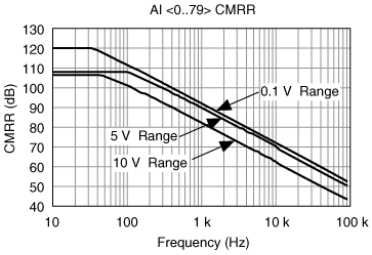

Analog Triggers	
Number of triggers	1
Source	
NI 6250/6251	AI <0..15>, APFI 0
NI 6254/6259	AI <0..31>, APFI <0..1>
NI 6255	AI <0..79>, APFI 0
Functions	Start Trigger, Reference Trigger, Pause Trigger, Sample Clock, Convert Clock, Sample Clock Timebase
Source level	
AI <0..79>	±full scale
APFI <0..1>	±10 V
Resolution	10 bits, 1 in 1,024
Modes	Analog edge triggering, analog edge triggering with hysteresis, and analog window triggering
Bandwidth (-3 dB)	
AI <0..79>	3.4 MHz
APFI <0..1>	3.9 MHz
Accuracy	±1%
APFI <0..1> characteristics	
Input impedance	10 kΩ
Coupling	DC
Protection	
Power on	±30 V
Power off	±15 V
Analog Output	
Number of channels	
NI 6250/6254	0

NI 6251/6255	2
NI 6259	4
DAC resolution	16 bits
DNL	±1 LSB
Monotonicity	16 bit guaranteed
Accuracy	Refer to the *AO Absolute Accuracy Table*
Maximum update rate	
1 channel	2.86 MS/s
2 channels	2.00 MS/s
3 channels	1.54 MS/s
4 channels	1.25 MS/s
Timing accuracy	50 ppm of sample rate
Timing resolution	50 ns
Output range	±10 V, ±5 V, ±external reference on APFI <0..1>
Output coupling	DC
Output impedance	0.2 Ω
Output current drive	±5 mA
Overdrive protection	±25 V
Overdrive current	20 mA
Power-on state	±5 mV[2]
Power-on glitch	1.5 V peak for 1.5 s
Output FIFO size	8,191 samples shared among channels used
Data transfers	
PCI/PCIe/PXI/PXIe devices	DMA (scatter-gather), interrupts, programmed I/O
USB devices	USB Signal Stream, programmed I/O
AO waveform modes: Non-periodic waveform Periodic waveform regeneration mode from onboard FIFO Periodic waveform regeneration from host buffer including dynamic update	
Settling time, full scale step 15 ppm (1 LSB)	2 µs
Slew rate	20 V/µs
Glitch energy at midscale transition, ±10 V range	
Magnitude	10 mV
Duration	1 µs

[2] For all USB-6251/6259 Screw Terminal devices, when powered on, the analog output signal is not defined until after USB configuration is complete.

External Reference	
APFI <0..1> characteristics	
Input impedance	10 kΩ
Coupling	DC
Protection	
Power on	±30 V
Power off	±15 V
Range	±11 V
Slew rate	20 V/µs

AO <0..3> Analog Output External Reference Bandwidth

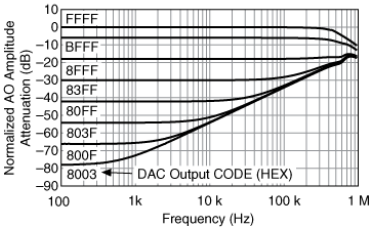

Calibration (AI and AO)

Recommended warm-up time	15 minutes
Calibration interval	2 years

AI Absolute Accuracy Table

Nominal Range		Residual Gain Error (ppm of Reading)	Gain Tempco (ppm/°C)	Reference Tempco	Residual Offset Error (ppm of Range)	Offset Tempco (ppm of Range/°C)	INL Error (ppm of Range)	Random Noise, σ (μVrms)	Absolute Accuracy at Full Scale[1] (μV)	Sensitivity[2] (μV)
Positive Full Scale	Negative Full Scale									
10	-10	60	13	1	20	21	60	280	1,920	112.0
5	-5	70	13	1	20	21	60	140	1,010	56.0
2	-2	70	13	1	20	24	60	57	410	22.8
1	-1	80	13	1	20	27	60	32	220	12.8
0.5	- 0.5	90	13	1	40	34	60	21	130	8.4
0.2	- 0.2	130	13	1	80	55	60	16	74	6.4
0.1	- 0.1	150	13	1	150	90	60	15	52	6.0

Accuracies listed are valid for up to two years from the device external calibration.

AbsoluteAccuracy = Reading · (GainError) + Range · (OffsetError) + NoiseUncertainty

GainError = ResidualAIGainError + GainTempco · (TempChangeFromLastInternalCal) + ReferenceTempco · (TempChangeFromLastExternalCal)

OffsetError = ResidualAIOffsetError + OffsetTempco · (TempChangeFromLastInternalCal) + INL_Error

$$\text{NoiseUncertainty} = \frac{\text{RandomNoise} \cdot 3}{\sqrt{100}} \qquad \text{For a coverage factor of 3 } \sigma \text{ and averaging 100 points.}$$

[1] Absolute accuracy at full scale on the analog input channels is determined using the following assumptions:

TempChangeFromLastExternalCal = 10 °C

TempChangeFromLastInternalCal = 1 °C

number_of_readings = 100

CoverageFactor = 3 σ

For example, on the 10 V range, the absolute accuracy at full scale is as follows:

GainError = 60 ppm + 13 ppm · 1 + 1 ppm · 10 GainError = 83 ppm

OffsetError = 20 ppm + 21 ppm · 1 + 60 ppm OffsetError = 101 ppm

$$\text{NoiseUncertainty} = \frac{275\ \mu\text{V} \cdot 3}{\sqrt{100}} \qquad \text{NoiseUncertainty} = 83\ \mu\text{V}$$

AbsoluteAccuracy = 10 V · (GainError) + 10 V · (OffsetError) + NoiseUncertainty AbsoluteAccuracy = 1920 µV

[2] Sensitivity is the smallest voltage change that can be detected. It is a function of noise.

AO Absolute Accuracy Table

Nominal Range		Residual Gain Error (ppm of Reading)	Gain Tempco (ppm/°C)	Reference Tempco	Residual Offset Error (ppm of Range)	Offset Tempco (ppm of Range/°C)	INL Error (ppm of Range)	Absolute Accuracy at Full Scale[1] (μV)
Positive Full Scale	Negative Full Scale							
10	-10	75	17	1	40	2	64	2,080
5	-5	85	8	1	40	2	64	1,045

[1] Absolute Accuracy at full scale numbers is valid immediately following internal calibration and assumes the device is operating within 10 °C of the last external calibration.
Accuracies listed are valid for up to two years from the device external calibration.

AbsoluteAccuracy = OutputValue · (GainError) + Range · (OffsetError)

GainError = ResidualGainError + GainTempco · (TempChangeFromLastInternalCal) + ReferenceTempco · (TempChangeFromLastExternalCal)

OffsetError = ResidualOffsetError + AOOffsetTempco · (TempChangeFromLastInternalCal) + INL_Error

Digital I/O/PFI	
Static Characteristics	
Number of channels	
NI 6250/6251/6255	24 total, 8 (P0.<0..7>), 16 (PFI <0..7>/P1, PFI <8..15>/P2)
NI 6254/6259	48 total, 32 (P0.<0..31>), 16 (PFI <0..7>/P1, PFI <8..15>/P2)
Ground reference	D GND
Direction control	Each terminal individually programmable as input or output
Pull-down resistor	50 kΩ typ, 20 kΩ min
Input voltage protection[3]	±20 V on up to two pins

[3] Stresses beyond those listed under Input voltage protection may cause permanent damage to the device.

Waveform Characteristics (Port 0 Only)	
Terminals used	
NI 6250/6251/6255	Port 0 (P0.<0..7>)
NI 6254/6259	Port 0 (P0.<0..31>)
Port/sample size	
NI 6250/6251/6255	Up to 8 bits
NI 6254/6259	Up to 32 bits
Waveform generation (DO) FIFO	2,047 samples
Waveform acquisition (DI) FIFO	2,047 samples
DI Sample Clock frequency	
PCI/PCIe/PXI/PXIe devices	0 to 10 MHz[4]
USB devices	0 to 1 MHz system dependent[4]
DO Sample Clock frequency	
PCI/PCIe/PXI/PXIe devices	
Regenerate from FIFO	0 to 10 MHz
Streaming from memory	0 to 1 MHz system dependent[4]
USB devices	
Regenerate from FIFO	0 to 10 MHz
Streaming from memory	0 to 1 MHz system dependent[4]
Data transfers	
PCI/PCIe/PXI/PXIe devices	DMA (scatter-gather), interrupts, programmed I/O
USB devices	USB Signal Stream, programmed I/O
DO or DI Sample Clock source[5]	Any PFI, RTSI, AI Sample or Convert Clock, AO Sample Clock, Ctr *n* Internal Output, and many other signals

[4] Performance can be dependent on bus latency and volume of bus activity.
[5] The digital subsystem does not have its own dedicated internal timing engine. Therefore, a sample clock must be provided from another subsystem on the device or an external source.

PFI/Port 1/Port 2 Functionality	
Functionality	Static digital input, static digital output, timing input, timing output
Timing output sources	Many AI, AO, counter, DI, DO timing signals

Debounce filter settings	125 ns, 6.425 µs, 2.56 ms, disable; high and low transitions; selectable per input

Recommended Operation Conditions[6]		
Level	**Min**	**Max**
Input high voltage (V_{IH})	2.2 V	5.25 V
Input low voltage (V_{IL})	0 V	0.8 V
Output high current (I_{OH}) P0.<0..31> PFI <0..15>/P1/P2	 — —	 -24 mA -16 mA
Output low current (I_{OL}) P0.<0..31> PFI <0..15>/P1/P2	 — —	 24 mA 16 mA

Electrical Characteristics		
Level	**Min**	**Max**
Positive-going threshold (VT+) Negative-going threshold (VT-)	— 0.8 V	2.2 V —
Delta VT hysteresis (VT+ - VT-)	0.2 V	—
I_{IL} input low current (V_{in} = 0 V) I_{IH} input high current (V_{in} = 5 V)	— —	-10 µA 250 µA

Digital I/O Characteristics[6]

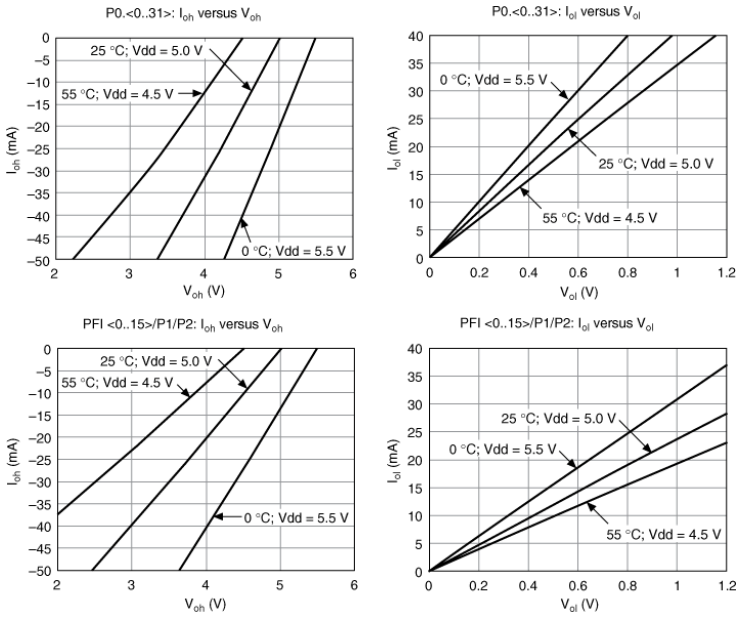

[6] On earlier versions of the USB-6251 Screw Terminal (part numbers 194929A/B/C-0*x*) and the USB-6259 Screw Terminal (part numbers 194021B/C-0*x*), the digital I/O characteristics of P0.<16..31> match the characteristics of PFI <0..15>. Refer to the November 2006 version of the *NI 625x Specifications* (part number 371291G-01) for more details.

General-Purpose Counter/Timers

Number of counter/timers	2
Resolution	32 bits

Counter measurements	Edge counting, pulse, semi-period, period, two-edge separation
Position measurements	X1, X2, X4 quadrature encoding with Channel Z reloading; two-pulse encoding
Output applications	Pulse, pulse train with dynamic updates, frequency division, equivalent time sampling
Internal base clocks	80 MHz, 20 MHz, 0.1 MHz
External base clock frequency	0 MHz to 20 MHz
Base clock accuracy	50 ppm
Inputs	Gate, Source, HW_Arm, Aux, A, B, Z, Up_Down
Routing options for inputs	Any PFI, RTSI, PXI_TRIG, PXI_STAR, analog trigger, many internal signals
FIFO	2 samples
Data transfers	
PCI/PCIe/PXI/PXIe devices	Dedicated scatter-gather DMA controller for each counter/timer; interrupts, programmed I/O
USB devices	USB Signal Stream, programmed I/O
Frequency Generator	
Number of channels	1
Base clocks	10 MHz, 100 kHz
Divisors	1 to 16
Base clock accuracy	50 ppm
Output can be available on any PFI or RTSI terminal.	
Phase-Locked Loop (PLL)	
Number of PLLs	1
Reference signal	PXI_STAR, PXI_CLK10, RTSI <0..7>
Output of PLL	80 MHz Timebase; other signals derived from 80 MHz Timebase including 20 MHz and 100 kHz Timebases
External Digital Triggers	
Source	Any PFI, RTSI, PXI_TRIG, PXI_STAR
Polarity	Software-selectable for most signals
Analog input function	Start Trigger, Reference Trigger, Pause Trigger, Sample Clock, Convert Clock, Sample Clock Timebase
Analog output function	Start Trigger, Pause Trigger, Sample Clock, Sample Clock Timebase
Counter/timer functions	Gate, Source, HW_Arm, Aux, A, B, Z, Up_Down
Digital waveform generation (DO) function	Sample Clock
Digital waveform acquisition (DI) function	Sample Clock
Device-To-Device Trigger Bus	
PCI/PCIe devices	RTSI <0..7>[7]
PXI/PXIe devices	PXI_TRIG <0..7>, PXI_STAR
USB devices	None
Output selections	10 MHz Clock; frequency generator output; many internal signals
Debounce filter settings	125 ns, 6.425 µs, 2.56 ms, disable; high and low transitions; selectable per input

[7] In other sections of this document, *RTSI* refers to RTSI <0..7> for PCI/PCIe devices or PXI_TRIG <0..7> for PXI/PXIe devices.

Bus Interface	
PCI/PXI devices	3.3 V or 5 V signal environment
PCIe devices	
Form factor	x1 PCI Express, specification v1.0a compliant
Slot compatibility	x1, x4, x8, and x16 PCI Express slots[8]

PXIe devices	
Form factor	x1 PXI Express peripheral module, specification rev 1.0 compliant
Slot compatibility	x1 and x4 PXI Express or PXI Express hybrid slots
USB devices	USB 2.0 Hi-Speed or full-speed[9,10]
DMA channels (PCI/PCIe/PXI/PXIe devices)	6, analog input, analog output, digital input, digital output, counter/timer 0, counter/timer 1
USB Signal Stream (USB devices)	4, can be used for analog input, analog output, digital input, digital output, counter/timer 0, counter/timer 1

All PXI-625*x* devices support one of the following features:

May be installed in PXI Express hybrid slots
Or, may be used to control SCXI in PXI/SCXI combo chassis

Table 1. PXI/SCXI Combo and PXI Express Chassis Compatibility

M Series Device	M Series Part Number	SCXI Control in PXI/SCXI Combo Chassis	PXI Express Hybrid Slot Compatible
PXI-6250	191325D-04/191325E-04L	No	Yes
PXI-6251	191325D-03/191325E-03L	No	Yes
	191325D-13/191325E-13L	Yes	No
PXI-6254	191325D-02/191325E-03L	No	Yes
PXI-6255	193618A-01	No	Yes
PXI-6259	191325D-01/191325E-01L	No	Yes
	191325D-11/191325E-11L	Yes	No
Earlier versions of PXI-6251/ 6254/6259	191325C-0*x* 191325B-0*x*	Yes	No

All NI PXIe-625*x* devices may be installed in PXI Express slots or PXI Express hybrid slots.

[8] Some motherboards reserve the x16 slot for graphics use. For PCI Express guidelines, refer to ni.com/pciexpress.

[9] If you are using a USB M Series device in full-speed mode, device performance will be lower and you will not be able to achieve maximum sampling/update rates.

[10] Operating on a full-speed bus may result in lower high-speed full-speed performance.

Power Requirements

Current draw from bus during no-load condition[11]	
PCI/PXI devices	
+5 V	0.03 A
+3.3 V	0.725 A
+12 V	0.35 A
PCIe devices	
+3.3 V	0.925 A
+12 V	0.35 A
PXIe devices	
+3.3 V	0.45 A
+12 V	0.5 A
Current draw from bus during AI and AO overvoltage condition[11]	
PCI/PXI devices	
+5 V	0.03 A
+3.3 V	1.2 A
+12 V	0.38 A
PCIe devices	
+3.3 V	1.4 A
+12 V	0.38 A
PXIe devices	
+3.3 V	0.48 A
+12 V	0.71 A

⚠ **Caution** USB-625*x* devices must be powered with NI offered AC adapter or a National Electric Code (NEC) Class 2 DC source that meets the power requirements for the device and has appropriate safety certification marks for country of use.

USB power supply requirements	11 to 30 VDC, 20 W, locking or non-locking power jack with 0.080" diameter center pin, 5/16-32 thread for locking collars

[11] Does not include P0/PFI/P1/P2 and +5 V terminals.

Power Limits	
Caution Exceeding the power limits may cause unpredictable behavior by the device and/or PC/chassis.	
PCI devices	
+5 V terminal (connector 0)	1 A max[12]
+5 V terminal (connector 1)	1 A max[12]
PCIe devices	
Without disk drive power connector installed	
+5 V terminals combined	0.35 A max[12]
P0/PFI/P1/P2 and +5 V terminals combined	0.39 A max
With disk drive power connector installed	
+5 V terminal (connector 0)	1 A max[12]
+5 V terminal (connector 1)	1 A max[12]
P0/PFI/P1/P2 combined	0.39 A max
PXI/PXIe devices	
+5 V terminal (connector 0)	1 A max[12]
+5 V terminal (connector 1)	1 A max[12]
P0/PFI/P1/P2 and +5 V terminals combined	2 A max
USB devices	
+5 V terminal	1 A max[12]
P0/PFI/P1/P2 and +5 V terminals combined	2 A max
Power supply fuse	2 A, 250 V

[12] Has a self-resetting fuse that opens when current exceeds this specification.

Physical Requirements	
Printed circuit board dimensions	
NI PCI-6250/6251/6254/6255/6259	9.7 × 15.5 cm (3.8 × 6.1 in.)
NI PCIe-6251/6259	9.9 × 16.8 cm (3.9 × 6.6 in.) (half-length)
NI PXI/PXIe-6250/6251/6254/6255/6259	Standard 3U PXI
Enclosure dimensions (includes connectors)	
NI USB-6251/6255/6259 Screw Terminal	26.67 × 17.09 × 4.45 cm (10.5 × 6.73 × 1.75 in.)
NI USB-6251/6259 BNC	28.6 × 17 × 6.9 cm (11.25 × 6.7 × 2.7 in.)
NI USB-6251/6255/6259 Mass Termination	18.8 × 17.09 × 4.45 cm (7.4 × 6.73 × 1.75 in.)
NI USB-6251/6255/6259 OEM	Refer to the *NI USB-622x/625x OEM User Guide*
Weight	
NI PCI-6250	142 g (5 oz)
NI PCI-6251	149 g (5.2 oz)
NI PCI-6254	152 g (5.3 oz)
NI PCI-6255	164 g (5.8 oz)
NI PCI-6259	162 g (5.6 oz)
NI PCIe-6251	161 g (5.7 oz)
NI PCIe-6259	175 g (6.1 oz)
NI PXI-6250	212 g (7.5 oz)
NI PXI-6251/6254	222 g (7.8 oz)
NI PXI-6255	236 g (8.3 oz)
NI PXI-6259	233 g (8.2 oz)

NI PXIe-6251	208 g (7.3 oz)
NI PXIe-6259	221 g (7.8 oz)
NI USB-6251 Screw Terminal	1.2 kg (2 lb 10 oz)
NI USB-6255/6259 Screw Terminal	1.24 kg (2 lb 11 oz)
NI USB-6251/6255/6259 Mass Termination	816 g (1 lb 12.8 oz)
NI USB-6251 OEM	140 g (4.9 oz)
NI USB-6255/6259 OEM	172 g (6.1 oz)
I/O connector	
NI PCI/PCIe/PXI/PXIe-6250/6251	1 68-pin VHDCI
NI PCI/PCIe/PXI/PXIe-6254/6255/6259	2 68-pin VHDCI
NI USB-6251 Screw Terminal	64 screw terminals
NI USB-6255/6259 Screw Terminal	128 screw terminals
NI USB-6251 BNC	21 BNCs and 30 screw terminals
NI USB-6259 BNC	32 BNCs and 60 screw terminals
NI USB-6251 Mass Termination	1 68-pin SCSI
NI USB-6255/6259 Mass Termination	2 68-pin SCSI
Disk drive power connector (PCIe devices)	Standard ATX peripheral connector (not serial ATA)
USB-6251/6255/6259 Screw Terminal/USB-6251/6259 BNC screw terminal wiring	16-28 AWG

Maximum Working Voltage[13]

NI 6250/6251/6254/6255/6259 channel-to-earth	11 V, Measurement Category I

Caution Do *not* use for measurements within Categories II, III, or IV.

[13] Maximum working voltage refers to the signal voltage plus the common-mode voltage.

Environmental

Operating temperature	
PCI/PXI/PXIe devices	0 to 55 °C
PCIe devices	0 to 50 °C
USB devices	0 to 45 °C
Storage temperature	-20 to 70 °C
Humidity	10 to 90% RH, noncondensing
Maximum altitude	2,000 m
Pollution Degree (indoor use only)	2
Shock and Vibration (PXI/PXIe Devices Only)	
Operational shock	30 g peak, half-sine, 11 ms pulse (Tested in accordance with IEC-60068-2-27. Test profile developed in accordance with MIL-PRF-28800F.)
Random vibration	
Operating	5 to 500 Hz, 0.3 g_{rms}
Nonoperating	5 to 500 Hz, 2.4 g_{rms} (Tested in accordance with IEC-60068-2-64. Nonoperating test profile exceeds the requirements of MIL-PRF-28800F, Class 3.)

Safety

This product is designed to meet the requirements of the following standards of safety for electrical equipment for measurement, control, and laboratory use:

IEC 61010-1, EN 61010-1
UL 61010-1, CSA 61010-1

Note For UL and other safety certifications, refer to the product label or visit ni.com/certification, search by model number or product line, and click the appropriate link in the Certification column.

Electromagnetic Compatibility

This product is designed to meet the requirements of the following standards of EMC for electrical equipment for measurement, control, and laboratory use:

EN 61326 EMC requirements; Minimum Immunity
EN 55011 Emissions; Group 1, Class A
CE, C-Tick, ICES, and FCC Part 15 Emissions; Class A

Note For EMC compliance, operate this device with shielded cables.

CE Compliance

This product meets the essential requirements of applicable European Directives, as amended for CE marking, as follows:

73/23/EEC; Low-Voltage Directive (safety)
89/336/EEC; Electromagnetic Compatibility Directive (EMC)

Note Refer to the Declaration of Conformity (DoC) for this product for any additional regulatory compliance information. To obtain the DoC for this product, visit ni.com/certification, search by model number or product line, and click the appropriate link in the Certification column.

Environmental Management

National Instruments is committed to designing and manufacturing products in an environmentally responsible manner. NI recognizes that eliminating certain hazardous substances from our products is beneficial not only to the environment but also to NI customers.

For additional environmental information, refer to the NI and the Environment Web page at ni.com/environment. This page contains the environmental regulations and directives with which NI complies, as well as other environmental information not included in this document.

Waste Electrical and Electronic Equipment (WEEE)

At the end of their life cycle, all products must be sent to a WEEE recycling center. For more information about WEEE recycling centers and National Instruments WEEE initiatives, visit ni.com/environment/weee.htm.

电子信息产品污染控制管理办法 （中国 RoHS）

中国客户 National Instruments 符合中国电子信息产品中限制使用某些有害物质指令 (RoHS)。
关于 National Instruments 中国 RoHS 合规性信息，请登录 ni.com/environment/rohs_china。
(For information about China RoHS compliance, go to ni.com/environment/rohs_china.)

Back to Top

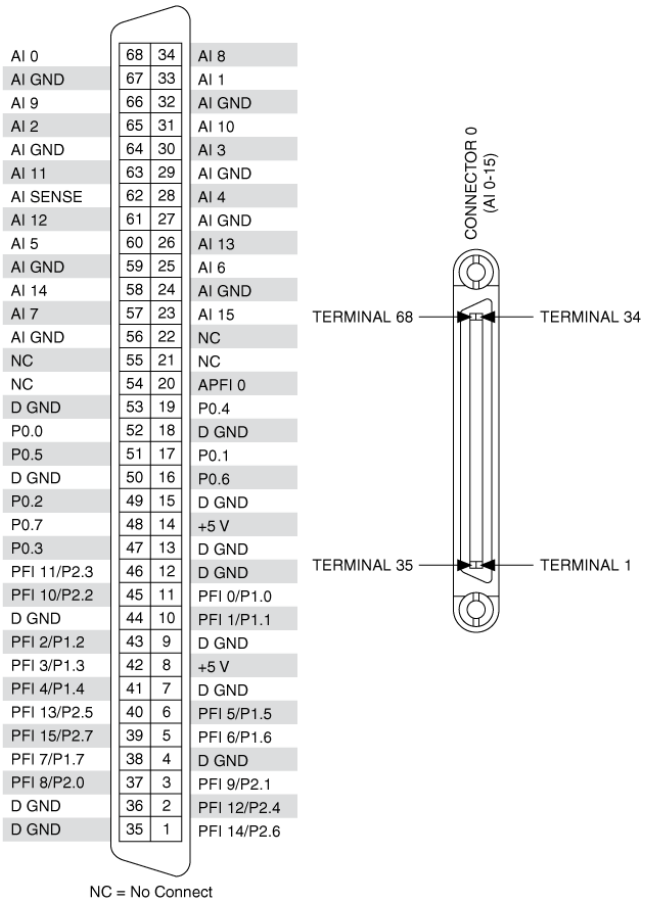

NI PCI/PXI-6250 Pinout

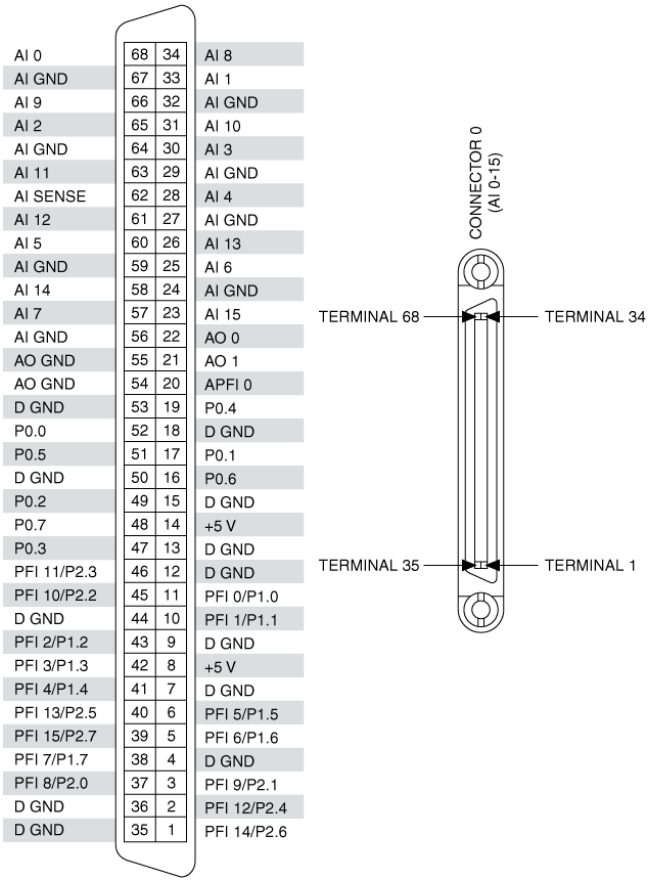

NI PCI/PCIe/PXI/PXIe-6251 Pinout

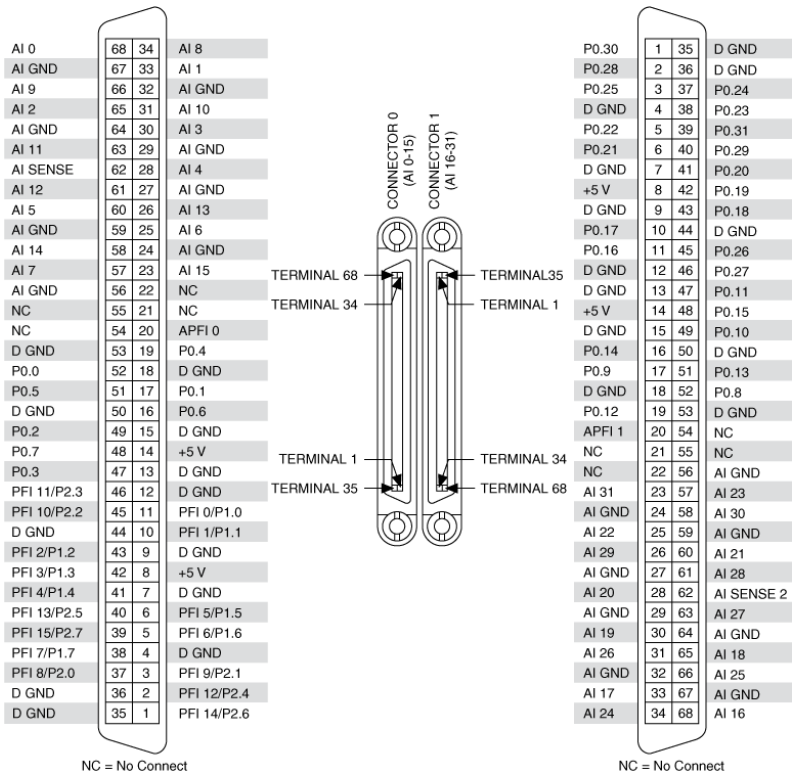

NI PCI/PXI-6254 Pinout

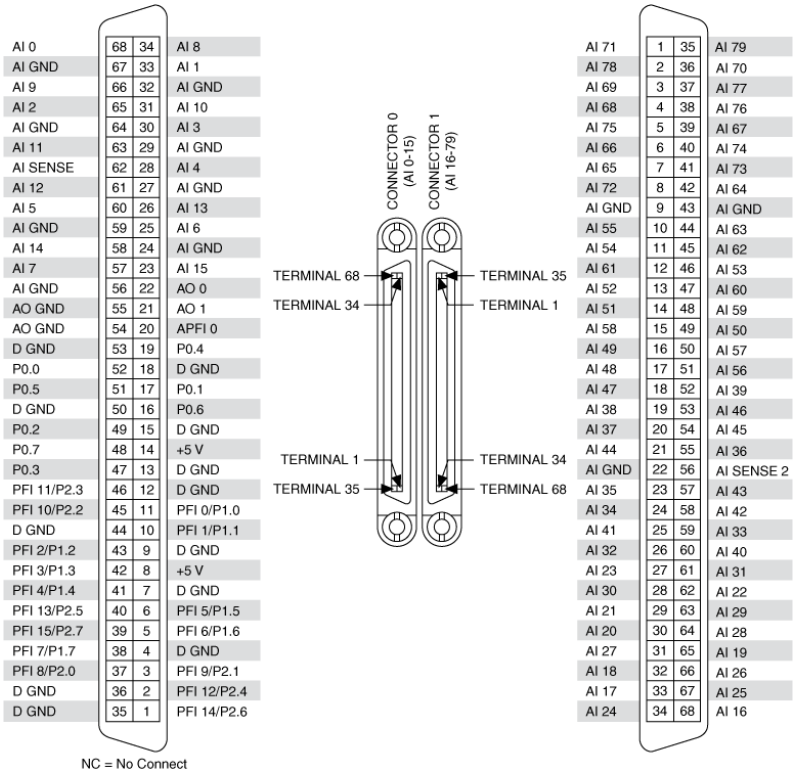

NI PCI/PXI-6255 Pinout

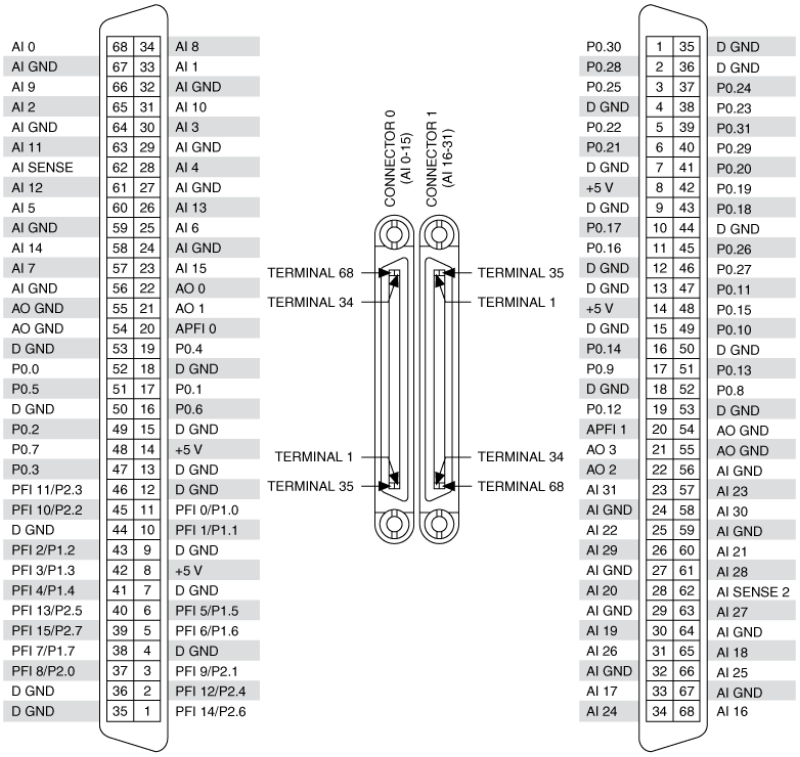

NI PCI/PCIe/PXI/PXIe-6259 Pinout

Back to Top